UNIVERSITY OF CALIFORNIA, SAN DIEGO

THREE-DIMENSIONAL RECONSTRUCTION OF THE NORMAL AND FIBROTIC SKELETAL MUSCLE EXTRACELLULAR COLLAGEN NETWORK

A dissertation submitted in partial satisfaction of the

requirements for the degree Doctor of Philosophy

in

Bioengineering

by

Allison R. Gillies

Committee in charge:

Professor Richard L. Lieber, Chair
Professor Shyni Varghese, Co-Chair
Professor Mark H. Ellisman
Professor Andrew D. McCulloch
Professor Samuel R. Ward

2013

The Dissertation of Allison R. Gillies is approved, and it is acceptable in quality and form for publication on microfilm and electronically:

_____

_____

_____

_____
Co-Chair

_____
Chair

University of California, San Diego

2013

This dissertation is dedicated to my father, Rodney, who encouraged me to follow my dreams. Your spirit lives on through the love you shared with those around you and your slightly inappropriate similes used to describe everyday situations. You will always be missed.

TABLE OF CONTENTS

LIST OF FIGURES AND TABLES

ACKNOWLEDGEMENTS

The work presented in this dissertation was a collaborative effort and many people have helped and supported me along the way. First, I would like to thank my advisor, Prof. Rick Lieber. When we met, he (who loves sarcomeres) was being forced to study the extracellular matrix because it kept coming up in his research models, and it just so happened I wanted to study the extracellular matrix. He temporarily excused my indifference toward sarcomeres and taught me everything I needed to know (and love) about muscle. Our quest for the truth about the extracellular matrix led us to Prof. Mark Ellisman, and I thank him and his team (especially Tom Deerinck) for allowing me to work with them. Without Dr. Ellisman's knowledge about muscle and expertise in microscopy, much of the work presented in this dissertation would not have been possible.

I have been lucky to work with amazing people in the Muscle Physiology Laboratory and I thank them for both technical and emotional support. Blair Conner and Michael Villongco helped enormously by tackling the mountain of data analysis and tissue processing that was required for this work. I would especially like to thank our lab manager, Shannon Bremner. I now know that her practice of hiding from me in lab was out of love—she knew I was close to finding the answer and she just wanted me to go a step farther. I also want to thank Prof. Sam Ward for sharing his expertise in imaging, which was an integral component of this dissertation.

Finally, I would like to thank my husband, Brett, and my family for supporting me during my graduate career. It has been a long and difficult road, and I thank all of you for believing in me. In Brett's absence during two deployments (15+ months), my

Navy and non-Navy community continued to encourage and support me in my studies, and for that I am grateful.

Chapter 2, in full, is a reprint of the material as it appears in Muscle and Nerve, 2011, Gillies AR, Lieber RL. The dissertation author was the primary investigator and author of this paper.

Chapter 3, in full, is a reprint of the material as it appears in Tissue Engineering Part C, 2011, Gillies AR, Smith LR, Lieber RL, Varghese S. The dissertation author was the primary investigator and author of this paper.

Chapter 4, in part, is currently being prepared for submission for publication of the material, Gillies AR, Bushong E, Deerinck TJ, Ellisman MH, Lieber RL. The dissertation author was the primary investigator and author of this material.

Chapter 5, in part, is currently being prepared for submission for publication of the material, Gillies AR, Bushong E, Deerinck TJ, Ellisman MH, Lieber RL. The dissertation author was the primary investigator and author of this material.

VITA

2007	Bachelor of Science, Biomedical Engineering North Carolina State University
2007-2009	Teaching Assistant, Department of Bioengineering University of California, San Diego
2008-2013	Graduate Student Researcher, Department of Bioengineering University of California, San Diego
2013	Doctor of Philosophy, Bioengineering University of California, San Diego

Journal Articles

Peutzer, J., Williams, J., **Gillies, A. R.**, Bernacki, S. H., and Loboa, E. G. (2013) The effects of cyclic hydrostatic pressure on chondrogenesis and viability of human adipose- and bone marrow-derived mesenchymal stem cells in three-dimensional agarose constructs. *Tissue Eng Part A* **19**, 299-306

Gillies, A. R., and Lieber, R. L. (2011) Structure and function of the skeletal muscle extracellular matrix. *Muscle Nerve* **44**, 318-331

Gillies, A. R., Smith, L. R., Lieber, R. L., and Varghese, S. (2011) Method for decellularizing skeletal muscle without detergents or proteolytic enzymes. *Tissue Eng Part C Methods* **17**, 383-389

Finger, A. R., Sargent, C. Y., Dulaney, K. O., Bernacki, S. H., and Loboa, E. G. (2007) Differential effects on messenger ribonucleic acid expression by bone marrow-derived human mesenchymal stem cells seeded in agarose constructs due to ramped and steady applications of cyclic hydrostatic pressure. *Tissue Eng* **13**, 1151-1158

Selected Abstracts

Gillies, A. R., Rodríguez-Soto, A. E., Ward, S. R., and Lieber, R. L. Discovery of fibrotic skeletal muscle perimysium ultrastructure. *The Orthopaedic Research Society, January 26-29, 2013*.

Gillies, A. R., and Lieber, R. L. Extracellular matrix organization in skeletal muscle fibrosis. *American Physical Therapy Association Section on Research Retreat, August 5-9, 2012.*

Gillies, A. R., and Lieber, R. L. Effect of desmin knockout on skeletal muscle extracellular matrix organization. *Experimental Biology, April 21-25, 2012.*

Gillies, A. R., Smith, L. R., Varghese, S., and Lieber, R. L. Method for investigating the structure and composition of striated muscle extracellular matrix. *Keystone Symposia on Extracellular Matrix and Cardiovascular Remodeling, January 23-28, 2011*.

ABSTRACT OF THE DISSERTATION

THREE-DIMENSIONAL RECONSTRUCTION OF THE NORMAL AND FIBROTIC SKELETAL MUSCLE EXTRACELLULAR COLLAGEN NETWORK

by

Allison R. Gillies

Doctor of Philosophy in Bioengineering

University of California, San Diego, 2013

Professor Richard Lieber, Chair

Professor Shyni Varghese, Co-Chair

Skeletal muscle fibrosis is a hallmark of muscle injury and disease, and is defined as a general increase in extracellular matrix components including collagen. In addition to an increase in collagen, fibrotic muscle stiffness increases which manifests clinically as decreased range of motion and contracture. Despite the lack of clinical treatment for skeletal muscle fibrosis, very little data exist on extracellular matrix collagen and its alterations with fibrosis. This dissertation aims to elucidate the structure of extracellular collagen and its role in fibrosis.

Because so little is known about the skeletal muscle extracellular matrix, Chapter 2 provides a review of the literature and original scanning electron micrographs of collagen structures that appear to be load-bearing. This review concluded that further study of the extracellular matrix was necessary to determine its normal structure and function before trying to interpret its fibrotic response.

As a first attempt to quantify normal properties of the extracellular matrix, Chapter 3 describes a method for direct investigation of structure, composition, and mechanical properties. In this method, muscle fibers were removed from muscle without proteolytic enzymes or detergents that could degrade extracellular components. Passive mechanical testing was performed on intact extracellular matrix to directly measure its mechanical properties for the first time.

With the observation of collagenous cable-like structures at the micron scale, a method was developed to better investigate extracellular collagen ultrastructure. Chapter 4 presents a three-dimensional electron microscopy method for reconstruction of skeletal muscle extracellular collagen structure. Collagen cable structures, fibroblasts, muscle fibers, and their interactions were modeled.

With this new tool, it was possible to investigate the structure of fibrotic extracellular matrix collagen. Chapter 5 investigates the structure and quantity of collagen cables structures in normal and fibrotic muscle. Previous studies indicated that fibrotic muscle was stiffer than normal, so it was hypothesized that the volume fraction of collagen cables increased in fibrotic muscle. Fibrotic muscle contained double the volume fraction of collagen cables compared to wild type muscle. Collagen

cables may therefore provide a future therapeutic target to reduce stiffness and improve function of fibrotic muscle.

CHAPTER 1

Introduction

1.1 General Introduction to the Dissertation

Skeletal muscle is a composite structure composed of multinucleated muscle fibers and the extracellular matrix that surrounds them. Muscle fibers generate force by contraction of sarcomeres, the basic functional unit of muscle, and this force is transmitted laterally through the extracellular matrix to tendons and bones to generate movement. The transmission of force from sarcomeres to the extracellular matrix occurs through a network of intermediate filaments, cytoskeletal proteins, and transmembrane complexes. In a number of muscle diseases, the genetic deletion or truncation of these proteins leads to reduced force transmission and therefore decreased muscle function. A common result of this disconnect of muscle fibers with the extracellular matrix is fibrosis, or a general increase in the amount of extracellular matrix material.

In addition to muscle disease, skeletal muscle fibrosis can occur in response to muscle injury. Patients with muscle fibrosis can have decreased range of motion and develop contracture. At the tissue level, fibrotic muscles are stiffer compared to normal muscle and this stiffness is a major factor in their limited function. This increase in stiffness is thought to arise from elastic components within the extracellular matrix, such as collagen. Fibrillar collagens have the necessary

mechanical properties to account for increased muscle stiffness, but structural studies have not been performed to determine if collagen organization is altered in fibrotic muscle. In fact, structural information on normal extracellular matrix is severely lacking. In addition, quantitative studies of the extracellular matrix to determine if the actual volume of extracellular components increase or if the apparent increase in extracellular matrix area in fibrosis is due solely to muscle fiber atrophy have not been performed. This dissertation examines the normal and fibrotic skeletal muscle extracellular matrix, with a focus on the structure, organization, and quantity of collagen.

Chapter 2, which has been published in *Muscle & Nerve*, is a review of the current understanding of skeletal muscle extracellular matrix structure, function, composition, and alterations with pathology. Original scanning electron micrographs of muscle extracellular matrix are included to provide evidence for previously unappreciated structures. This review calls attention to the paucity of information on the extracellular matrix structure and alterations with muscle pathology, and outlines specific questions that warrant further investigation.

Chapter 3, which has been published in *Tissue Engineering Part C Methods*, describes a method for analyzing the native structure and biochemistry of isolated extracellular matrix. Decellularization of skeletal muscle was achieved without the use of detergents or proteolytic enzymes that could alter the extracellular matrix composition and structure. Cellular components were successfully removed based upon Western blot and DNA quantification, and extracellular components largely remained intact as determined by scanning electron microscopy investigation of

structure and collagen and glycosaminoglycan quantification. This method also allowed for direct investigation of extracellular matrix mechanical properties, which previously could only be inferred.

Chapter 4 describes a method for three dimensional electron microscopy and reconstruction of skeletal muscle extracellular matrix. Previous tools available for studying the structure of the extracellular matrix were inadequate to answer our questions about collagen structure and organization in fibrotic skeletal muscle. Serial block face scanning electron microscopy is a new tool that allows for high resolution determination of tissue ultrastructure over relatively large volumes. This tool has been used for brain and tendon research, but not for skeletal muscle extracellular matrix. Imaging parameters and modifications to previous protocols, as well as reconstruction and segmentation methods are described. Reconstructions of extracellular collagen, fibroblasts, capillaries, and myonuclei are shown at a scale that has not been seen before.

Chapter 5 examines the extracellular matrix of fibrotic muscle compared to normal muscle. Collagen that surrounds bundles of muscle fibers forms long cables that extend throughout the muscle and have a wavy morphology. To determine if the increased muscle stiffness in a model of progressive muscle fibrosis (desmin knockout) could be due to extracellular matrix alterations, collagen cables were reconstructed by 3D electron microscopy and quantified by stereological analysis. Collagen cables were generally aligned with the muscle fiber axis, but appeared to be more prevalent in fibrotic muscle. Stereology confirmed this finding; the volume fraction of collagen cables is almost doubled in fibrotic muscle, while the volume of

disassociated collagen is unchanged. Interesting connections of collagen cables with fibroblasts and myonuclei are discussed.

Chapter 6 summarizes the findings of this dissertation and discusses the clinical implications of these findings. Future research directions are also provided.

1.2 Basic Skeletal Muscle Anatomy and Physiology

The skeletal muscle structural hierarchy forms a basis for its physiological function. Muscles are composed of fascicles, which contain many muscle cells. These specialized muscle cells, called muscle fibers, are multinucleated and composed of many myofibrils arranged in parallel. Each myofibril contains sarcomeres, the functional unit of muscle, in series. Sarcomeres are formed from overlapping actin and myosin myofilaments (Fig. 1.1A), and the interaction of these myofilaments forms the basis for force generation in muscle.

The thick and thin myofilaments in sarcomeres are formed from polymers of myosin and actin, respectively. The thick filament of myosin molecules is highly asymmetrical and termed the myosin heavy chain (MHC). The globular motor head of myosin heavy chain cyclically binds actin allowing it to “slide” relative to thin filaments. Myosin heavy chain isoforms vary among muscle fibers, and can be identified in muscle cross-sections by immunohistochemistry (1). Muscle fibers expressing primarily type I MHC are generally slow contracting, and muscle fibers expressing type 2A, 2B, and/or 2X MHC are generally fast contracting (2). The thin filament is a polymer of actin monomers arranged into an α-helix. Actin regulates

tension generation by controlling its availability for myosin binding, which is achieved through the troponin protein.

The structure of thick and thin filaments forms the basis for the amount of tension that can be generated by a sarcomere. Isolated single frog muscle fibers undergoing isometric contraction were studied at varying sarcomere lengths and the maximum tension produced by the fiber was recorded. These experiments formed the basis for the sarcomere length-tension relationship which is shown in Figure 1.1B (3, 4). Actively contracting fibers produced little tension at short and long sarcomere lengths, and the maximum tension was produced over a plateau region corresponding to 2.0-2.2 μm sarcomere lengths. This region corresponds to sarcomere lengths that have maximum overlap, or cross-bridge formation, between thick and thin filaments. At sarcomere lengths greater than 2.2 μm, known as the descending limb region of the length-tension curve, fewer and fewer cross-bridges are formed between thick and thin filaments and therefore less force is generated. At sarcomere lengths shorter than 2.0 μm actin filaments begin to overlap and interfere with cross-bridge formation, decreasing tension produced. As sarcomeres continue to shorten, myosin filaments begin to push on the Z-disks that separate serial sarcomeres resulting in a rapid decline in sarcomere tension. The length-tension curve presented here is a function of thick and thin filament lengths in frog muscle, and filament lengths vary among species and between muscles. Therefore, the length-tension curve for human muscles will be slightly different.

1.3 Skeletal Muscle Extracellular Matrix

The extracellular matrix (ECM) is composed of a network of structural proteins and glycoproteins that surrounds muscle fibers. It is traditionally defined as the endomysium surrounding muscle fibers, perimysium surrounding groups of muscle fibers, and epimysium surrounding the muscle, although the true organization appears to be more complex. The original description of ECM is based upon its morphology in a cross-section of normal muscle tissue, in which these three levels can easily be distinguished. However, the typical cross-sectional view of ECM gives little insight into differences that may exist between these different levels since most general histological stains visualize ECM as randomly organized connective tissue. Detailed structural information of the ECM is severely lacking, and current understanding is based upon scanning electron micrographs of mesh-like endomysial networks (5-7) and larger collagen fibers believed to be perimysial in nature (5, 8).

ECM remodeling is an important aspect of muscle regeneration, and in this context the ECM serves as a reservoir for growth factors, matrix remodeling enzymes, and fibroblasts, the cells that produce many of these proteins and enzymes. Structural proteins, mainly fibrillar type I and III collagens (9), provide support for muscle fibers, capillaries, and nerves during this process. Collagen networks may also play a role in muscle lateral force transmission and passive tension as outlined below. It is important to note that the detailed structure-function relationship of the ECM, and particularly collagen in the ECM, has not yet been elucidated. A more detailed

description of the structure, composition, and mechanical properties of the ECM are presented in Chapter 2.

1.4 Lateral Force Transmission in Muscle

As discussed above, sarcomeres generate force allowing for muscle contraction. That force, however, must somehow be transmitted to tendons and then bones to produce movement. Force may be transmitted longitudinally within a muscle fiber from the proximal tendon to the distal tendon. Overwhelming evidence supports the theory that force may also be transmitted laterally out of the muscle fiber to the surrounding ECM and then to the tendon. This type of force transmission occurs through a series of intermediate filaments and is transmitted to the ECM through a complex of transmembrane proteins.

Intermediate filaments transmit forces developed within sarcomeres to the cytoskeleton. These intermediate filaments include desmin and vimentin, which co-localize with the Z-disk (10, 11) and bind cytoskeletal actin (γ-actin). The intermediate filament network transmits forces out of the cell through a series of focal adhesion complexes. In skeletal muscle, these focal adhesions are termed “costameres” (12). Dystrophin and its associated glycoproteins compose the stronger of two linkages to the ECM within costameres. Dystrophin binds on one end to α-actinin, linking it to the intermediate filament network, and on the other to dystroglycan and sarcoglycan transmembrane proteins. Dystrophin’s importance to force transmission is highlighted by the functional deficits observed in patients with Duchenne muscular dystrophy

(DMD), which is caused by a mutation in the dystrophin gene. The other route of force transmission from intermediate filaments to the ECM is through vinculin, talin, and integrin complexes (13). Integrins are important for the normal function of skeletal muscle, as evidenced by progressive dystrophy with genetic deletion of the α7 integrin (14), although the α7 integrin-null phenotype is not as severe as that of DMD.

Outside the myofibers, components of the ECM bind to transmembrane proteins in costameres. Laminins in the basement membrane bind to integrins, α-dystroglycan, and other ECM proteins (15). Type IV collagen and fibronectin are also predominant components of the basement membrane (16) and form a mesh-like network that surrounds muscle fibers. The specific linkages that exist between the basement membrane and the endomysium, perimysium, and epimysium to transmit force in skeletal muscle are unknown.

1.5 Passive Mechanical Properties of Muscle

Most skeletal muscle mechanics studies have focused on active mechanics, but passive tension is also generated when muscle is stretched to long lengths without the formation of actin and myosin cross bridges. Passive tension arises as sarcomeres are stretched beyond optimum length (on the descending limb of the length-tension curve) and a typical passive tension curve is shown in Figure 1.1B. However passive tension, unlike active tension, could not be predicted based upon filament lengths, so the search began for the source of passive tension in muscle. In 1985, Magid and Law performed a study in which frog whole muscle passive tension was compared to that

of single fibers and single fibers with the sarcolemma removed (17). They found that passive tension was similar in muscle fibers and whole muscle and from this concluded that most passive tension in skeletal muscle developed within muscle fibers and not in the connective tissue, which was previously postulated.

Around the same time, titin, a giant protein in skeletal muscle, had been implicated in skeletal muscle passive elasticity based on structural evidence. Immunoelectron labeling of titin indicated that the protein spanned from Z-disk to neighboring Z-disk and was aligned parallel to thick filaments (18). Horowits *et al.* presented physiological data that titin and/or nebulin, another giant protein found in skeletal muscle, were implicated in passive tension development since degradation of these proteins reduced the ability of rabbit muscle fibers to produce passive tension (19). The contribution of titin, intermediate filaments, and collagen to passive tension in the rat heart were studied by selectively degrading each of these components to reveal that titin maintained passive tension at short sarcomere lengths, but became less important as sarcomere lengths increased (20).

For many years titin has been believed to be primarily responsible for the presence of passive elasticity in muscle, however recent evidence suggests that it may not be as important for whole muscle passive tension as originally thought. Passive tension varies systematically between muscles, yet titin isoform/size alone does not predict total muscle stiffness (21, 22). Initial research on titin and passive tension was performed on frog muscle, which contains very little connective tissue. Evidence suggests that connective tissue from mammalian muscle, composed mostly of collagen, could contribute to passive tension more than what has been measured in

frog muscle (5). Still, the factors that determine at what sarcomere length passive tension develops in different muscles are unknown and the parameters required to successfully model muscle passive mechanical properties have not yet been determined (23).

1.6 Skeletal Muscle Fibrosis

Fibrosis of various organs occurs in response to disease and injury, and skeletal muscle is no exception. Skeletal muscle fibrosis commonly develops in muscular dystrophies, myopathy (24), and with aging (25), and is identified by an increase in extracellular matrix material. Clinically, fibrotic muscle can be painful and have decreased range of motion and places patients at a higher risk for developing contracture. Another example of skeletal muscle fibrosis comes from cerebral palsy (CP), caused by an upper motoneuron lesion. The injury to the central nervous system causes secondary adaptations in skeletal muscle including fibrosis and contracture. Bundles of muscle fibers obtained from children with CP were stiffer than muscle from typically developing children (22). Additionally, CP muscles contained a higher collagen content than typically developing muscle.

Initially, the observation that muscle stiffness and collagen content increased in fibrotic muscle was exciting because it suggested that collagen content could be predictive of muscle stiffness and therefore function. However, when stiffness values were linearly regressed against the corresponding collagen content in both typically developing and cerebral palsy muscle biopsies, it was found that collagen content

alone does not correlate with muscle stiffness (Fig. 1.2). This forced the question, what about collagen (besides quantity) could affect tissue stiffness? Previous observations of collagen extracellular structures seemed likely candidates for load-bearing in muscle, but only limited data on these structures were available in the literature (5, 8). In order to determine how tissue stiffness increases in fibrotic muscle, a better understanding of the extracellular matrix structure and function is required in normal and pathologic conditions.

The desmin knockout mouse was used in this dissertation as progressive skeletal muscle fibrosis model to study the structure and composition of fibrotic extracellular matrix. These mice develop stiffer muscle, increased collagen content, and increased ECM area fraction compared to age-matched controls (26). Desmin is a component in the putative lateral force transmission pathway, and its deletion induces a constant state of inflammation and regeneration in muscle.

1.7 Extracellular Matrix Microscopy

Many microscopy techniques are available for investigating the skeletal muscle ECM structure. In order of low to high magnification, optical, laser, and electron microscopes are used to study biological specimens. Each of these methods has advantages and disadvantages for application to ECM, and an understanding of each of these tools is required to determine which tools are necessary to answer questions about collagen ECM structure.

Optical microscopy includes light and fluorescence microscopy, which are quick and relatively easy methods to obtain information about the presence or absence of an ECM component and the ECM area fraction. Optical microscopy shines light through a specimen, and the magnified image can be viewed by eye (Fig. 1.3A). Histology stains that identify collagen via light microscopy include Masson's trichrome and picrosirius red. Fluorescence microscopy is more commonly used to determine the presence or absence of a particular ECM component by antibody binding and indirect visualization with fluorophores. These methods however are only semi-quantitative, and do not have the magnification or resolution capabilities necessary for studying ECM structures on the micron scale.

Higher resolution and 3D visualization can be obtained with laser microscopy methods including confocal and second harmonic generation microscopy. Confocal microscopy also uses fluorophores to indirectly detect matrix components, but with the capability to "optically" section the specimen creating a z-stack of images. Second harmonic generation has the unique advantage of detecting collagen fibrils without indirect detection due to fibrillar collagen's crystalline non-centrosymmetric triple-helix structure (27). Unfortunately, small working distances at higher magnification limit the 3D imaging potential of these methods and tissue preparation methods can be disruptive to the native ECM structure.

Scanning electron microscopy (SEM) and transmission electron microscopy (TEM) can magnify skeletal muscle structures by 100,000x, making them the microscopy methods of choice for investigating structures on the micron and nano-scale. SEM and TEM produce images in different ways (Fig. 1.3). SEM specimens

must first be coated with metal to make them electrically conductive, and usually must be free of any moisture (biological specimen dehydration is required). An electron beam hits the specimen causing high-energy electrons to be emitted from the specimen, called secondary electrons (Fig. 1.3C). Alternatively, electrons within the electron beam may hit the specimen and be deflected off the surface, or backscattered. SEMs have both secondary and backscattered electron detectors. SEM images provide good 3D visualization of tissue surface or structures, however structures that are internal to the tissue must first be exposed. Exposing internal structures can damage the native tissue structure. In addition, coating specimens with metal particles may obscure fine structural details. TEM generates images by focusing an electron beam to pass through an ultrathin section of embedded tissue. Electrons pass through areas of the section depending on the density of the material and are detected by a camera at the bottom of the column (Fig. 1.3B). 3D imaging with TEM is possible through manually collecting and imaging serial sections or by using electron tomography, but these methods are laborious and usually only provide information over a small depth of tissue.

The collagen structures of interest to this dissertation are small in muscle cross-section (on the order of a few microns), yet they traverse through the tissue for at least several hundred microns. Because of their wavy morphology, the chances of obtaining a thin section that contains a continuous collagen structure are exceedingly small. A method that combines the 3D visualization of SEM with the resolution and non-disruptive preparation techniques of TEM was optimized and is described in Chapter 4.

1.8 References

1. Schiaffino, S., Gorza, L., Sartore, S., Saggin, L., Ausoni, S., Vianello, M., Gundersen, K., and Lomo, T. (1989) Three myosin heavy chain isoforms in type 2 skeletal muscle fibres. *J Muscle Res Cell Motil* **10**, 197-205

2. Bottinelli, R., Canepari, M., Pellegrino, M. A., and Reggiani, C. (1996) Force-velocity properties of human skeletal muscle fibres: myosin heavy chain isoform and temperature dependence. *J Physiol* **495 (Pt 2)**, 573-586

3. Gordon, A. M., Huxley, A. F., and Julian, F. J. (1966) Tension development in highly stretched vertebrate muscle fibres. *J Physiol* **184**, 143-169

4. Gordon, A. M., Huxley, A. F., and Julian, F. J. (1966) The variation in isometric tension with sarcomere length in vertebrate muscle fibres. *J Physiol* **184**, 170-192

5. Borg, T. K., and Caulfield, J. B. (1980) Morphology of connective tissue in skeletal muscle. *Tissue Cell* **12**, 197-207

6. Purslow, P. P., and Trotter, J. A. (1994) The morphology and mechanical properties of endomysium in series-fibred muscles: variations with muscle length. *J Muscle Res Cell Motil* **15**, 299-308

7. Trotter, J. A., and Purslow, P. P. (1992) Functional morphology of the endomysium in series fibered muscles. *J Morphol* **212**, 109-122

8. Passerieux, E., Rossignol, R., Chopard, A., Carnino, A., Marini, J. F., Letellier, T., and Delage, J. P. (2006) Structural organization of the perimysium in bovine skeletal muscle: Junctional plates and associated intracellular subdomains. *J Struct Biol* **154**, 206-216

9. Light, N., and Champion, A. E. (1984) Characterization of muscle epimysium, perimysium and endomysium collagens. *Biochem J* **219**, 1017-1026

10. Lazarides, E. (1980) Intermediate filaments as mechanical integrators of cellular space. *Nature* **283**, 249-256

11. Wang, K., and Ramirez-Mitchell, R. (1983) A network of transverse and longitudinal intermediate filaments is associated with sarcomeres of adult vertebrate skeletal muscle. *J Cell Biol* **96**, 562-570

12. Pardo, J. V., Siliciano, J. D., and Craig, S. W. (1983) A vinculin-containing cortical lattice in skeletal muscle: transverse lattice elements ("costameres") mark sites of attachment between myofibrils and sarcolemma. *Proc Natl Acad Sci U S A* **80**, 1008-1012

13. Miyamoto, S., Teramoto, H., Coso, O. A., Gutkind, J. S., Burbelo, P. D., Akiyama, S. K., and Yamada, K. M. (1995) Integrin function: molecular hierarchies of cytoskeletal and signaling molecules. *J Cell Biol* **131**, 791-805

14. Mayer, U., Saher, G., Fassler, R., Bornemann, A., Echtermeyer, F., von der Mark, H., Miosge, N., Poschl, E., and von der Mark, K. (1997) Absence of integrin alpha 7 causes a novel form of muscular dystrophy. *Nat Genet* **17**, 318-323

15. Talts, J. F., Andac, Z., Gohring, W., Brancaccio, A., and Timpl, R. (1999) Binding of the G domains of laminin alpha1 and alpha2 chains and perlecan to heparin, sulfatides, alpha-dystroglycan and several extracellular matrix proteins. *EMBO J* **18**, 863-870

16. Sanes, J. R. (1982) Laminin, fibronectin, and collagen in synaptic and extrasynaptic portions of muscle fiber basement membrane. *J Cell Biol* **93**, 442-451

17. Magid, A., and Law, D. J. (1985) Myofibrils bear most of the resting tension in frog skeletal muscle. *Science* **230**, 1280-1282

18. Maruyama, K., Yoshioka, T., Higuchi, H., Ohashi, K., Kimura, S., and Natori, R. (1985) Connectin filaments link thick filaments and Z lines in frog skeletal muscle as revealed by immunoelectron microscopy. *J Cell Biol* **101**, 2167-2172

19. Horowits, R., Kempner, E. S., Bisher, M. E., and Podolsky, R. J. (1986) A physiological role for titin and nebulin in skeletal muscle. *Nature* **323**, 160-164

20. Granzier, H. L., and Irving, T. C. (1995) Passive tension in cardiac muscle: contribution of collagen, titin, microtubules, and intermediate filaments. *Biophys J* **68**, 1027-1044

21. Prado, L. G., Makarenko, I., Andresen, C., Kruger, M., Opitz, C. A., and Linke, W. A. (2005) Isoform diversity of giant proteins in relation to passive and active contractile properties of rabbit skeletal muscles. *J Gen Physiol* **126**, 461-480

22. Smith, L. R., Lee, K. S., Ward, S. R., Chambers, H. G., and Lieber, R. L. (2011) Hamstring contractures in children with spastic cerebral palsy result from a stiffer extracellular matrix and increased in vivo sarcomere length. *J Physiol* **589**, 2625-2639

23. Winters, T. M., Takahashi, M., Lieber, R. L., and Ward, S. R. (2011) Whole muscle length-tension relationships are accurately modeled as scaled sarcomeres in rabbit hindlimb muscles. *J Biomech* **44**, 109-115

24. Goldfarb, L. G., Park, K. Y., Cervenakova, L., Gorokhova, S., Lee, H. S., Vasconcelos, O., Nagle, J. W., Semino-Mora, C., Sivakumar, K., and Dalakas, M. C. (1998) Missense mutations in desmin associated with familial cardiac and skeletal myopathy. *Nat Genet* **19**, 402-403

25. Carlson, M. E., Hsu, M., and Conboy, I. M. (2008) Imbalance between pSmad3 and Notch induces CDK inhibitors in old muscle stem cells. *Nature* **454**, 528-532

26. Meyer, G. A., and Lieber, R. L. (2012) Skeletal muscle fibrosis develops in response to desmin deletion. *Am J Physiol Cell Physiol* **302**, C1609-1620

27. Cox, G., Kable, E., Jones, A., Fraser, I., Manconi, F., and Gorrell, M. D. (2003) 3-dimensional imaging of collagen using second harmonic generation. *J Struct Biol* **141**, 53-62

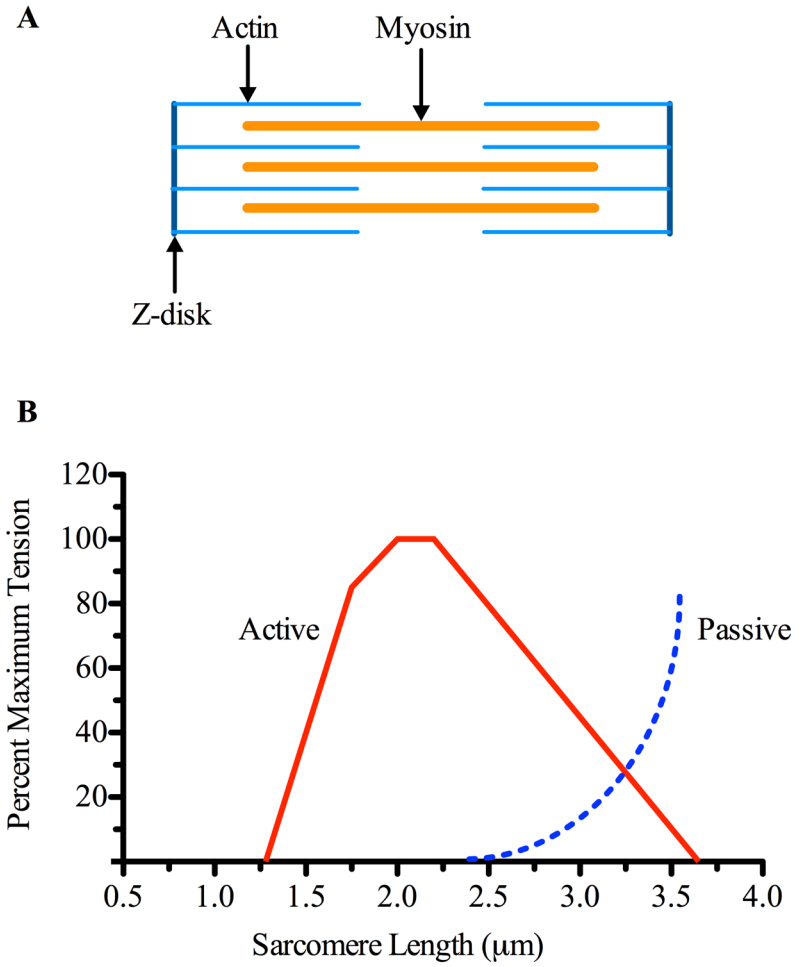

Figure 1.1: A) Schematic diagram of a sarcomere. Actin and myosin filaments overlap and can slide relative to each other. Sarcomeres are bounded on either end by the z-disk. B) Sarcomere length-tension relationship for frog muscle undergoing isometric contractions. The red solid line denotes tension generated by actively contracting sarcomeres, and the blue dotted line represents passive muscle tension.

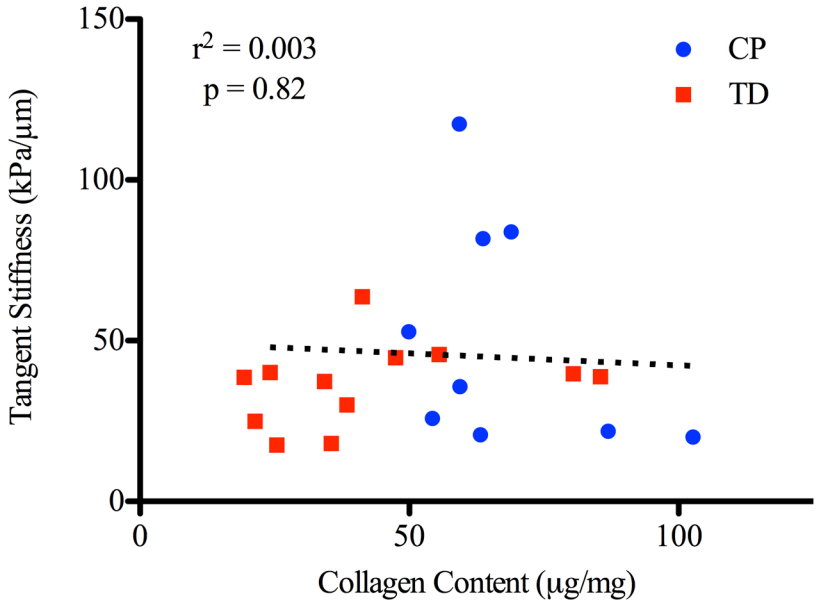

Figure 1.2: Collagen content is not predictive of tangent stiffness for muscle isolated from typically developing children (TD) or children with cerebral palsy (CP). Each data point represents one subject. Linear regression analysis of all data (dotted black line) revealed no correlation between collagen content and tangent stiffness. Data courtesy of L.R. Smith.

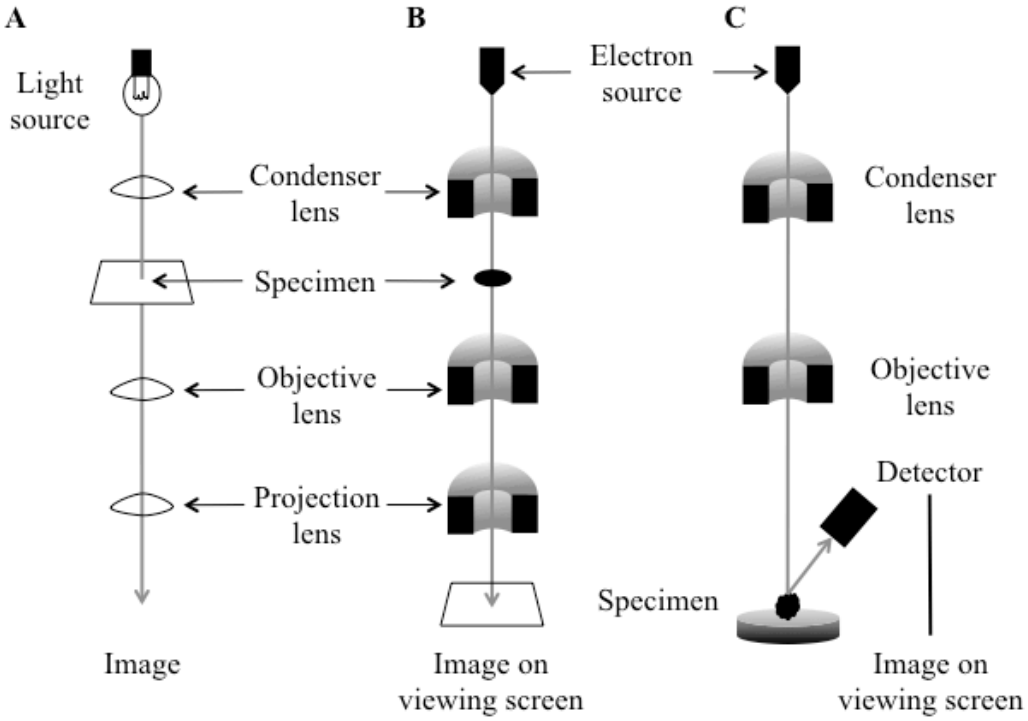

Figure 1.3: Schematic representations of A) optical microscopy, B) transmission electron microscopy, and C) scanning electron microscopy. These techniques are routinely used to investigate skeletal muscle structure. Note that the light and electron paths from source to image have been highly simplified and are shown as a single gray arrow.

CHAPTER 2

Structure and Function of the Skeletal Muscle Extracellular Matrix

2.1 Abstract

The skeletal muscle extracellular matrix (ECM) plays an important role in muscle fiber force transmission, maintenance, and repair. In both injured and diseased states, ECM adapts dramatically, a property that has clinical manifestations and alters muscle function. Here, we review the structure, composition, and mechanical properties of skeletal muscle ECM, describe the cells that contribute to the maintenance of the ECM and, finally, overview changes that occur with pathology. New scanning electron micrographs of ECM structure are also presented with hypotheses about ECM structure-function relationships. Detailed structure-function relationships of the ECM have yet to be defined and, as a result, we propose areas for future studies.

2.2 Introduction

Skeletal muscles are composed primarily of contractile material. Thus, it is no surprise that the vast majority of skeletal muscle studies focus on its contractile properties. However, because muscle is a composite tissue of connective tissue, blood vessels, and nerves as well as contractile material, these “minor” tissues (in terms of

relative mass) may strongly influence muscle function. In this review, we focus on the skeletal muscle extracellular matrix (ECM) because of the growing body of evidence indicating that ECM strongly affects muscle's normal function, its ability to adapt, and the biological reservoir of muscle stem cells that it provides. Specifically, recent biomechanical studies support the idea the ECM bears the majority of muscle passive load which implies that clinical examination of patient range of motion and stiffness primarily reflect their ECM properties. In addition, while muscle pathology is typically described in terms of altered fiber type, fiber size distribution or centralized nuclei, nearly every pathological change reported in muscle is also associated to some degree with ECM fibrosis. Therefore, based on its important functional role, its consistent response to disease and injury, and its clinically significant manifestations, it is timely to review our current understanding of muscle ECM structure, function, and biology.

2.3 Skeletal Muscle ECM Structure

Unfortunately, there is a paucity of objective information about muscle ECM compared to the other connective tissues of mesenchymal origin, such as tendon, ligament, bone, and cartilage. It follows logically that much of the muscle ECM literature simply represents extrapolation of knowledge gleaned from other tissues. This is especially true in terms of understanding muscle ECM's functional properties, primarily because the geometry of muscle ECM is tremendously complex compared to other connective tissues. Didactic presentations regarding muscle ECM often

subdivide it into endomysial (around the muscle cell), perimysial (around groups of muscle cells), and epimysial (around the muscle) connective tissues (Fig. 2.1). However, direct inspection of actual skeletal muscle samples by light, transmission or scanning electron microscopy reveals that such definitive subdivisions are relatively arbitrary. Systematic studies of muscle ECM, in which the proper rules of three-dimensional sampling are followed, are lacking, resulting in a literature where sampling is typically biased according to what "appears" most prominent in tissue sections. Those studying ECM are encouraged to emulate the outstanding morphometric studies of muscle sarcoplasmic reticulum (SR) that led to our current understanding of the excitation-contraction coupling mechanism. These studies revealed that, while the SR is unimpressive in any single EM plane, reconstruction of the SR network reveals a highly ordered, extensive, and functionally critical component of muscle that would have been missed if it were simply viewed in any single traditional plane (1). It is therefore likely that a higher order organization of muscle ECM exists that is yet to be defined, and our understanding of the "three" subdivisions of ECM is of a rudimentary nature.

The muscle endomysium

An exception to the casual sampling performed in most ECM studies is the systematic and quantitative description of the muscle endomysial ECM reported for feline and bovine muscle by Purslow and Trotter (2, 3). They showed that a highly ordered network surrounds individual muscle fibers that deforms nonlinearly with increasing sarcomere length. The result is a load-bearing network whose mechanical

properties reflect more the network geometry than the constitutive properties of the composite collagen fibers (except at very long lengths). The significance of this geometry is that force is most likely transmitted by shear through the endomysium. Their dramatic topographical photographs (Fig. 2.2) and quantitative models (3), although performed about 25 years ago, still form our basic understanding of muscle cell-endomysium structural interactions. Because other muscles have not been studied at the same level of detail, it is not clear whether this level of organization is typical of all muscles across species or even different muscles within the same species.

We have examined the endomysial structure of mouse extensor digitorum longus (EDL) muscles using scanning electron microscopy. When fixed at resting length, we observed discreet patches of ECM that could be lifted away from myofibers in regions where fibers were apparently pulled apart during processing (Fig. 2.3A). Based on the fact that the edges of this "patch" appeared to become contiguous with the muscle fiber (Figs. 2.3B and 2.3D), we suspect that this patch represents an elevated piece of muscle fiber ECM, presumably endomysium. Interestingly, on muscle fibers adjacent to this patch, endomysial ECM appeared has a longitudinal periodicity on the myofiber surface (see lines in Fig. 2.3B), but no such longitudinal periodicity is obvious on the released patches (Fig. 2.3C). Often a large tubular extension passed over the surface of the fiber, which may represent a portion of the microcirculation or, perhaps an axon traversing the tissue (Fig. 2.3B).

The muscle perimysium

Muscle perimysial studies are much more sparse, variable and less defined

compared to the studies described above for the endomysium primarily because there is no strict definition of perimysium. Light micrographic cross-sections reveal thickened ECM that "surrounds" bundles of muscle cells. Thus, this "thicker" ECM region is often considered a distinct entity simply because it presents a more visually obvious pattern; its higher order arrangement (if any) is not known. For example, it is not known whether perimysium surrounds a bundle of fibers from origin to insertion analogous to a telephone cable or whether it is interconnected across the muscle belly similar to the endomysial network. Addressing this issue has profound implications for understanding the normal and pathological properties of the muscle perimysium and has not previously been systematically addressed.

Surface topology of the perimysium suggests that, unlike the endomysium, perimysial collagen fibers are organized into more-or-less discrete populations that extend along and across muscle fibers (4-7). This can be observed on micrographs where longitudinally oriented fibers form a dense series of bands along fibers while transverse collagen fibers interconnect muscle fibers at discrete points ("Perimysial Plate," Fig. 2.4). Intriguingly, it has been reported that these transverse connection points are colocalized with focal adhesions and intracellular subdomains (7, 8), suggesting that the perimysium may be involved in cellular signaling. The degree of intimacy between the muscle cell and the perimysium can be appreciated based on the fact that cellular landmarks such as Z-bands and A-bands are visualized at the fiber surface (Fig. 2.4). However, it is not clear to what extent this arrangement is typical of all muscle fibers, and no data exist for human muscle. In the context of our understanding of normal muscle physiology, it would be interesting to determine

whether perimysial arrangements vary among muscles of different functions, such as those that are chronically active, perform antigravity functions, operate at long lengths, or are involved in rapid movements. In the same way that muscle fiber type has come to be understood in the context of muscle's physiological function (9), it is likely that some degree of ECM customization exists across muscles of different function. We frequently observed extended perimysial cables in the interstitium between muscle cells. Under conditions where the cells were extended (by about 30%) long cables were observed to be taut (Fig. 2.5A) and sometimes even frayed (Fig. 2.5B) as they passed between fibers. The cables themselves were organized as bundles of collagen fibers but the actual collagen isoform or the presence/absence of proteoglycan in these cables is not known. These cables terminated on muscle cells as the perimysial plate (Fig. 2.4). Under conditions where the muscle was fixed while slack, the perimysial cables were tortuous and intimately associated with the fiber surface (Fig. 2.6). It is of interest that the cable reproduced in the montage of Figure 2.6 has a gross structure reminiscent of strain relief (arrow) that is commonly present in load bearing structures that are subjected to length changes. Also visible in this micrograph is the close association between the so-called perimysial cables and the endomysial mesh (arrowheads). Clearly, "unraveling" the biological and biomechanical associations between these structures represents a formidable challenge.

To understand the organization of collagen fibrils in ECM more completely, confocal microscopy can be used to examine ECM components (10, 11). This method offers the ability to measure real-time deformation in ECM components in response to

loading. Taken together, the above descriptive studies of skeletal muscle ECM strongly suggest that there is a well-organized collagen network that can be quantified in terms of fibril size distribution, interconnection, and orientation as a function of muscle length and activity. However, the exact nature of the network and its site(s) of mechanical integration with the surrounding muscle tissue, including the microcirculation and motor unit axons, remain to be determined.

The muscle epimysium

The epimysial layer of muscle ECM can be discretely isolated by dissection and, thus, lends itself to a more discrete definition and mechanical testing. Gao and colleagues described the deep and superficial surfaces of epimysium as being primarily composed of very large collagen bundles with a familiar "crimp" pattern reminiscent of that seen in tendon (12, 13). In light of this structural specialization, a micromechanical model was developed that could describe the highly nonlinear behavior of this connective tissue (14). These investigators speculated that stiffness of the epimysium changed with age, which could have implications for understanding biomechanical properties of aged muscle both in terms of normal function and response to injury. In addition to the epimysium, connective tissue linkages may be involved in force transmission between muscles, but this will not be discussed here (see review (15)). Based on the morphological appearance of epimysium (Fig. 2.7), it is not clear whether epimysium has truly distinct structural properties compared to perimysium. Apparent sarcomere length periodicity (Fig. 2.7A, lines) as well as longitudinal ECM periodicity are both observable in the epimysium (Fig. 2.7B, lines).

However, because these preparatory and visualization methods are so disruptive, it is not clear that these properties reflect native ECM structure.

Putative structure hierarchy of skeletal muscle ECM

The hierarchical organization of ECM into endo-, peri-, and epimysium is generally accepted, but this simplified organization does not explain how ECM transitions through these "zones" from muscle to tendon. Passerieux and colleagues digested muscle fibers in bovine flexor carpi radialis muscles and visualized the resulting connective tissue using scanning electron microscopy (16). The images they obtained suggest that sheets of perimysial collagen join and become continuous with tendon. It is interesting to note that tendon and perimysium both contain primarily type I collagen, and the primary proteoglycan (PG) for both structures is decorin. In contrast, epimysium and endomysium are made up of almost equal amounts of types I and III collagen and contain other PGs (see below). The structure of perimysium is also different from the mesh-like structure of endomysium. This evidence supports the hypothesis that perimysium is continuous with tendon (Fig. 2.1B). Using this logic, muscle fascicles are viewed as being surrounded by perimysium, and endomysium is continuous within fascicles, but does not cross the perimysial border. Collagen in tendon is much more organized than collagen in perimysium, but collagen organization may have initially been similar during development before differentiating as a result of loading conditions. High tensile loads on the tendon may organize collagen fibers to align with the muscle axis while complex stress and strain distributions within the muscle belly may allow perimysial collagen to maintain a less

organized structure. Based on the fact that muscle fibers within a motor unit do not extend the length of a fascicle (17) and the observation of an intimate interaction between tendon and perimysium, a current structural model for muscle tissue is one in which muscle fibers are embedded within a matrix of ECM that forms discrete layers that are mechanically interconnected. Thus, muscle fiber force generated by actin-myosin interactions will be transmitted to the ECM at multiple focal adhesions along the muscle fiber itself (18). Once force is transmitted to the ECM, there would be nearly infinite paths of force transmission to the external tendon. In this way, focal ECM or muscle fiber injuries would have negligible functional significance due to the mechanical redundancy built into the ECM. It would be extremely helpful to pursue detailed studies of the transition zones between endomysium, perimysium, epimysium, and tendon.

2.4 Composition

Skeletal muscle collagens

Collagen is the major structural protein in skeletal muscle ECM accounting for 1-10% of muscle mass dry weight (19, 20). Collagen structure has been extensively studied and will not be described here (see review (21)). Types I, III, IV, V, VI, XI, XII, XIV, XV, and XVIII collagen are expressed during skeletal muscle development (22-26), although fibrillar types I and III predominate in adult endo-, peri-, and epimysium (27, 28). Several studies suggest that perimysial collagen is predominantly type I, whereas type III collagen appears to be more evenly distributed between

endomysium and epimysium (28). However, these studies are largely qualitative due to difficulty isolating various "regions" of ECM; thus, it is not clear if collagen ratios vary in muscles with different functions. Type V collagen, another fibril-forming collagen, associates with types I and III and may form a core for type I collagen fibrils in perimysium and endomysium (29). No data exist regarding the effect of a type V collagen core on type I collagen fibril crimp pattern, tensile strength, or fibril diameter. Types XII and XIV collagen are fibril associated collagens with interrupted triple helices (FACITs) localized primarily to perimysium (23). While they appear to link fibrillar collagen to other ECM components, their precise function is not known.

Muscle basement membrane consists primarily of a type IV collagen network, however types VI, XV, and XVIII are also present (22, 24-26, 30). Types XV and XVIII collagen are classified as multiplexins, which are heparan sulfate proteoglycans (HSPGs). The multiplexins can bind growth factors and also aid in linking the basement membrane to other basement membrane glycoproteins and endomysium (31). Although the basement membrane is considered distinct from endomysium, the two are intimately connected and probably involved in the transmission of force from the myofiber to the tendon (3, 32).

Attempts to characterize skeletal muscle collagens fully have been hampered by inadequate biochemical techniques that do not accurately differentiate and/or quantify collagen types. This is partially due to the complex and conserved structure of collagen molecules. Current methods include quantification by the ratio of hydroxyproline to collagen, Western blots of digested collagen fractions, antibody binding assays, and high pressure liquid chromatography (HPLC). Identification by

hydroxyproline and HPLC does not allow for differentiation of specific collagen types, whereas Western blotting may be used to successfully quantify collagen types. However, this method is laborious, fairly insensitive, difficult to quantify and not suitable for large-scale screening. Immunohistochemistry may be used to localize collagen in muscle tissue, however this approach suffer from the fact that antibody affinities vary tremendously and, as described above, collagen "visualization" is highly biased due to the complex geometry of ECM itself. Visualization is further complicated by the presence of heterotrimers of different collagen types because antibody-binding epitopes may be masked by associated collagen fibrils. New techniques must be developed to identify and quantify different collagen types.

Proteoglycans and glycosaminoglycans

Proteoglycans are ubiquitous in connective tissue, and muscle ECM is no exception. A number of PGs are present in muscle ECM, with many belonging to the family of small leucine-rich proteoglycans (SLRPs). SLRPs consist of a core protein with attached GAG chains and include decorin, biglycan, fibromodulin, and lumican. The most abundant PGs in skeletal muscle ECM have chondroitin sulfate and dermatan sulfate GAG chains, including decorin and biglycan (33). The heparan sulfate PGs collagen XVIII, perlecan, and agrin comprise approximately 30% of the PGs in ECM (33) and are known to bind growth factors (34, 35). Growth factors in skeletal muscle can be stored and released by negatively charged GAGs, particularly HSPGs. This is especially important in the basement membrane and endomysium, which surround muscle fibers where they can act in an autocrine fashion. Importantly,

enzymes in the ECM can cleave GAG chains with their associated growth factors (36-38), allowing for their interaction in cell signaling and mechanotransduction. Again, this field is in its infancy.

Collagen-proteoglycan interactions

Because they comprise the major structural components of ECM, collagen and proteoglycans have unique interactions that maintain the structure and organization of the matrix. Proteoglycans bind to collagen in specific locations (39-41) and are present in different ratios throughout ECM. Decorin, the major PG in the perimysium (42), is arch shaped (43, 44), and its leucine-rich repeats bind to type I collagen (45) near the d and e bands (40). Due to its binding interaction with type I collagen *in vitro*, decorin has been proposed to be a regulator of type I collagen fibrillogenesis in skeletal muscle. Decorin inhibits the lateral growth of collagen fibrils, both with and without its GAG chain, implying the core protein is the source of inhibition (46). Biglycan is structurally similar to decorin and also binds to type I collagen, likely at the same position as decorin (47). The binding of proteoglycans to collagen and the location of collagen crosslinks might be key factors that determine the structural organization of skeletal muscle ECM. In the absence of decorin (48) or biglycan (49) collagen fibril diameter in tendon is irregular. Additionally, biglycan-null mice display a mild muscular dystrophic phenotype (50) and skin from decorin-null mice has reduced tensile strength (48), indicating the importance of these PGs in maintaining normal tissue function and mechanical properties (see review (51)).

Glycoproteins and matricellular proteins

Many glycoproteins function as linker molecules between type IV collagen in the basement membrane and sarcolemma (muscle fiber membrane). At the sarcolemma, laminins are bound by integrins and α-dystroglycan (52, 53), and fibronectin may also bind to integrins (54). Laminins can bind directly to type IV collagen (55, 56), but may also be indirectly linked by fibronectin (55, 57) or nidogen (58, 59). Interactions between these glycoproteins provide potential mechanisms for lateral force transmission from the myofiber and have been reviewed (32). Together with the branched network structure of type IV collagen, these glycoproteins form the basis for basement membrane architecture (see reviews (60, 61)).

Matricellular proteins are secreted into the extracellular matrix but do not play a structural role and in skeletal muscle include osteopontin, secreted protein acidic and rich in cysteine (SPARC), thrombospondin, and tenascin-C. Osteopontin has cytokine-like functions and is not normally observed in normal skeletal muscle, but appears during muscle regeneration. Although typically secreted by inflammatory cells, myoblasts may also secrete osteopontin (62). SPARC has been shown to bind collagen and may chaperone collagen interactions in the extracellular matrix (63). Thrombospondin has been identified in skeletal muscle ECM and thrombospondin knockout mice had higher skeletal muscle capillarity than wildtype mice, indicating that its role may be to prevent excessive capillary formation (64). Tenascin-C is localized to the neuromuscular junction (NMJ) (65) and binds perlecan and agrin (66, 67), which could indicate that it plays a role in maintaining NMJ architecture (68).

Although these proteins do not provide structural support, they are vital in ECM signaling and maintaining ECM organization.

Matrix remodeling enzymes

In normal skeletal muscle, a delicate balance exists between enzymes responsible for ECM synthesis and their inhibitors. Turnover of the ECM is required for cell migration, myotube formation, and reorganization of the matrix during muscle adaptation. Matrix metalloproteinase (MMP) levels in uninjured muscle are generally low, but secreted MMPs that can be expressed in skeletal muscle include the gelatinases MMP-2 and MMP-9 (69) that degrade type IV collagen, fibronectin, proteoglycans, and laminin, as well as the collagenases MMP-1 (70) and MMP-13 (71) that degrade types I and III collagen. In addition to secreted MMPs, membrane type-1 MMP activates MMP-2 and has proteolytic functions near the cell surface (72). Their inhibitors, tissue inhibitors of matrix metalloproteinases (TIMPs) 1-3 (70, 73), either bind to active MMPs or stabilize inactive forms, thereby inhibiting their enzymatic activity. Given the wide range of components involved in ECM synthesis, degradation, and inhibition of this degradation, it is clear that skeletal muscle ECM composition and, therefore, its mechanical properties, are under tight regulation.

2.5 ECM Mechanics

Muscle ECM mechanical properties

Muscle develops passive tension as it is stretched beyond its slack length and,

within fibers, passive tension has been attributed primarily to titin, a giant protein that spans from the Z-disc to the M-line within sarcomeres (74). Magid and Law demonstrated in frog muscle fibers that passive tension originated from within myofibrils, not extracellularly, which led to decades of defining titin's structure and function (75). However, a correlation between titin size and fiber or myofibrillar stiffness is only weak (76), suggesting that other aspects of titin's structure may be more functionally important than size (e.g. protein phosphorylation) or that other structures are significantly involved. Biomechanical studies of muscle fiber bundles and even whole muscle provide more evidence that titin plays only a minor role in passive load-bearing at the tissue level. For example, when measuring the passive mechanical modulus of muscle from single fibers to fiber bundles, the modulus often increases two-fold (Table 2.1) (77-80). Given that the ECM comprises only about 5% of the area fraction of these muscle samples, these studies suggest that the ECM is a tremendously stiff structure surrounding relatively compliant fibers.

As mentioned above, to date, measurement of ECM biomechanical properties has consisted of studying epimysial sheets that are easily dissected and tested or isolation studies that remove all components from muscle with the exception of endomysium, perimysium, and epimysium collagen fibrils. However, biaxial testing of ECM sheets or isolated collagen fibrils may not represent the *in vivo* loading or structural environment of ECM, and new methods are needed to accurately measure the *in vivo* mechanical properties of the composite ECM.

<u>Direct and indirect measurement of composite ECM mechanical properties</u>

Two recent studies provide examples of novel methods that indirectly (79) or directly (81) define muscle ECM mechanical properties. To indirectly define ECM mechanical properties, a single muscle fiber modulus can be measured and compared to the modulus of muscle bundles. ECM modulus can then be calculated using the rule of mixtures for composites after the load-bearing area of fiber and ECM are first defined (79). Using this approach, isolated muscle fiber stress-strain behavior was shown to be linear, and muscle bundle stress-strain behavior was nonlinear (Fig. 2.8A). However, it was not clear whether the inherent nonlinearities in the ECM material properties were due to the fact that muscle fiber bundles are composed of numerous individual muscle fibers with slightly different linear material properties or whether the ECM itself was nonlinear. It is possible that nonlinear stress-strain behavior of muscle bundles can be a manifestation of fibers with linear stress-strain relationships that develop tension at different sarcomere lengths. To address this question, mechanical experiments were performed in which numerous single fibers were isolated to exclude ECM and then "grouped" together to be the size of a muscle fiber bundle. Then, a comparison between fiber "groups" and fiber bundles provided a comparison between multiple muscle fibers with and without ECM. The results clearly demonstrated that the modulus of a fiber group was nearly identical to that of single fibers; in contrast, the modulus of bundles was about five times higher (Fig. 2.8B). These experiments demonstrate that ECM is inherently stiffer than muscle fibers and that its material properties are highly nonlinear.

In a different approach, instead of using a subtractive method to define ECM properties, ECM properties were directly measured by treating the muscle in such a

way that removes everything *except* the ECM from a muscle (81). Unlike previous maceration techniques used to observe collagen in the ECM (82) or enzymatic and detergent digestion methods that remove glycosaminoglycans that may affect mechanical properties (83, 84), this so-called "decellularization" protocol did not remove glycosaminoglycans from the muscle. Importantly, biomechanical properties of the decellularized muscles were nearly identical to those of intact muscles. Creative experiments such as these will provide a first step toward elucidating the mechanical properties of skeletal muscle ECM.

2.6 ECM Mononuclear Cells

While most descriptions of "cells" within muscle tissue refer to the multinucleated, post-mitotic, highly differentiated muscle fibers, muscle tissue, in general, and ECM, in particular, is resident to a wide variety of mononuclear cell types that are involved in the maintenance of ECM and the regeneration of muscle. Satellite cells within muscle have been described in detail in a number of recent reviews (85, 86) and will not be discussed further in this review. Instead, we focus on the cell types in muscle that contribute to the production and maintenance of ECM. In terms of the "minor" cell types, nerve axons secrete agrin, a HSPG that aids in clustering acetylcholine receptors at the neuromuscular junction (87). Their supporting Schwann cells are capable of producing laminins both *in vitro* and *in vivo* (88), and, when cultured with nerve cells, they secrete types I and III collagen (89). The primary mononuclear cell in normal muscle ECM is the fibroblast, which is responsible for

producing the majority of ECM components, including collagen, fibronectin, MMPs, and PGs (90-92). In cases of muscle injury, however, other cell types may contribute to the production of ECM components. For example, satellite cells have been shown to secrete MMPs in culture (93), which may aid in their migration through the ECM to sites of muscle injury. It is even possible that multinucleated myofibers contribute to ECM production in normal muscle. Myogenic cells secrete collagen (94), MMP-2 (69), and decorin (95) in culture, and embryonic myoblasts secrete collagens prior to fusion (96), but fibroblasts appear to be necessary to organize these ECM components into a functional matrix (92, 97). Fibroblasts are sensitive to mechanical loading and convert mechanical signals into altered gene expression (see review (98)). Fibroblasts near the myotendinous junction likely experience a different mechanical environment compared to those located in the midbelly of the muscle, and this could be responsible for increased collagen production to aid in tendon development and maintenance as well as laminins and talins that link the ends of muscle fibers to the basement membrane at the myotendinous junction. Because the amount of collagen in muscle varies, it is reasonable to speculate that muscles may have phenotypically different fibroblasts for ECM production that correspond to the needs of that muscle type. There is precedent for such a differential function of generically identified "fibroblasts": extraocular fibroblasts are phenotypically distinct from leg muscle fibroblasts even when isolated from the same species. These fibroblasts are derived from neural ectoderm and mesenchymal origin, respectively, so transcriptional differences would not be surprising (99). A recent study found that fibroblasts isolated from different muscle types have different *in vitro* growth potentials and expression

different levels of MMP-2 (90). Fibroblasts cultured from bovine semitendinosus and sternomandibularis muscles had higher growth capacity than fibroblasts from longissimus dorsi muscle, and active MMP-2 expression was generally highest in semitendinosus fibroblast cultures and lowest in sternomandibularis fibroblast cultures. The mechanical properties and collagen content of these muscles were not analyzed in parallel, so these differences cannot be correlated with muscle function or ECM turnover. The location and number of fibroblasts in skeletal muscle have not been systematically addressed, but fluorescence-activated cell sorting (FACS) makes it possible to identify and separate fibroblasts from muscle tissue. Measuring changes in the fibroblast compartment of muscle after injury and pathology could explain the measured changes in ECM of these muscles.

The fact that a significant fraction of muscle resident mononuclear cells have stem cell properties (86) is especially provocative in light of recent studies that clearly demonstrate that the biomechanical properties of the cell substrate strongly affects gene expression patterns that pertain to fate determination (100). This raises the distinct possibilities that mechanical properties of ECM are not only modified in disease and injury, but that mechanical modifications or the ECM affect subsequent tissue properties. Again, this field is in its infancy.

2.7 ECM Pathological Changes

Fibrosis

A common theme across almost all myopathies is the accumulation of excess

ECM, which is generically termed “fibrosis.” This term actually has no objective definition but is typically used as a qualitative descriptor in muscle pathology. Fibrosis in skeletal muscle is clinically relevant especially in light of the very strong mechanical influence that the ECM plays in muscle function. It is unclear, however, whether fibrosis in muscle is characterized by excessive production of ECM components, altered activity or gene expression of ECM-degrading MMPs and their inhibitors, or a combination of these. Skeletal muscle fibrosis occurs in muscular dystrophies, diabetes, immobilization, and aging (101-105). Histological analysis of fibrosis in muscle (Fig. 2.9) is characterized by increased endomysium and perimysium. This type of description is highly sensitive but entirely nonspecific. Fibroblasts are typically the collagen producing cells in mature muscle, but other cell types, including inflammatory cells, myofibers, endothelial cells, and satellite cells, may contribute to collagen production in fibrotic muscle, as described above. To answer the question of which cell types produce collagen in fibrotic muscle, it would be interesting to study a Cre recombinase expressing mouse under the control of the type I collagen promoter (106) in a fibrosis-inducing injury model. In this model Cre protein is co-expressed with the α2 chain of type I collagen so that the presence of Cre, and therefore the cells expressing type I collagen, can be identified by immunofluorescence staining with an anti-Cre antibody. Furthermore, multiple reaction monitoring may be used in the future to quantify proteins from labeled cell types in muscle (107). This method can detect and quantify peptides in multiplex format using a triple quadrupole instrument. An advantage to this method is that it might be used to identify protein signals in fibrotic muscle that cause cells to

overexpress collagen.

Transforming growth factor-beta (TGF-β) is a cytokine with many functions in skeletal muscle. The role of TGF-β in fibrosis has been the subject of many studies (see reviews (108, 109)). Activated TGF-β induces fibroblasts to produce type I collagen, fibronectin, and connective tissue growth factor (CTGF) and suppresses matrix metalloproteinases. When repeated muscle injury occurs, elevated TGF-β continues to signal ECM production and eventually leads to a fibrotic response. In the case of Duchenne muscular dystrophy (DMD), decorin and biglycan, which normally sequester TGF-β, are differentially expressed (110-112), which may lead to altered TGF-β signaling and eventual fibrosis. CTGF has only recently been discovered, and its role in muscle fibrosis is not fully understood, but the expression of TGF-β and CTGF seem to be related (113-116). Mechanical stress appears to stimulate CTGF expression (117, 118), and CTGF may be involved in the muscle fibrosis that occurs after stretch injury.

In addition to changes in composition, fibrosis has been associated with changes in muscle mechanics. Spastic muscle from patients with cerebral palsy is characterized by increased extracellular material (119) and stiffer fibers (78, 120). Interestingly, the modulus of spastic muscle fibers is about two times greater than normal fibers, but the modulus of spastic muscle bundles is significantly lower than normal bundles (78). It is tempting to speculate that the reduced spastic bundle modulus occurs in response to the altered stiffness of the muscle fibers themselves. Collagen content is increased in spastic muscle (119) and correlates with the clinical severity of muscle spasticity (121), again demonstrating the clinical importance of

ECM in pathology. Analysis of muscle from children with wrist flexion contractures revealed significant changes in transcripts related to ECM in a way that differed from other altered use or disease models such as DMD, immobilization-induced atrophy or hereditary spastic paraplegia (122). Thus, it is possible that the "final" observable effect is fibrosis, but there are numerous cellular processes that can produce it.

An equally provocative muscle adaptation was recently observed in a desmin knockout model (123). Incremental stress-relaxation tests were performed on EDL muscle fibers and fiber bundles from desmin knockout and wildtype mice. The linear modulus was defined as the slope of the stress-strain curve—a measure of tissue stiffness. Loss of the intermediate filament network ultimately resulted in ECM hypertrophy and, mechanically, stiffer muscle tissue. Thus, data from children with CP and transgenic animal models both suggest the possibility that muscle fiber mechanical properties and ECM properties are dependent upon each other. The detailed mechanistic basis for such an interaction remains to be defined.

Profibrotic cytokines and ECM components that interact with them have been specific targets for antifibrotic therapies for skeletal muscle based on their potential to directly affect ECM production. Huard and colleagues have implemented this mechanistic approach by using IGF-1, decorin, and TGF-β inhibitors to prevent fibrosis in skeletal muscle (124-126). These treatments enhance regeneration and prevent fibrosis in injured muscle, but their efficacy in muscle that is already fibrotic has not yet been determined.

Intramuscular fat

Another pathological response of skeletal muscle to disease or injury is the accumulation of intramuscular, extracellular fat. This is distinct from the positive adaptation of muscle to exercise that includes increased intracellular fat deposition (127). Pathological examples of intramuscular fat deposition include fatty deposits that occur in advanced cases of DMD (128), obesity (129), type 2 diabetes (129), and aged muscle (129, 130), as well as the "fatty atrophy" that accompanies rotator cuff tears (131, 132) and low back pathology in humans (133).

Only recently has it been possible to address, in a relatively mechanistic fashion, the biological basis for fatty deposition in muscle tissue. This is based on the discovery of several cells types within muscle that have clear adipogenic potential, including satellite cells, mesenchymal stem cells, and certain side population cells (134-136). However, until recently, it was not clear which of these cells are responsible for adipose tissue in muscle. Uezumi and colleagues identified a PDGFRα^+ progenitor cell population distinct from satellite cells that can differentiate into adipose tissue *in vivo* under non-regenerating conditions (135). Interestingly, these cells were observed more in perimysium than endomysium, consistent with the idea that fat accumulation in disease is generally localized to the perimysium (137). A detailed mechanism for the activation of these cells and the factor(s) that regulate their proliferation is not yet known.

2.8 Conclusions

The role of ECM in muscle mechanics and pathology is not well understood,

but it is becoming more evident that changes in ECM are clinically significant. Further studies are required to define the detailed structure and composition of ECM, characterize its mechanical properties, and determine the way in which these relationships change in diseased states. Several studies have been proposed in this review that could address these areas, and the key questions are summarized below:

1. What is the three-dimensional perimysial collagen structure in muscle? How does this differ amongst muscles with different function, e.g. those that are chronically active, perform antigravity functions, operate at long lengths, or are involved in rapid movements?
2. What is the nature of the transition between structures of the endomysium, perimysium, epimysium, and tendon? How do these structures interconnect to transmit force along and across muscle?
3. What is the nature of the biological and biomechanical communication between muscle cells and the ECM? Which structures are responsible for transmission of biological and mechanical signals between muscle cells and the ECM?
4. What are the changes that occur in the fibroblast and mononuclear cell compartment of muscle with normal development, pathology, and injury? What cell types contribute to the fibrosis or fatty accumulation that occurs in muscle disease?

Answers to these questions will vastly improve our basic understanding of the ECM and how it contributes to normal muscle function. Only then can we begin to understand how compositional and structural changes in the ECM affect muscle

function in disease and injury. Finally, identifying mechanisms by which ECM hypertrophies in disease will provide potential targets for therapeutic interventions.

2.9 Acknowledgements

I would like to acknowledge my co-author from Chapter 2, which is a reprint of the material as it appears in Muscle and Nerve, 2011, Gillies AR, Lieber RL. No authors had competing interests regarding the publication of this research. ARG carried out SEM tissue preparation, SEM imaging, and drafted the manuscript. RLL conceived of the study, participated in its design and coordination, and supervised writing of the manuscript.

The authors acknowledge Dr. Wolfgang A. Linke for providing original data from Prado et al. 2005, Kim Battista for drawing Figure 1, Dr. Orrin Franko for critical reading of the manuscript, the Department of Veterans Affairs, NIH grant R24HD050837, and NSF for a Graduate Research Fellowship.

2.10 References

1. Eisenberg, B. R. (1983) Quantitative ultrastructure of mammalian skeletal muscle. In *Skeletal Muscle* (Peachey, L. D., Adrian, R. H., and Geiger, S. R., eds) pp. 73-112, American Physiological Society, Baltimore, MD

2. Trotter, J. A., and Purslow, P. P. (1992) Functional morphology of the endomysium in series fibered muscles. *J Morphol* **212**, 109-122

3. Purslow, P. P., and Trotter, J. A. (1994) The morphology and mechanical properties of endomysium in series-fibred muscles: variations with muscle length. *J Muscle Res Cell Motil* **15**, 299-308

4. Jarvinen, T. A., Jozsa, L., Kannus, P., Jarvinen, T. L., and Jarvinen, M. (2002) Organization and distribution of intramuscular connective tissue in normal and immobilized skeletal muscles. An immunohistochemical, polarization and scanning electron microscopic study. *J Muscle Res Cell Motil* **23**, 245-254

5. Borg, T. K., and Caulfield, J. B. (1980) Morphology of connective tissue in skeletal muscle. *Tissue Cell* **12**, 197-207

6. Rowe, R. W. (1981) Morphology of perimysial and endomysial connective tissue in skeletal muscle. *Tissue Cell* **13**, 681-690

7. Passerieux, E., Rossignol, R., Chopard, A., Carnino, A., Marini, J. F., Letellier, T., and Delage, J. P. (2006) Structural organization of the perimysium in bovine skeletal muscle: Junctional plates and associated intracellular subdomains. *J Struct Biol* **154**, 206-216

8. Young, M., Paul, A., Rodda, J., Duxson, M., and Sheard, P. (2000) Examination of intrafascicular muscle fiber terminations: implications for tension delivery in series-fibered muscles. *J Morphol* **245**, 130-145

9. Schiaffino, S., and Reggiani, C. (1994) Myosin isoforms in mammalian skeletal muscle. *J Appl Physiol* **77**, 493-501

10. Hanley, P. J., Young, A. A., LeGrice, I. J., Edgar, S. G., and Loiselle, D. S. (1999) 3-Dimensional configuration of perimysial collagen fibres in rat cardiac muscle at resting and extended sarcomere lengths. *J Physiol* **517**, 831-837

11. Nakamura, Y. N., Iwamoto, H., Yamaguchi, T., Ono, Y., Nakanishi, Y., Tabata, S., Nishimura, S., and Gotoh, T. (2007) Three-dimensional reconstruction of intramuscular collagen networks of bovine muscle: A demonstration by an immunohistochemical/confocal laser-scanning microscopic method. *Animal Science Journal* **78**, 445-447

12. Butler, D. L., Grood, E. S., Noyes, F. R., and Zernicke, R. F. (1978) Biomechanics of ligaments and tendons. *Exerc Sport Sci Rev* **6**, 125-181

13. Gao, Y., Kostrominova, T. Y., Faulkner, J. A., and Wineman, A. S. (2008) Age-related changes in the mechanical properties of the epimysium in skeletal muscles of rats. *J Biomech* **41**, 465-469

14. Gao, Y., Waas, A. M., Faulkner, J. A., Kostrominova, T. Y., and Wineman, A. S. (2008) Micromechanical modeling of the epimysium of the skeletal muscles. *J Biomech* **41**, 1-10

15. Huijing, P. A. (1999) Muscle as a collagen fiber reinforced composite: a review of force transmission in muscle and whole limb. *J Biomech* **32**, 329-345

16. Passerieux, E., Rossignol, R., Letellier, T., and Delage, J. P. (2007) Physical continuity of the perimysium from myofibers to tendons: involvement in lateral force transmission in skeletal muscle. *J Struct Biol* **159**, 19-28

17. Ounjian, M., Roy, R. R., Eldred, E., Garfinkel, A., Payne, J. R., Armstrong, A., Toga, A. W., and Edgerton, V. R. (1991) Physiological and developmental implications of motor unit anatomy. *J Neurobiol* **22**, 547-559

18. Patel, T. J., and Lieber, R. L. (1997) Force transmission in skeletal muscle: from actomyosin to external tendons. *Exerc Sport Sci Rev* **25**, 321-363

19. Bendall, J. R. (1967) Elastin Content of Various Muscles of Beef Animals. *Journal of the Science of Food and Agriculture* **18**, 553-558

20. Dransfield, E. (1977) Intramuscular Composition and Texture of Beef Muscles. *Journal of the Science of Food and Agriculture* **28**, 833-842

21. Gelse, K., Poschl, E., and Aigner, T. (2003) Collagens--structure, function, and biosynthesis. *Adv Drug Deliv Rev* **55**, 1531-1546

22. Halfter, W., Dong, S., Schurer, B., and Cole, G. J. (1998) Collagen XVIII is a basement membrane heparan sulfate proteoglycan. *J Biol Chem* **273**, 25404-25412

23. Listrat, A., Lethias, C., Hocquette, J. F., Renand, G., Menissier, F., Geay, Y., and Picard, B. (2000) Age-related changes and location of types I, III, XII and

XIV collagen during development of skeletal muscles from genetically different animals. *Histochem J* **32**, 349-356

24. Marvulli, D., Volpin, D., and Bressan, G. M. (1996) Spatial and temporal changes of type VI collagen expression during mouse development. *Dev Dyn* **206**, 447-454

25. Myers, J. C., Dion, A. S., Abraham, V., and Amenta, P. S. (1996) Type XV collagen exhibits a widespread distribution in human tissues but a distinct localization in basement membrane zones. *Cell Tissue Res* **286**, 493-505

26. Nishimura, T., Ojima, K., Hattori, A., and Takahashi, K. (1997) Developmental expression of extracellular matrix components in intramuscular connective tissue of bovine semitendinosus muscle. *Histochem Cell Biol* **107**, 215-221

27. Bailey, A. J., Restall, D. J., Sims, T. J., and Duance, V. C. (1979) Meat Tenderness - Immunofluorescent Localization of the Isomorphic Forms of Collagen in Bovine Muscles of Varying Texture. *Journal of the Science of Food and Agriculture* **30**, 203-210

28. Light, N., and Champion, A. E. (1984) Characterization of muscle epimysium, perimysium and endomysium collagens. *Biochem J* **219**, 1017-1026

29. Fitch, J. M., Gross, J., Mayne, R., Johnson-Wint, B., and Linsenmayer, T. F. (1984) Organization of collagen types I and V in the embryonic chicken cornea: monoclonal antibody studies. *Proc Natl Acad Sci U S A* **81**, 2791-2795

30. Sanes, J. R. (1982) Laminin, fibronectin, and collagen in synaptic and extrasynaptic portions of muscle fiber basement membrane. *J Cell Biol* **93**, 442-451

31. Eklund, L., Piuhola, J., Komulainen, J., Sormunen, R., Ongvarrasopone, C., Fassler, R., Muona, A., Ilves, M., Ruskoaho, H., Takala, T. E., and Pihlajaniemi, T. (2001) Lack of type XV collagen causes a skeletal myopathy and cardiovascular defects in mice. *Proc Natl Acad Sci U S A* **98**, 1194-1199

32. Grounds, M. D., Sorokin, L., and White, J. (2005) Strength at the extracellular matrix-muscle interface. *Scandinavian Journal of Medicine & Science in Sports* **15**, 381-391

33. Brandan, E., and Inestrosa, N. C. (1987) Isolation of the heparan sulfate proteoglycans from the extracellular matrix of rat skeletal muscle. *J Neurobiol* **18**, 271-282

34. Mundhenke, C., Meyer, K., Drew, S., and Friedl, A. (2002) Heparan sulfate proteoglycans as regulators of fibroblast growth factor-2 receptor binding in breast carcinomas. *Am J Pathol* **160**, 185-194

35. Iozzo, R. V., and San Antonio, J. D. (2001) Heparan sulfate proteoglycans: heavy hitters in the angiogenesis arena. *J Clin Invest* **108**, 349-355

36. Imai, K., Hiramatsu, A., Fukushima, D., Pierschbacher, M. D., and Okada, Y. (1997) Degradation of decorin by matrix metalloproteinases: Identification of the cleavage sites, kinetic analyses and transforming growth factor-beta 1 release. *Biochem J* **322**, 809-814

37. Ishai-Michaeli, R., Eldor, A., and Vlodavsky, I. (1990) Heparanase activity expressed by platelets, neutrophils, and lymphoma cells releases active fibroblast growth factor from extracellular matrix. *Cell Regul* **1**, 833-842

38. Whitelock, J. M., Murdoch, A. D., Iozzo, R. V., and Underwood, P. A. (1996) The degradation of human endothelial cell-derived perlecan and release of bound basic fibroblast growth factor by stromelysin, collagenase, plasmin, and heparanases. *J Biol Chem* **271**, 10079-10086

39. Hedbom, E., and Heinegard, D. (1993) Binding of fibromodulin and decorin to separate sites on fibrillar collagens. *J Biol Chem* **268**, 27307-27312

40. Pringle, G. A., and Dodd, C. M. (1990) Immunoelectron Microscopic Localization of the Core Protein of Decorin near the D-Bands and E-Bands of Tendon Collagen Fibrils by Use of Monoclonal-Antibodies. *J Histochem Cytochem* **38**, 1405-1411

41. Scott, J. E., and Haigh, M. (1985) 'Small'-proteoglycan:collagen interactions: keratan sulphate proteoglycan associates with rabbit corneal collagen fibrils at the 'a' and 'c' bands. *Biosci Rep* **5**, 765-774

42. Nakano, T., Li, X., Sunwoo, H. H., and Sim, J. S. (1997) Immunohistochemical localization of proteoglycans in bovine skeletal muscle and adipose connective tissues. *Canadian J Animal Sci* **77**, 169-172

43. Scott, J. E. (1996) Proteodermatan and proteokeratan sulfate (decorin, lumican/fibromodulin) proteins are horseshoe shaped. Implications for their interactions with collagen. *Biochemistry* **35**, 8795-8799

44. Weber, I. T., Harrison, R. W., and Iozzo, R. V. (1996) Model structure of decorin and implications for collagen fibrillogenesis. *J Biol Chem* **271**, 31767-31770

45. Svensson, L., Heinegard, D., and Oldberg, A. (1995) Decorin-Binding Sites for Collagen Type-I Are Mainly Located in Leucine-Rich Repeats 4-5. *J Biol Chem* **270**, 20712-20716

46. Vogel, K. G., Koob, T. J., and Fisher, L. W. (1987) Characterization and interactions of a fragment of the core protein of the small proteoglycan (PGII) from bovine tendon. *Biochem Biophys Res Commun* **148**, 658-663

47. Schonherr, E., Witschprehm, P., Harrach, B., Robenek, H., Rauterberg, J., and Kresse, H. (1995) Interaction of Biglycan with Type-I Collagen. *J Biol Chem* **270**, 2776-2783

48. Danielson, K. G., Baribault, H., Holmes, D. F., Graham, H., Kadler, K. E., and Iozzo, R. V. (1997) Targeted disruption of decorin leads to abnormal collagen fibril morphology and skin fragility. *J Cell Biol* **136**, 729-743

49. Corsi, A., Xu, T., Chen, X. D., Boyde, A., Liang, J., Mankani, M., Sommer, B., Iozzo, R. V., Eichstetter, I., Robey, P. G., Bianco, P., and Young, M. F. (2002) Phenotypic effects of biglycan deficiency are linked to collagen fibril abnormalities, are synergized by decorin deficiency, and mimic Ehlers-Danlos-like changes in bone and other connective tissues. *J Bone Miner Res* **17**, 1180-1189

50. Mercado, M. L., Amenta, A. R., Hagiwara, H., Rafii, M. S., Lechner, B. E., Owens, R. T., McQuillan, D. J., Froehner, S. C., and Fallon, J. R. (2006) Biglycan regulates the expression and sarcolemmal localization of dystrobrevin, syntrophin, and nNOS. *FASEB J* **20**, 1724-1726

51. Ameye, L., and Young, M. F. (2002) Mice deficient in small leucine-rich proteoglycans: novel in vivo models for osteoporosis, osteoarthritis, Ehlers-Danlos syndrome, muscular dystrophy, and corneal diseases. *Glycobiology* **12**, 107R-116R

52. Ervasti, J. M., and Campbell, K. P. (1993) A Role for the Dystrophin-Glycoprotein Complex as a Transmembrane Linker between Laminin and Actin. *J Cell Biol* **122**, 809-823

53. von der Mark, H., Durr, J., Sonnenberg, A., von der Mark, K., Deutzmann, R., and Goodman, S. L. (1991) Skeletal myoblasts utilize a novel beta 1-series integrin and not alpha 6 beta 1 for binding to the E8 and T8 fragments of laminin. *J Biol Chem* **266**, 23593-23601

54. Wu, C., Keivens, V. M., O'Toole, T. E., McDonald, J. A., and Ginsberg, M. H. (1995) Integrin activation and cytoskeletal interaction are essential for the assembly of a fibronectin matrix. *Cell* **83**, 715-724

55. Rao, C. N., Margulies, I. M., and Liotta, L. A. (1985) Binding domain for laminin on type IV collagen. *Biochem Biophys Res Commun* **128**, 45-52

56. Charonis, A. S., Tsilibary, E. C., Yurchenco, P. D., and Furthmayr, H. (1985) Binding of laminin to type IV collagen: a morphological study. *J Cell Biol* **100**, 1848-1853

57. Laurie, G. W., Bing, J. T., Kleinman, H. K., Hassell, J. R., Aumailley, M., Martin, G. R., and Feldmann, R. J. (1986) Localization of binding sites for laminin, heparan sulfate proteoglycan and fibronectin on basement membrane (type IV) collagen. *J Mol Biol* **189**, 205-216

58. Mayer, U., Nischt, R., Poschl, E., Mann, K., Fukuda, K., Gerl, M., Yamada, Y., and Timpl, R. (1993) A single EGF-like motif of laminin is responsible for high affinity nidogen binding. *EMBO J* **12**, 1879-1885

59. Fox, J. W., Mayer, U., Nischt, R., Aumailley, M., Reinhardt, D., Wiedemann, H., Mann, K., Timpl, R., Krieg, T., Engel, J., and et al. (1991) Recombinant nidogen consists of three globular domains and mediates binding of laminin to collagen type IV. *EMBO J* **10**, 3137-3146

60. Sanes, J. R. (2003) The basement membrane/basal lamina of skeletal muscle. *J Biol Chem* **278**, 12601-12604

61. Ervasti, J. M. (2003) Costameres: the Achilles' heel of Herculean muscle. *J Biol Chem* **278**, 13591-13594

62. Uaesoontrachoon, K., Yoo, H. J., Tudor, E. M., Pike, R. N., Mackie, E. J., and Pagel, C. N. (2008) Osteopontin and skeletal muscle myoblasts: association with muscle regeneration and regulation of myoblast function in vitro. *Int J Biochem Cell Biol* **40**, 2303-2314

63. Bradshaw, A. D. (2009) The role of SPARC in extracellular matrix assembly. *J Cell Commun Signal* **3**, 239-246

64. Malek, M. H., and Olfert, I. M. (2009) Global deletion of thrombospondin-1 increases cardiac and skeletal muscle capillarity and exercise capacity in mice. *Exp Physiol* **94**, 749-760

65. Chiquet, M., and Fambrough, D. M. (1984) Chick myotendinous antigen. II. A novel extracellular glycoprotein complex consisting of large disulfide-linked subunits. *J Cell Biol* **98**, 1937-1946

66. Cotman, S. L., Halfter, W., and Cole, G. J. (1999) Identification of extracellular matrix ligands for the heparan sulfate proteoglycan agrin. *Exp Cell Res* **249**, 54-64

67. Chung, C. Y., and Erickson, H. P. (1997) Glycosaminoglycans modulate fibronectin matrix assembly and are essential for matrix incorporation of tenascin-C. *J Cell Sci* **110 (Pt 12)**, 1413-1419

68. Cifuentes-Diaz, C., Faille, L., Goudou, D., Schachner, M., Rieger, F., and Angaut-Petit, D. (2002) Abnormal reinnervation of skeletal muscle in a tenascin-C-deficient mouse. *J Neurosci Res* **67**, 93-99

69. Kherif, S., Lafuma, C., Dehaupas, M., Lachkar, S., Fournier, J. G., Verdiere-Sahuque, M., Fardeau, M., and Alameddine, H. S. (1999) Expression of matrix metalloproteinases 2 and 9 in regenerating skeletal muscle: a study in experimentally injured and mdx muscles. *Dev Biol* **205**, 158-170

70. Singh, A., Nelson-Moon, Z. L., Thomas, G. J., Hunt, N. P., and Lewis, M. P. (2000) Identification of matrix metalloproteinases and their tissue inhibitors type 1 and 2 in human masseter muscle. *Arch Oral Biol* **45**, 431-440

71. Wu, N., Jansen, E. D., and Davidson, J. M. (2003) Comparison of mouse matrix metalloproteinase 13 expression in free-electron laser and scalpel incisions during wound healing. *J Invest Dermatol* **121**, 926-932

72. Ohuchi, E., Imai, K., Fujii, Y., Sato, H., Seiki, M., and Okada, Y. (1997) Membrane type 1 matrix metalloproteinase digests interstitial collagens and other extracellular matrix macromolecules. *J Biol Chem* **272**, 2446-2451

73. Chin, J. R., and Werb, Z. (1997) Matrix metalloproteinases regulate morphogenesis, migration and remodeling of epithelium, tongue skeletal muscle and cartilage in the mandibular arch. *Development* **124**, 1519-1530

74. Granzier, H., and Labeit, S. (2007) Structure-function relations of the giant elastic protein titin in striated and smooth muscle cells. *Muscle Nerve* **36**, 740-755

75. Magid, A., and Law, D. J. (1985) Myofibrils bear most of the resting tension in frog skeletal muscle. *Science* **230**, 1280-1282

76. Prado, L. G., Makarenko, I., Andresen, C., Kruger, M., Opitz, C. A., and Linke, W. A. (2005) Isoform diversity of giant proteins in relation to passive and active contractile properties of rabbit skeletal muscles. *J Gen Physiol* **126**, 461-480

77. Ward, S. R., Tomiya, A., Regev, G. J., Thacker, B. E., Benzl, R. C., Kim, C. W., and Lieber, R. L. (2009) Passive mechanical properties of the lumbar multifidus muscle support its role as a stabilizer. *J Biomech* **42**, 1384-1389

78. Lieber, R. L., Runesson, E., Einarsson, F., and Friden, J. (2003) Inferior mechanical properties of spastic muscle bundles due to hypertrophic but compromised extracellular matrix material. *Muscle Nerve* **28**, 464-471

79. Meyer, G. A., and Lieber, R. L. (2011) Elucidation of extracellular matrix mechanics from muscle fibers and fiber bundles. *J Biomech* **44**, 771-773

80. Winters, T. M., Takahashi, M., Lieber, R. L., and Ward, S. R. (2009) Nonlinear scaling of passive tension in skeletal muscle. In *Workshop on Multi-Scale Muscle Mechanics* p. 38, Woods Hole, MA

81. Gillies, A., Smith, L. R., Lieber, R. L., and Varghese, S. (2011) Method for decellularizing skeletal muscle without detergents or proteolytic enzymes. *Tissue Eng Part C Methods* **17**, 383-389

82. Ohtani, O., Ushiki, T., Taguchi, T., and Kikuta, A. (1988) Collagen fibrillar networks as skeletal frameworks: a demonstration by cell-maceration/scanning electron microscope method. *Arch Histol Cytol* **51**, 249-261

83. Schenke-Layland, K., Vasilevski, O., Opitz, F., Konig, K., Riemann, I., Halbhuber, K. J., Wahlers, T., and Stock, U. A. (2003) Impact of decellularization of xenogeneic tissue on extracellular matrix integrity for tissue engineering of heart valves. *J Struct Biol* **143**, 201-208

84. Stern, M. M., Myers, R. L., Hammam, N., Stern, K. A., Eberli, D., Kritchevsky, S. B., Soker, S., and Van Dyke, M. (2009) The influence of extracellular matrix derived from skeletal muscle tissue on the proliferation and differentiation of myogenic progenitor cells ex vivo. *Biomaterials* **30**, 2393-2399

85. Cosgrove, B. D., Sacco, A., Gilbert, P. M., and Blau, H. M. (2009) A home away from home: challenges and opportunities in engineering in vitro muscle satellite cell niches. *Differentiation* **78**, 185-194

86. Péault, B., Rudnicki, M., Torrente, Y., Cossu, G., Tremblay, J. P., Partridge, T., Gussoni, E., Kunkel, L. M., and Huard, J. (2007) Stem and progenitor cells in skeletal muscle development, maintenance, and therapy. *Mol Ther* **15**, 867-877

87. Reist, N. E., Magill, C., and McMahan, U. J. (1987) Agrin-like molecules at synaptic sites in normal, denervated, and damaged skeletal muscles. *J Cell Biol* **105**, 2457-2469

88. Cornbrooks, C. J., Carey, D. J., McDonald, J. A., Timpl, R., and Bunge, R. P. (1983) In vivo and in vitro observations on laminin production by Schwann cells. *Proc Natl Acad Sci U S A* **80**, 3850-3854

89. Bunge, M. B., Williams, A. K., Wood, P. M., Uitto, J., and Jeffrey, J. J. (1980) Comparison of nerve cell and nerve cell plus Schwann cell cultures, with particular emphasis on basal lamina and collagen formation. *J Cell Biol* **84**, 184-202

90. Archile-Contreras, A. C., Mandell, I. B., and Purslow, P. P. (2010) Phenotypic differences in matrix metalloproteinase 2 activity between fibroblasts from three bovine muscles. *J Anim Sci* **88**, 4006-4015

91. Gatchalian, C. L., Schachner, M., and Sanes, J. R. (1989) Fibroblasts that proliferate near denervated synaptic sites in skeletal muscle synthesize the adhesive molecules tenascin(J1), N-CAM, fibronectin, and a heparan sulfate proteoglycan. *J Cell Biol* **108**, 1873-1890

92. Kuhl, U., Ocalan, M., Timpl, R., Mayne, R., Hay, E., and von der Mark, K. (1984) Role of muscle fibroblasts in the deposition of type-IV collagen in the basal lamina of myotubes. *Differentiation* **28**, 164-172

93. Guerin, C. W., and Holland, P. C. (1995) Synthesis and secretion of matrix-degrading metalloproteases by human skeletal muscle satellite cells. *Dev Dyn* **202**, 91-99

94. Beach, R. L., Rao, J. S., and Festoff, B. W. (1985) Extracellular-matrix synthesis by skeletal muscle in culture. Major secreted collagenous proteins of clonal myoblasts. *Biochem J* **225**, 619-627

95. Brandan, E., Fuentes, M. E., and Andrade, W. (1991) The proteoglycan decorin is synthesized and secreted by differentiated myotubes. *Eur J Cell Biol* **55**, 209-216

96. Sasse, J., von der Mark, H., Kuhl, U., Dessau, W., and von der Mark, K. (1981) Origin of collagen types I, III, and V in cultures of avian skeletal muscle. *Dev Biol* **83**, 79-89

97. Kuhl, U., Timpl, R., and von der Mark, K. (1982) Synthesis of type IV collagen and laminin in cultures of skeletal muscle cells and their assembly on the surface of myotubes. *Dev Biol* **93**, 344-354

98. Chiquet, M., Gelman, L., Lutz, R., and Maier, S. (2009) From mechanotransduction to extracellular matrix gene expression in fibroblasts. *Biochim Biophys Acta* **1793**, 911-920

99. Kusner, L. L., Young, A., Tjoe, S., Leahy, P., and Kaminski, H. J. (2010) Perimysial fibroblasts of extraocular muscle, as unique as the muscle fibers. *Invest Ophthalmol Vis Sci* **51**, 192-200

100. Engler, A. J., Sen, S., Sweeney, H. L., and Discher, D. E. (2006) Matrix elasticity directs stem cell lineage specification. *Cell* **126**, 677-689

101. Alexakis, C., Partridge, T., and Bou-Gharios, G. (2007) Implication of the satellite cell in dystrophic muscle fibrosis: a self-perpetuating mechanism of collagen overproduction. *Am J Physiol Cell Physiol* **293**, C661-669

102. Alnaqeeb, M. A., Alzaid, N. S., and Goldspink, G. (1984) Connective tissue changes and physical properties of developing and ageing skeletal muscle. *J Anat* **139**, 677-689

103. Berria, R., Wang, L., Richardson, D. K., Finlayson, J., Belfort, R., Pratipanawatr, T., De Filippis, E. A., Kashyap, S., and Mandarino, L. J. (2006) Increased collagen content in insulin-resistant skeletal muscle. *Am J Physiol Endocrinol Metab* **290**, E560-565

104. Duance, V. C., Stephens, H. R., Dunn, M., Bailey, A. J., and Dubowitz, V. (1980) A role for collagen in the pathogenesis of muscular dystrophy? *Nature* **284**, 470-472

105. Williams, P. E., and Goldspink, G. (1984) Connective tissue changes in immobilised muscle. *J Anat* **138 (Pt 2)**, 343-350

106. Florin, L., Alter, H., Grone, H. J., Szabowski, A., Schutz, G., and Angel, P. (2004) Cre recombinase-mediated gene targeting of mesenchymal cells. *Genesis* **38**, 139-144

107. Fu, Q., Schoenhoff, F. S., Savage, W. J., Zhang, P., and Van Eyk, J. E. (2010) Multiplex assays for biomarker research and clinical application: translational science coming of age. *Proteomics Clin Appl* **4**, 271-284

108. Leask, A., and Abraham, D. J. (2004) TGF-beta signaling and the fibrotic response. *FASEB J* **18**, 816-827

109. Border, W. A., and Noble, N. A. (1994) Transforming growth factor beta in tissue fibrosis. *N Engl J Med* **331**, 1286-1292

110. Fadic, R., Mezzano, V., Alvarez, K., Cabrera, D., Holmgren, J., and Brandan, E. (2006) Increase in decorin and biglycan in Duchenne Muscular Dystrophy: role of fibroblasts as cell source of these proteoglycans in the disease. *J Cell Mol Med* **10**, 758-769

111. Zanotti, S., Negri, T., Cappelletti, C., Bernasconi, P., Canioni, E., Di Blasi, C., Pegoraro, E., Angelini, C., Ciscato, P., Prelle, A., Mantegazza, R., Morandi, L., and Mora, M. (2005) Decorin and biglycan expression is differentially altered in several muscular dystrophies. *Brain* **128**, 2546-2555

112. Zanotti, S., Saredi, S., Ruggieri, A., Fabbri, M., Blasevich, F., Romaggi, S., Morandi, L., and Mora, M. (2007) Altered extracellular matrix transcript expression and protein modulation in primary Duchenne muscular dystrophy myotubes. *Matrix Biol* **26**, 615-624

113. Blalock, T. D., Duncan, M. R., Varela, J. C., Goldstein, M. H., Tuli, S. S., Grotendorst, G. R., and Schultz, G. S. (2003) Connective tissue growth factor expression and action in human corneal fibroblast cultures and rat corneas after photorefractive keratectomy. *Invest Ophthalmol Vis Sci* **44**, 1879-1887

114. Duncan, M. R., Frazier, K. S., Abramson, S., Williams, S., Klapper, H., Huang, X. F., and Grotendorst, G. R. (1999) Connective tissue growth factor mediates transforming growth factor beta-induced collagen synthesis: downregulation by cAMP. *FASEB J* **13**, 1774-1786

115. Maeda, N., Kanda, F., Okuda, S., Ishihara, H., and Chihara, K. (2005) Transforming growth factor-beta enhances connective tissue growth factor expression in L6 rat skeletal myotubes. *Neuromuscul Disord* **15**, 790-793

116. Mezzano, V., Cabrera, D., Vial, C., and Brandan, E. (2007) Constitutively activated dystrophic muscle fibroblasts show a paradoxical response to TGF-beta and CTGF/CCN2. *J Cell Commun Signal* **1**, 205-217

117. Schild, C., and Trueb, B. (2002) Mechanical stress is required for high-level expression of connective tissue growth factor. *Exp Cell Res* **274**, 83-91

118. Kivela, R., Kyrolainen, H., Selanne, H., Komi, P. V., Kainulainen, H., and Vihko, V. (2007) A single bout of exercise with high mechanical loading induces the expression of Cyr61/CCN1 and CTGF/CCN2 in human skeletal muscle. *J Appl Physiol* **103**, 1395-1401

119. Smith, L. R., Lee, K. S., Ward, S. R., Chambers, H. G., and Lieber, R. L. (2011) Hamstring contractures in children with spastic cerebral palsy result from a stiffer ECM and increased in vivo sarcomere length. *J Physiol* **589**, 2625-2639

120. Friden, J., and Lieber, R. L. (2003) Spastic muscle cells are shorter and stiffer than normal cells. *Muscle Nerve* **27**, 157-164

121. Booth, C. M., Cortina-Borja, M. J., and Theologis, T. N. (2001) Collagen accumulation in muscles of children with cerebral palsy and correlation with severity of spasticity. *Dev Med Child Neurol* **43**, 314-320

122. Smith, L. R., Ponten, E., Hedstrom, Y., Ward, S. R., Chambers, H. G., Subramaniam, S., and Lieber, R. L. (2009) Novel transcriptional profile in wrist muscles from cerebral palsy patients. *BMC Med Genomics* **2**, 44

123. Meyer, G. A., McCulloch, A. D., Ward, S. R., and Lieber, R. L. (2010) Intermediate filament and ECM mechanics deduced from desmin knockout muscles. In *Biophysical Society 54th Annual Meeting* Vol. 98 p. 545a, Biophys J, San Francisco, CA

124. Chan, Y. S., Li, Y., Foster, W., Fu, F. H., and Huard, J. (2005) The use of suramin, an antifibrotic agent, to improve muscle recovery after strain injury. *Am J Sports Med* **33**, 43-51

125. Fukushima, K., Badlani, N., Usas, A., Riano, F., Fu, F., and Huard, J. (2001) The use of an antifibrosis agent to improve muscle recovery after laceration. *Am J Sports Med* **29**, 394-402

126. Sato, K., Li, Y., Foster, W., Fukushima, K., Badlani, N., Adachi, N., Usas, A., Fu, F. H., and Huard, J. (2003) Improvement of muscle healing through enhancement of muscle regeneration and prevention of fibrosis. *Muscle Nerve* **28**, 365-372

127. Schenk, S., and Horowitz, J. F. (2007) Acute exercise increases triglyceride synthesis in skeletal muscle and prevents fatty acid-induced insulin resistance. *J Clin Invest* **117**, 1690-1698

128. Leroy-Willig, A., Willig, T. N., Henry-Feugeas, M. C., Frouin, V., Marinier, E., Boulier, A., Barzic, F., Schouman-Claeys, E., and Syrota, A. (1997) Body composition determined with MR in patients with Duchenne muscular dystrophy, spinal muscular atrophy, and normal subjects. *Magn Reson Imaging* **15**, 737-744

129. Goodpaster, B. H., and Wolf, D. (2004) Skeletal muscle lipid accumulation in obesity, insulin resistance, and type 2 diabetes. *Pediatr Diabetes* **5**, 219-226

130. Visser, M., Goodpaster, B. H., Kritchevsky, S. B., Newman, A. B., Nevitt, M., Rubin, S. M., Simonsick, E. M., and Harris, T. B. (2005) Muscle mass, muscle strength, and muscle fat infiltration as predictors of incident mobility limitations in well-functioning older persons. *J Gerontol A Biol Sci Med Sci* **60**, 324-333

131. Goutallier, D., Postel, J. M., Bernageau, J., Lavau, L., and Voisin, M. C. (1994) Fatty muscle degeneration in cuff ruptures. Pre- and postoperative evaluation by CT scan. *Clin Orthop Relat Res* **304**, 78-83

132. Nakagaki, K., Ozaki, J., Tomita, Y., and Tamai, S. (1996) Fatty degeneration in the supraspinatus muscle after rotator cuff tear. *J Shoulder Elbow Surg* **5**, 194-200

133. Danneels, L. A., Vanderstraeten, G. G., Cambier, D. C., Witvrouw, E. E., and De Cuyper, H. J. (2000) CT imaging of trunk muscles in chronic low back pain patients and healthy control subjects. *Eur Spine J* **9**, 266-272

134. Asakura, A., Komaki, M., and Rudnicki, M. (2001) Muscle satellite cells are multipotential stem cells that exhibit myogenic, osteogenic, and adipogenic differentiation. *Differentiation* **68**, 245-253

135. Uezumi, A., Fukada, S., Yamamoto, N., Takeda, S., and Tsuchida, K. (2010) Mesenchymal progenitors distinct from satellite cells contribute to ectopic fat cell formation in skeletal muscle. *Nat Cell Biol* **12**, 143-152

136. Uezumi, A., Ojima, K., Fukada, S., Ikemoto, M., Masuda, S., Miyagoe-Suzuki, Y., and Takeda, S. (2006) Functional heterogeneity of side population cells in skeletal muscle. *Biochem Biophys Res Commun* **341**, 864-873

137. Greco, A. V., Mingrone, G., Giancaterini, A., Manco, M., Morroni, M., Cinti, S., Granzotto, M., Vettor, R., Camastra, S., and Ferrannini, E. (2002) Insulin resistance in morbid obesity: reversal with intramyocellular fat depletion. *Diabetes* **51**, 144-151

Table 2.1: Comparison of single fiber and fiber bundle modulus values from various muscles.

Muscle	Single Fiber Modulus (kPa)	Fiber Bundle Modulus (kPa)	Bundle:Fiber Modulus Ratio	Reference no.
Human Iliocostalis	37.05	58.83	1.59	77
Human Longissimus	32.80	62.85	1.92	77
Human Multifidus	33.71	91.34	2.71	77
Human Upper Extremity	28.2	462.5	16.4	78
Spastic Human Upper Extremity	55	111.15	2.02	78
Mouse Fifth Toe EDL	6.26	40.53	6.48	79
Rabbit Diaphragm	30.14*	57.01*	1.89	76
Rabbit EDL	70.95*	158.47*	2.23	76
	81.31	89.41	1.10	80
Rabbit Gastrocnemius	53.52*	106.53*	1.99	76
Rabbit Psoas	157.11*	91.59*	0.58	76
Rabbit Tibialis Anterior	112.08	127.69	1.14	80
Rabbit EDII	80.52	90.91	1.13	80
Mean ± Standard Deviation	60 ± 41	119 ± 108	3.2 ± 4.2	

Abbreviations: No data (ND), extensor digitorum longus (EDL), extensor digitorum II (EDII)
*Modulus values calculated as the tangent modulus corresponding to a strain of 0.449.

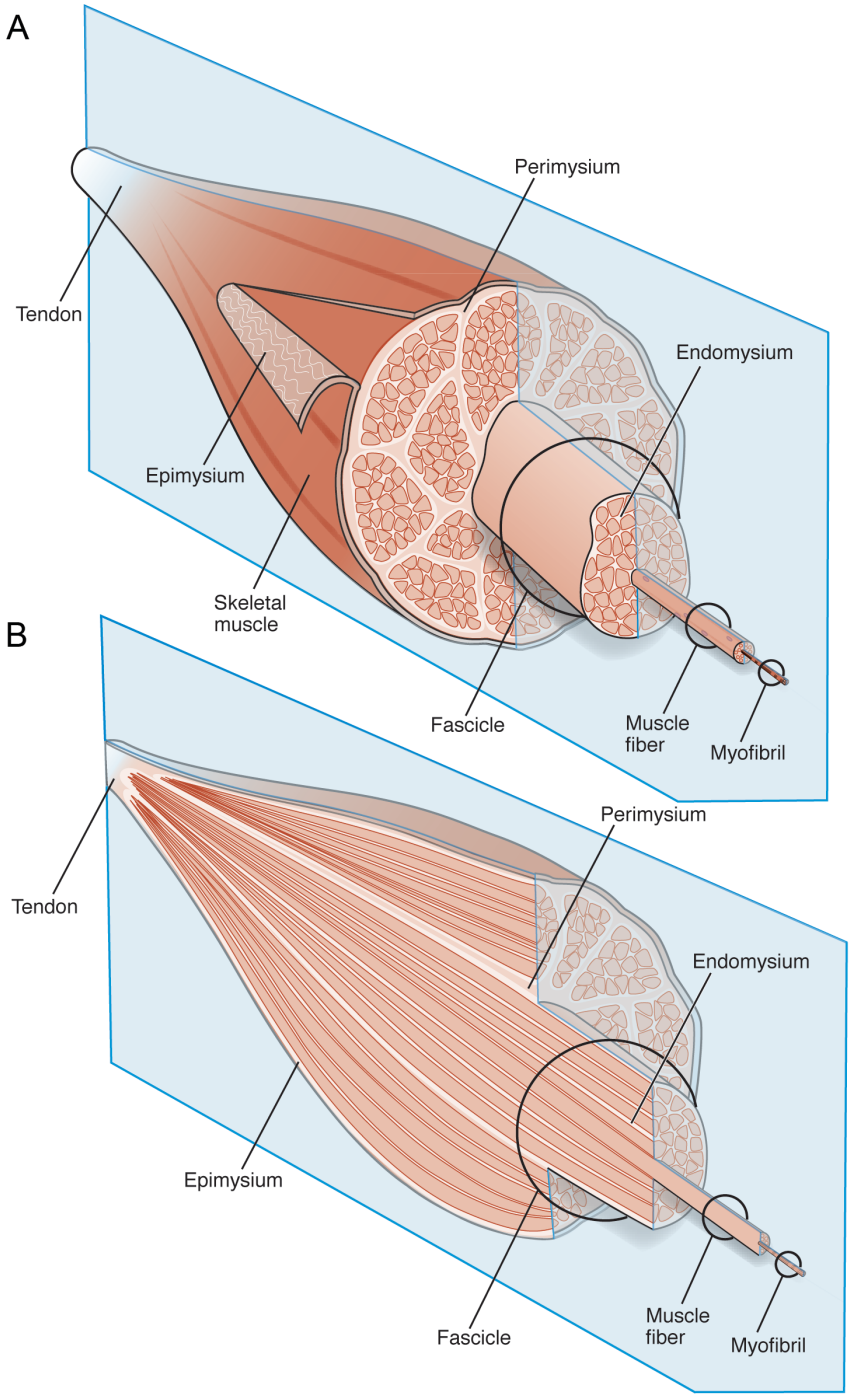

Figure 2.1: Schematic diagram of the gross organization of muscle tissue and muscle ECM-tendon organization. **(A)** Muscle ECM can be categorized as epimysium (surrounding the muscle), perimysium (surrounding muscle fascicles), and endomysium (surrounding muscle fibers). **(B)** Cross-section of muscle tissue indicating that the perimysium may be continuous with the tendon, whereas endomysium is contained within muscle fascicles.

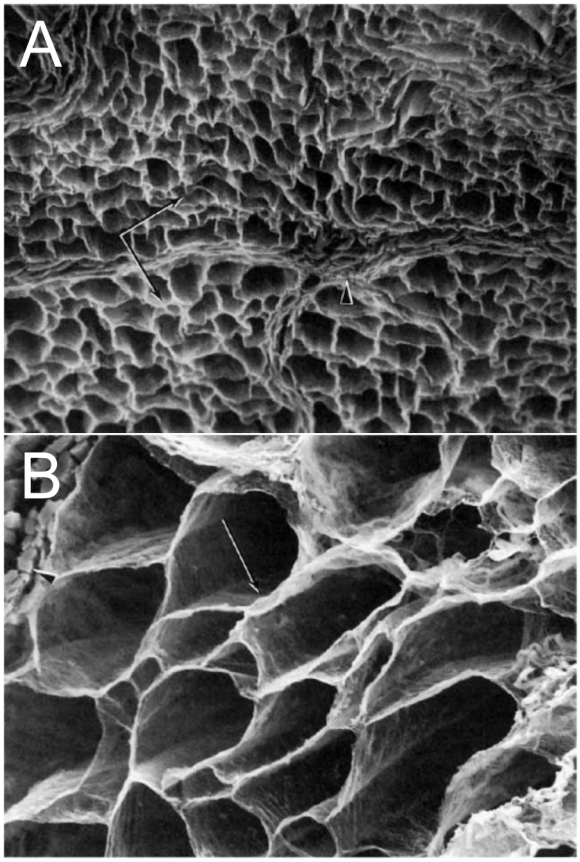

Figure 2.2: Scanning EM of the collagenous endomysial network around muscle fibers observed after digesting fibers with NaOH. **(A)** Low power overview of the endomysium reveals an array of "tubes" into which muscle fibers insert (arrows) as well as a thickened area surrounding the fibers that is presumably perimysium (arrowhead). **(B)** Higher power view of endomysial network revealing the fine structure of the endomysial surfaces (arrow) as well as some undigested muscle fiber (arrowhead). This picture suggests that muscle fibers are embedded in a complex connective tissue matrix and are intimately associated with ECM. Figure from reference (2) used with permission.

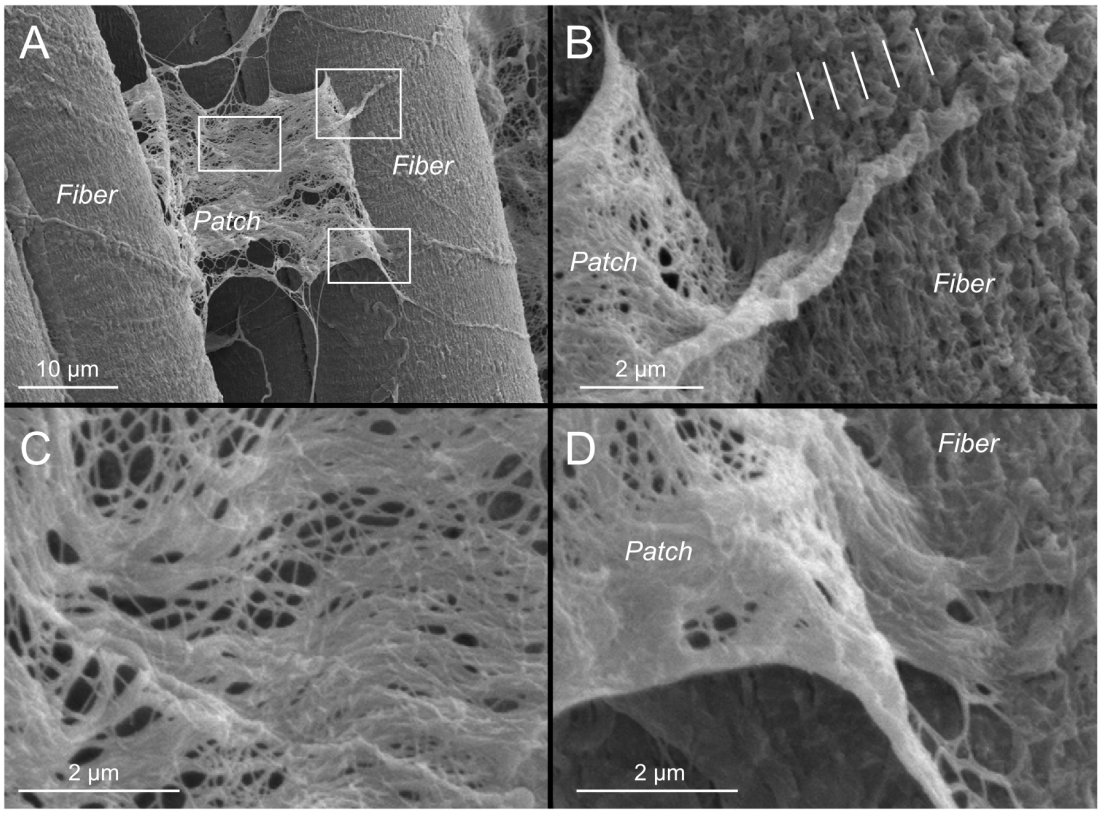

Figure 2.3: Mouse extensor digitorum longus muscles formalin-fixed at resting length, dehydrated in graded ethanol, lyophilized, and observed by SEM (same preparatory method used for Figs 2.4, 2.5, 2.6, and 2.7). **(A)** Patch of ECM pulled away from muscle fibers during sample preparation. Each white rectangle is enlarged in subsequent figure components. **(B)** A regular, longitudinal organization of ECM structures is observable on the fiber surface and its periodicity is noted with lines. **(C)** Central region of the patch of ECM pulled away from muscle fiber surface showing the wavy collagen fiber organization and collagen fibril network. **(D)** Apparent connection between the ECM patch pulled away and the muscle fiber surface. The patch appears to be continuous with the ECM on the fiber surface.

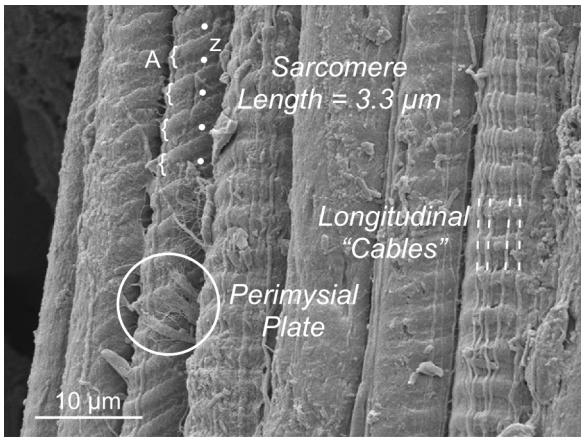

Figure 2.4: Scanning electron micrograph of 7 adjacent muscle fibers. Note that the surface topology varies among the fibers. In 5 cases, surface striations are visible, some of which clearly show A-band (curved brackets) and Z-band periodicity (dots). In 3 fibers, stout longitudinal "cables" extend a distance of at least 100 µm. In one case, a discrete connection is seen on the surface of a fiber that presumably represents the "perimysial plate" (circled) that connects adjacent fibers. Micrograph was obtained from a mouse EDL muscle stretched to a sarcomere length of 3.3 µm.

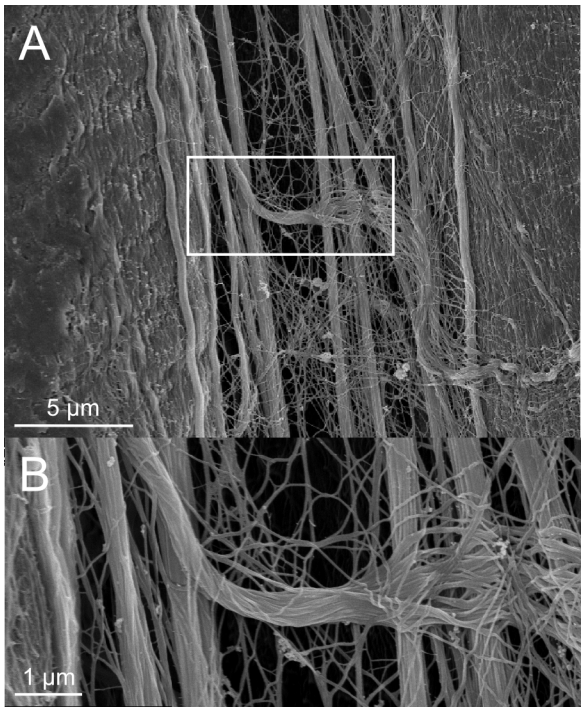

Figure 2.5: Scanning electron micrograph of mouse EDL muscle stretched about 30% beyond resting length showing longitudinally aligned perimysial collagen cables. **(A)** Two muscle fibers separated by stretched collagen cables. The collagen cables are distinct from the muscle fiber surface. **(B)** A collagen cable becomes frayed as it traverses across collagen cables.

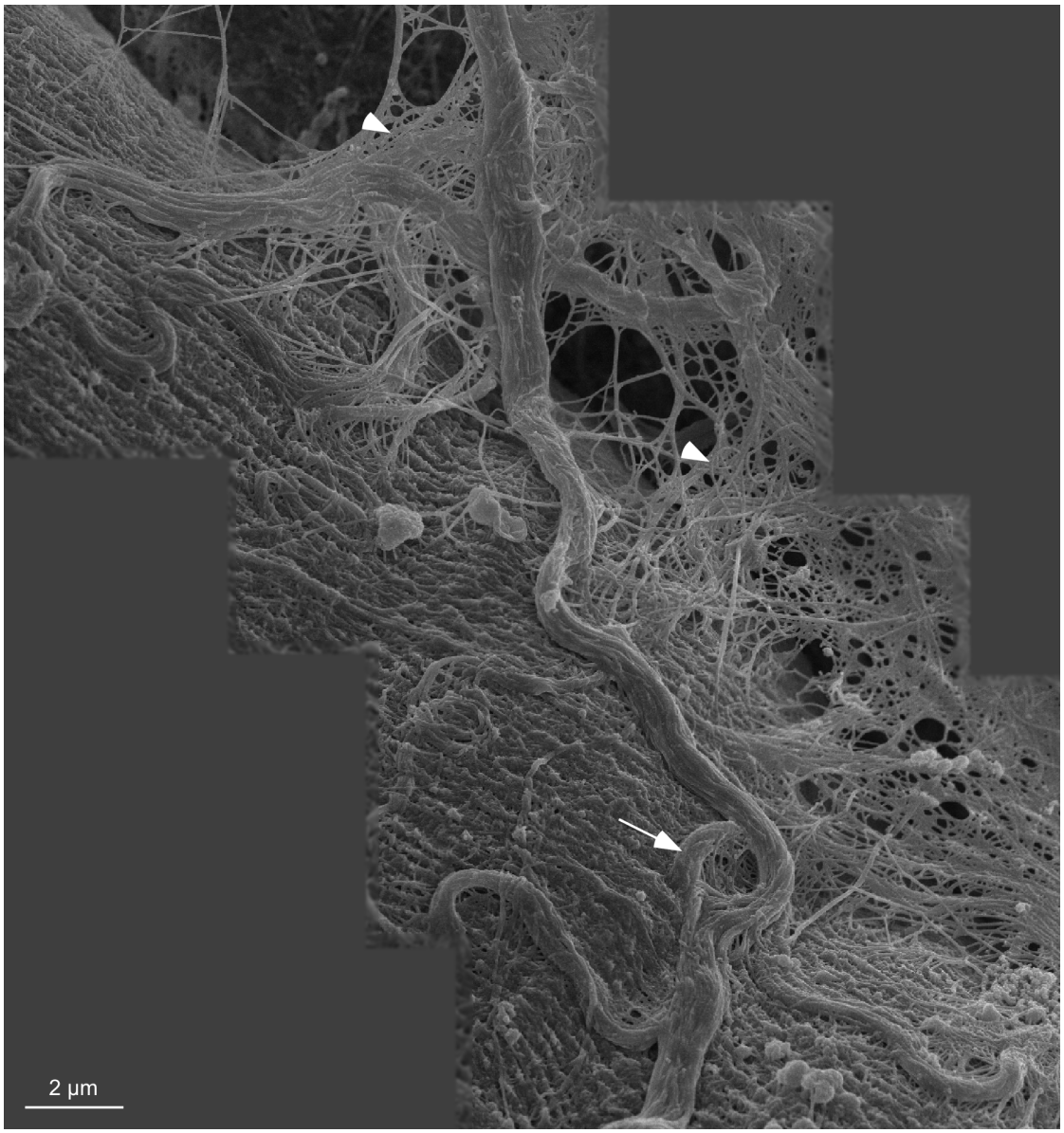

Figure 2.6: Montage of scanning electron micrographs from shortened mouse EDL muscle. Large collagen cables arranged in a slack configuration are visible on the surface of the muscle fiber and integrated with the fiber surface. Coils in the collagen cables may indicate that the cables have a strain relief function (arrow). These large cables are believed to be perimysial in nature while the mesh in the background of the montage (arrow heads) is believed to be endomysial. It is clear that these two levels of ECM are intimately associated.

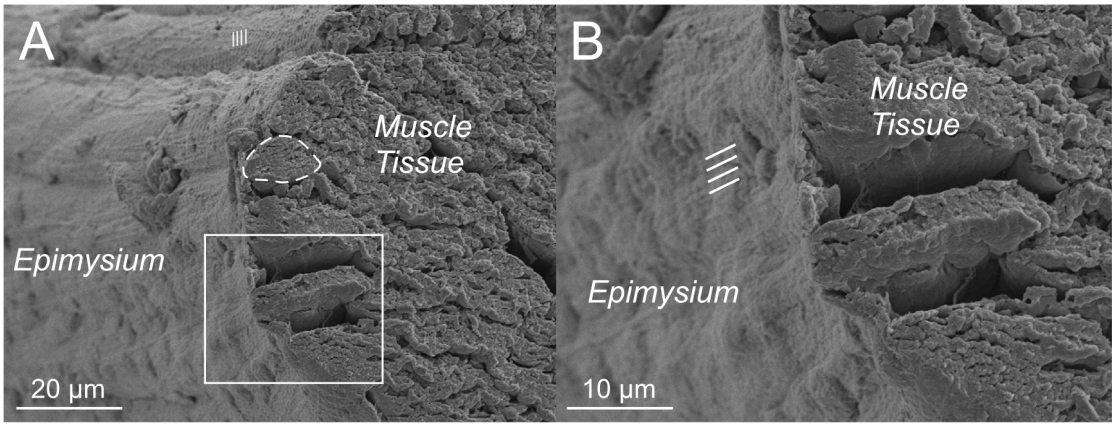

Figure 2.7: Epimysial layer of a mouse EDL muscle viewed in cross-section. A connective tissue sheath is clearly seen surrounding muscle fibers. **(A)** Survey view of the muscle where a region can be observed with sarcomere periodicity through the connective tissue layer. An individual muscle fiber is outlined (dashed line) **(B)** Closer view of the epimysium reveals longitudinal periodicities (lines) with approximately 1 µm of spacing.

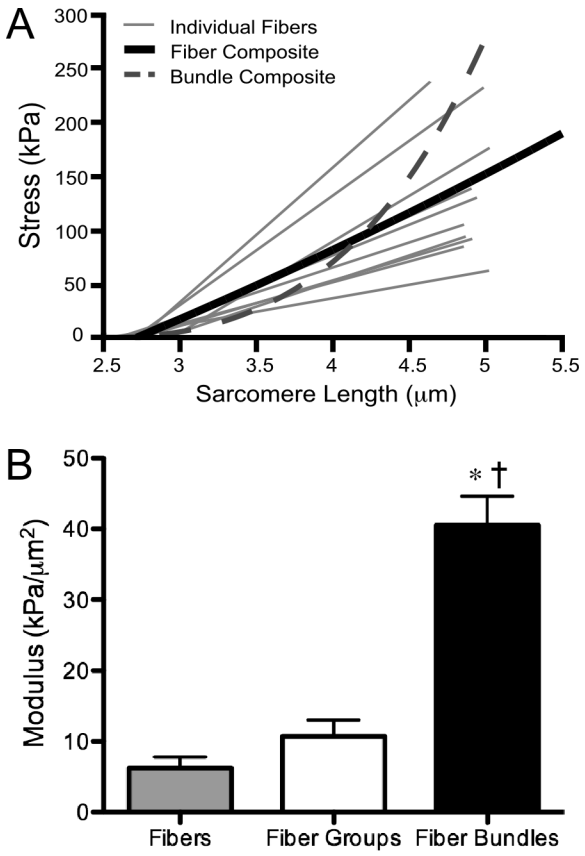

Figure 2.8: Mechanical contribution of the ECM to muscle bundle modulus. **(A)** Individual fibers display linear stress-strain behavior, whereas muscle bundles composed of these fibers and ECM display a nonlinear relationship. **(B)** Fiber groups do not contain ECM (see text), and the modulus value is comparable to that of single fibers. Fiber bundles do contain ECM and have a significantly higher modulus, suggesting that the addition of ECM is responsible for the increased modulus (data replotted from reference (79)). Asterisk indicates $p<0.05$ compared to fibers, dagger indicates $p<0.05$ compared to fiber groups.

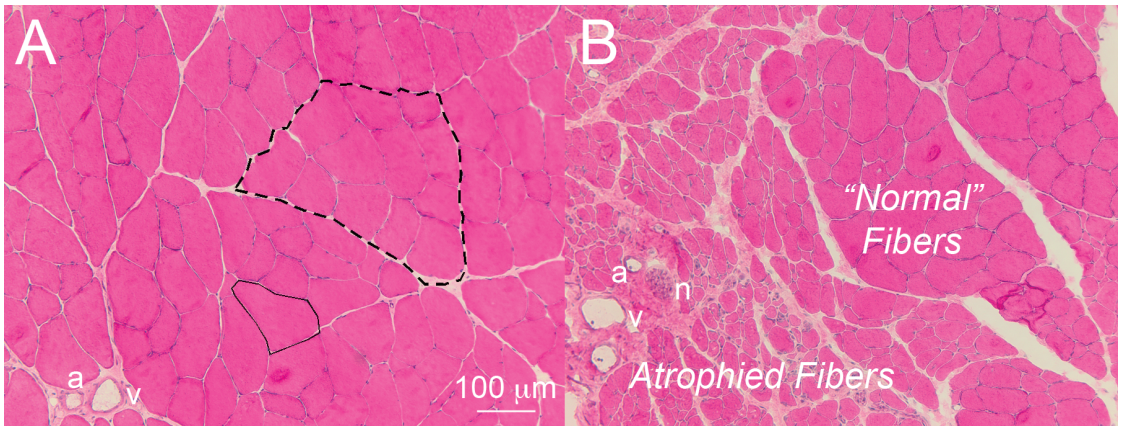

Figure 2.9: Cross-sectional view of normal and neurotoxin-injected rat tibialis anterior muscle stained with hematoxylin and eosin. **(A)** Normal muscle showing endomysium connective tissue (sample outlined in solid line) separating muscle fibers and perimysium (sample outlined in dashed line) separating bundles of muscle fibers (artery, a; vein, v). **(B)** Increased connective tissue around atrophied fibers in neurotoxin -injected muscle (nerve, n). Unaffected regions show normal fiber morphology (image courtesy of Drs. Sam Ward and Viviane Minamoto).

CHAPTER 3

Method for Decellularizing Skeletal Muscle Without Detergents or Proteolytic Enzymes

3.1 Abstract

Decellularized skeletal muscle is a promising model that can be used to study cell-matrix interactions and changes that occur in muscle extracellular matrix (ECM) in myopathies and muscle wasting diseases. The goal of this study was to develop a novel method to decellularize skeletal muscle that maintains the native biochemical composition and structure of the ECM. This method consists of sequential incubation of mouse tibialis anterior muscles in latrunculin B, high ionic strength salt solution, and DNase I and avoids use of proteases or detergents that degrade the ECM. Characterization of the decellularized muscles using hematoxylin and eosin staining along with DNA quantification suggested complete removal of DNA, while biochemical analyses indicated no loss of collagens and only a slight reduction in glycosaminoglycans. Western blot analysis of decellularized tissues showed removal of the vast majority of the contractile proteins actin and myosin, and morphological analysis using scanning electron microscopy suggested removal of myofibers from decellularized muscle tissues. Passive mechanical testing of decellularized muscle bundles revealed the typical non-linear behavior, similar to that of intact muscle.

Together these results suggest that the protocol developed successfully decellularizes skeletal muscle without altering its composition and mechanical function.

3.2 Introduction

Decellularized tissues are useful for a number of biomedical applications such as understanding the physicochemical properties of extracellular matrix (ECM) and providing a tissue specific scaffold for engineering functional tissues. For instance, by harnessing the cell-matrix interactions that are crucial for cell growth and differentiation (1), several studies have promoted tissue formation by combining cells with tissue derived extracellular matrix from decellularized heart, urinary bladder, skeletal muscle, and small intestinal submucosa (2-6). A number of different decellularization methods have been developed (7), but the native biochemical, mechanical, and structural properties of the decellularized ECM are altered depending upon the method used.

This study describes the development of a decellularization method that maintains the mechanical and structural integrity of skeletal muscle connective tissue with minimal disruption to the ECM. Skeletal muscle ECM plays an important role in tissue maintenance and regeneration of skeletal muscle (8), and modulates cell adhesion and migration, growth factor storage and release, and satellite cell activation and differentiation (9-11). The composition, structure, and mechanical properties of skeletal muscle ECM may change with age and various muscle pathologies, and these ECM associated changes could play an important role in determining the success of

therapeutic interventions that rely on multiple biological and biomechanical cues from the ECM.

Previous attempts to decellularize skeletal muscles have incorporated relatively harsh physical methods such as freeze-thawing (12, 13) and detergent and enzymatic treatment with Triton X-100, sodium deoxycholate, sodium dodecyl sulfate (SDS), and trypsin (2, 14-22). These methods inherently result in ECM degradation and/or compromised mechanical and structural properties, which is not desirable for studies that require maintenance of skeletal muscle ECM biochemical and mechanical properties. To this end, we developed a decellularization method that utilizes only osmotic shock and actin and myosin depolymerization, and specifically does not use either proteases or detergents.

3.3 Materials and Methods

Decellularization of muscle tissue

All animal handling and experimental procedures were in accordance with the protocol approved by the UCSD Institutional Animal Care and Use Committee (IACUC) and NIH guidelines for animal welfare. After euthanasia, tibialis anterior (TA) muscles were removed from 2-month-old female C57BL/6 mice (Harlan Sprague Dawley, Indianapolis, IN). Upon removal, TA muscles were incubated in 50nM latrunculin B (Cayman Chemical, Ann Arbor, Michigan) in high glucose Dulbecco's Modified Eagle Medium (DMEM, Gibco, Carlsbad, CA) for 2h at 37°C with agitation. All further steps were performed with agitation at room temperature unless otherwise

stated. Muscle tissues were washed with distilled water twice for 15 min between incubation steps. After incubation in latrunculin B, muscles were incubated in 0.6M potassium chloride (KCl, Fluka Chemicals, Milwaukee, WI) for 2h followed by 1.0M potassium iodide (KI, Fisher Scientific, Waltham, MA) for 2h (23). After the salt solution incubations, muscles were washed in distilled water overnight then the KCl and KI incubations were repeated, followed by incubation in DNase I (1 kU/ml, Sigma, St. Louis, MO) for 2h. Finally, treated muscles were washed in distilled water for a minimum of 2 days with daily water changes to remove remaining reagents. Control muscles were analyzed immediately after harvesting.

For comparative purposes, the decellularization method of Stern *et al.* (21) was performed on intact TA muscles from 2-month-old female C57BL/6 mice for comparison. Briefly, the following steps were performed at 4°C with continuous agitation: ultrapure water for 2 days, 1 hr in 0.05% trypsin with EDTA (Mediatech, Manassas, VA), neutralized in DMEM with 10% fetal bovine serum (Gemini Bio-Products, West Sacramento, CA) overnight, 5 days of exposure to 1% Triton X-100 (Sigma), rinsed in ultrapure water for 2 days, and rinsed in phosphate buffered saline for 1 day. Biochemical assays for DNA, glycosaminoglycan, and collagen quantification were performed on these tissues. Note that this method was originally optimized for slices of muscle tissue (<500 μm). Here, we have performed this method on intact muscle tissues in order to make a valid direct comparison.

DNA quantification

Total DNA from lyophilized and papain-digested (4 μg/mg tissue, Worthington Biochemical, Lakewood, NJ) muscles (16-18h at 65°C) was quantified using the fluorescent Quant-iT Picogreen reagent (Life Technologies, Carlsbad, CA) according to the manufacturer's instructions. Fluorescence was measured using a Beckman Coulter DTX 880 Multimode Detector (excitation: 480nm, emission: 520nm) and values were compared to a lambda DNA standard.

Sulfated glycosaminoglycan (GAG) content

Sulfated GAG content of the samples was quantified using the dimethylmethylene blue dye assay (DMMB, Sigma) (24). Muscles were lyophilized and papain-digested followed by incubation with DMMB dye. Absorbance of the samples at 525nm was measured with a Beckman Coulter DU730 UV/Vis Spectrophotometer using chondroitin sulfate (Sigma) as the standard.

Collagen content

The proximal half of TA muscles were hydrolyzed in 6N HCl for 18h at 115°C. Hydroxyproline content was then measured after reaction with chloramine T (EMD Chemicals, Gibbstown, NJ) and p-dimethylaminobenzaldehyde (Fluka Chemicals) (25). Absorbance of the samples was measured at 550nm using a Bio-Tek Synergy HT1 microplate reader and values were compared to a L-4-hydroxyproline (Fluka Chemicals) standard. Collagen content was calculated using a 1:7.46 hydroxyproline:collagen ratio (26).

Histology and immunohistochemistry

Muscles were allowed to equilibrate in 1:1 phosphate buffered saline (PBS):optimal cutting temperature compound (OCT, Sakura Finetek, Torrance, CA) for 30 min before being frozen in OCT in liquid nitrogen cooled isopentane. Embedded muscles were cryosectioned at 10μm thickness perpendicular to the fiber direction as evidenced by tightly packed polygonal fibers with no preferred long axis. Hematoxylin and eosin staining (H&E, Statlab Medical Products, McKinney, TX) was performed and sections were mounted with Permount mounting medium (Fisher Scientific). Sections for immunohistochemistry were permeabilized in 3% bovine serum albumin (BSA, Sigma) and 0.5% Triton X-100 (Fisher Scientific) in PBS for 30 min and incubated in primary antibody (Pax7 diluted 1:250; Developmental Studies Hybridoma Bank, Iowa City, IA) for 1h. The secondary antibody (Alexa Fluor 568 goat anti-mouse IgG diluted 1:250; Life Technologies) was applied for 1h and slides were coverslipped in mounting medium containing 4',6-diamidino-2-phenylindole (DAPI, Vector Laboratories, Burlingame, CA). Slides were viewed using a Zeiss Axio Observer A1 fluorescence microscope and images were recorded using AxioView software.

SDS-PAGE and Western blot analysis

Muscles were homogenized in the presence of protease and phosphatase inhibitors. Total protein content was measured using the Bradford dye-binding method. Equal amounts of protein from each sample were loaded into wells of 4-15% gradient polyacrylamide gels (Bio-Rad, Hercules, CA). Proteins were transferred to

PVDF membranes that were blocked in tris buffered saline with 0.1% Tween-20 (TBST) and 5% nonfat dry milk for 1h at room temperature. The primary antibody [actin (JLA20) diluted 1:1,000 or myosin (A4.1519) diluted 1:20,000; Developmental Studies Hybridoma Bank] was applied for 1h at room temperature. Membranes were washed and incubated with the secondary antibody (goat anti-mouse IgG horseradish peroxidase-conjugated diluted 1:10,000; Santa Cruz Biotechnology, Santa Cruz, CA) for 30 min at room temperature. Membranes were washed followed by incubation with chemiluminescent substrate (ECL Plus, GE Healthcare, Waukesha, WI) and imaged using a Storm Imager 840. Precision Plus Protein Standard (Bio-Rad) was used for molecular weight indication.

Scanning electron microscopy (SEM) analysis

Muscles were lightly fixed in 4% paraformaldehyde for 45 min at room temperature and subsequently dehydrated in graded ethanol. Muscles were then snap frozen in liquid nitrogen and broken transversely to the fiber direction into 3 slices (approximately 2mm thickness) and lyophilized. Lyophilized muscle slices were sputter coated with chromium using an Emitech K575X Sputter Coater and observed using a Philips XL30 Environmental Scanning Electron Microscope.

Passive mechanics testing on decellularized muscles

Tissue was placed in a relaxing solution composed of (mmol/L) ethylene–glycol tetraacetic acid (EGTA; 7.5), potassium propionate (170), magnesium acetate (2), imidazole (5), creatine phosphate (10), adenosine triphosphate (ATP; 4),

leupeptin, a protease inhibitor, 17 mg/ml; and E64 (a protease inhibitor) 4 mg/ml (27). This relaxing solution has been shown to prevent proteolytic degradation and has therefore been used for mechanical characterization of intact muscle tissues (28). Small bundles of approximately 20 endomysial sheaths were dissected free from the tissue for mechanical testing.

Dissected bundles were secured on either side to 125 μm titanium wires using 10-0 silk suture loops. One wire was secured to an ultrasensitive force transducer (Model 405A, sensitivity 10 V/g, Aurora Scientific, Ontario, Canada) and the other was secured to a servomotor (Model 318B, Aurora Scientific, Ontario, Canada) on a micromanipulator as previously described for muscle fibers (28). Bundle length was set to the minimum length that produced measurable forces. Baseline sample diameters were measured optically with a cross-hair reticule mounted on a dissecting microscope and micromanipulators on an x–y mobile stage. Force–strain data were generated for each mounted bundle in approximately 10% strain increments with force recorded for 3-min to allow stress-relaxation. Bundles were elongated to approximately 100% strain. Force data were converted to stress by dividing force by the baseline cross-sectional area. Data were fit to a viscoelastic model that contained a spring in parallel with a series of a spring and dashpot. Relaxed stress was fit with a strain dependent parallel spring creating a quadratic stress-strain equation. Quadratic curve fits were averaged for untreated and decellularized samples and plotted at 10% strain increments.

Culture of C2C12 cells on decellularized muscles

To evaluate cytocompatibility of the decellularized muscles, C2C12 cells were cultured on decellularized tissues. C2C12 cells (4×10^5 cells in 40 µl culture medium) were pipetted onto intact decellularized muscles in low adhesion petri dishes. The seeded muscles were maintained at 37°C for 30 min prior to adding medium to allow adhesion of cells onto the decellularized tissues. Growth medium (DMEM, Gibco; 10% fetal bovine serum, Atlanta Biologicals, Atlanta, GA; 2 mM L-glutamine, Gibco; 1% penicillin/streptomycin, Gibco) was then added and cell seeded muscles were maintained at 37°C and 5% CO2 for 4 days. The C2C12-seeded muscles were then fixed in 4% paraformaldehyde for 1.5h, embedded in OCT, frozen, and cryosectioned at 10µm. Sections were mounted with DAPI and viewed as described above.

Statistical analysis

Biochemical data were obtained from four animals with one TA muscle from each animal being decellularized and the remaining TA muscle serving as the untreated control, and from three animals for TA muscles decellularized using the Stern *et al.* method (21). Experiments involving mechanical testing were performed on untreated (n = 9) and decellularized (n = 8) TA bundles. Data were calculated as mean ± standard error (SE) and significance was determined by performing one-way ANOVA with Tukey-Kramer multiple comparison post tests or 2-tailed Student's T tests (Prism 5, GraphPad Software, La Jolla, CA).

3.4 Results

Removal of cellular components

DNA content was significantly reduced from 2.92 ± 0.14 μg/mg dry weight in untreated muscle to 0.12 ± 0.01 μg/mg dry weight in decellularized muscle ($p<0.001$). Cell nuclei were absent in decellularized muscles stained with H & E compared to untreated muscle (Fig. 3.1). Similar findings were observed with DAPI and Pax7 staining, where the latter is a marker for satellite cells (data not shown). Evidence for removal of sarcomeric components was based on actin and myosin protein analysis. Western blotting for actin revealed bands at 43, 35, and 30 kDa with the 43 kDa band corresponding to full size actin (Fig. 3.2A). The amount of intact actin in decellularized muscles was greatly decreased compared to that of untreated muscles. Western blotting for myosin detected no full size myosin (200 kDa) in decellularized muscles, but several bands corresponding to low molecular weight fragments (<50 kDa size) were observed, which indicates degradation of myosin (Fig. 3.2B).

Decellularized muscle composition and structure

Major ECM components were quantified to determine the effect of decellularization on the biochemical composition of the ECM. Total GAG content was decreased from 4.93 ± 0.18 μg/mg dry weight in untreated muscles to 2.93 ± 0.18 μg/mg dry weight in decellularized muscles ($p<0.001$). Collagen content remained constant between the untreated and decellularized muscles (3.01 ± 0.11 and 3.49 ± 0.24 μg/mg wet weight respectively; $p=0.10$). We next examined the structure of the muscles to ensure that the decellularization process did not alter the gross structure of the ECM. SEM images obtained from untreated and decellularized muscles showed

that, unlike untreated muscles, decellularized muscles showed a hollow, tubular structure (Fig. 3.3). This observation implied that fibers were still present in the untreated muscle, but had been removed from the decellularized muscle.

Mechanical properties of decellularized muscle

Passive mechanical testing of untreated and decellularized muscle bundles yielded the non-linear stress-strain behavior as reported previously for muscle fiber bundles (Fig. 3.4) (29). Relaxed stress values were not significantly different between untreated and decellularized samples at any strain ranging from 10-100% strain ($p=0.06$-0.56). Similarly, the tangent modulus value at 100% strain was not significantly different between untreated and decellularized samples (308 ± 51.1 kPa and 218 ± 24.5 kPa respectively, $p=0.14$).

Decellularized muscles support cell survival

The C2C12 cells cultured on decellularized muscles were viable after four days in culture as evidenced by positive DAPI staining (Fig. 3.5). Cells were seeded on the surface of the muscle and, while the majority of cells remained on the surface of the muscle, some cells had begun to migrate into the decellularized tissue after four days.

Comparison with an existing decellularization method

Finally, we compared the decellularization method described in this manuscript to the existing method of Stern *et al.* (21). When performed on whole muscles, the latter method was unable to remove the nuclear components completely as

characterized by the DNA content. Specifically, the Stern *et al.* method resulted in a DNA content of 1.71 ± 0.17 μg/mg dry weight compared to 0.12 ± 0.01 μg/mg dry weight for our method ($p<0.001$ compared to our method and untreated).

We also compared the biochemical composition of the decellularized tissues. A significant reduction in the GAG content of the decellularized tissues was found using the Stern *et al.* method where the GAG content decreased from 4.93 ± 0.18 μg/mg dry weight in untreated muscles to 1.23 ± 0.04 μg/mg dry weight ($p<0.001$; $p<0.001$ compared to our method). This corresponds to a 75% of reduction in GAG compared to a 40% reduction observed with our method. In contrast to GAG, the collagen content remained relatively constant between the untreated and decellularized muscles for both methods (3.80 ± 0.14 μg/mg wet weight for Stern et al.; $p<0.05$ compared to untreated).

3.5 Discussion

The present study describes a decellularization method for intact skeletal muscle without the use of detergents or proteolytic enzymes. The method utilized actin disruption by treatment with latrunculin B, cell lysis by osmotic shock, myosin depolymerization by exposure to high ionic strength salt solution, and DNase I treatment to remove residual DNA from skeletal muscle. This method successfully removed muscle fibers and degraded sarcomeric components in the muscle tissue without altering the ECM structure or mechanical properties.

Since DNA quantification indicated the presence of a small amount of DNA in the decellularized tissue, tissue sections were stained for satellite cells that may be more resistant to the decellularization protocol. Negative Pax7 (satellite cells) and DAPI staining indicated that any DNA remaining in the decellularized muscles was degraded and not contained within intact cell nuclei.

An approximately 40% reduction in the GAG content of the decellularized tissue was observed, which could be due to removal of GAGs associated with the cell membrane; almost 30% of GAGs are associated with the cell membrane (30), and these GAGs may have been removed with the sarcolemma during the decellularization process. Decellularization methods using trypsin and Triton X-100 remove GAGs from skeletal muscle (21), but this effect appears to be tissue dependent since the use of trypsin and/or Triton X-100 on other tissues has yielded disparate results (31-33). Collagen content was unchanged in decellularized muscle showing that this method did not remove the most abundant ECM structural component. Together, these results provide evidence that the decellularization method described here is minimally disruptive to native ECM. Furthermore, comparison with the method of Stern *et al.* showed that our decellularization method was more efficient at removing DNA and retaining GAGs in intact muscle compared to a method that uses a proteolytic enzyme (trypsin) and a detergent (Triton X-100) (21).

SEM images from decellularized muscles (Fig. 3.3) suggested that muscle fibers were removed from the tissue, but that the overall architecture of the ECM was maintained when compared with the untreated tissue. SEM images of skeletal muscle endomysium obtained by Trotter and Purslow show a thinner, more fibrous matrix

than we obtained in this study (34, 35). The differences in the endomysial thickness could be attributed to the different sample preparation methods. Totter et al. treated muscles with NaOH, which removed the sarcolemma, basement membrane, and any GAGs associated with the endomysium, leaving only collagen fibrils within the ECM (35). The thicker ECM observed in our decellularized tissues is likely due to the presence of GAGs and the basement membrane.

Mechanical analysis of the decellularized muscles confirmed the mechanical integrity of the decellularized tissue since no difference was observed between the untreated and decellularized muscle bundle stress-strain relationship (Fig. 3.4). These results provide support for the concept that the ECM is the primary passive load bearing structure in skeletal muscle, not the fibers themselves. This result must be tempered by the fact that there was no unambiguous reference length available for determination of the stress-strain relation for decellularized muscle bundles. However, future studies can potentially overcome this limitation by referencing strain to sarcomere length before decellularization or by measuring the relationship between collagen crimp pattern and tissue strain.

The ability of the decellularized muscles to support adhesion and survival of C2C12 cells indicates their cytocompatibility, which is in agreement with other studies (2, 3, 21). The use of decellularized muscle has clinical applications in repair of severe skeletal muscle injuries where the muscles cannot undergo complete regeneration. Detergent-decellularized muscle has been used as a scaffold to repair muscle defects in animal models (2, 3, 18), however, complete functional regeneration has not yet been shown. Biochemical and mechanical signals of the ECM play a key role in the

activation of muscle progenitor cells and their differentiation (9, 21, 36), and thus the use of muscle ECM that contains these signals may be more effective at achieving functional regeneration of impaired muscles. This decellularization method may be used to study the changes that occur in muscle ECM with various myopathies and may serve as a diagnostic tool by identifying characteristic patterns in muscle ECM composition or architecture. In addition, tissues decellularized by this method may be used to measure directly the passive mechanical properties of skeletal muscle ECM. Since the decellularization method described here relies on diffusion of reagents into the tissue, extending this protocol to other tissues may require optimization depending upon the size and composition of the targeted tissue. The development of this method is a first step toward understanding not only the biochemical cues that exist within skeletal muscle ECM, but also the structural and mechanical signals for tissue maintenance.

3.6 Acknowledgements

I would like to acknowledge my co-authors from Chapter 3, which is a reprint of the material as it appears in Tissue Engineering Part C Methods, 2011, Gillies AR, Smith LR, Lieber RL, Varghese S. No authors had competing interests regarding the publication of this research. ARG carried out tissue decellularization, biochemical analyses, SEM analysis, cell viability assay, and drafted the manuscript. LRS carried out tissue mechanical testing. RLL provided expertise on skeletal muscle mechanics

and critical review of the manuscript. SV conceived of the study, participated in its design and coordination, and supervised writing of the manuscript.

The authors thank Dr. Ramsés Ayala, Dr. Chien-Wen Chang, Phil Kyriakakis, Gretchen Meyer, YongSung Hwang, Evie Lin, Ryan Anderson, and Soo Yeon Kim for discussion and technical support. The Pax7 monoclonal antibody developed by Atsushi Kawakami, actin monoclonal antibody developed by Jim Jung-Ching Lin, and myosin monoclonal antibody developed by Helen M. Blau were obtained from the Developmental Studies Hybridoma Bank developed under the auspices of the NICHD and maintained by The University of Iowa, Department of Biology, Iowa City, IA 52242. This work was supported by California Institute of Regenerative Medicine grant (#RN2-00945-1), NIH Grants AR057393 and R01AR057393, and a National Science Foundation Graduate Research Fellowship (A.R.G.).

3.7 References

1. Juliano, R. L., and Haskill, S. (1993) Signal transduction from the extracellular matrix. *J Cell Biol* **120**, 577-585

2. Conconi, M. T., De Coppi, P., Bellini, S., Zara, G., Sabatti, M., Marzaro, M., Zanon, G. F., Gamba, P. G., Parnigotto, P. P., and Nussdorfer, G. G. (2005) Homologous muscle acellular matrix seeded with autologous myoblasts as a tissue-engineering approach to abdominal wall-defect repair. *Biomaterials* **26**, 2567-2574

3. De Coppi, P., Bellini, S., Conconi, M. T., Sabatti, M., Simonato, E., Gamba, P. G., Nussdorfer, G. G., and Parnigotto, P. P. (2006) Myoblast-acellular skeletal muscle matrix constructs guarantee a long-term repair of experimental full-thickness abdominal wall defects. *Tissue Eng* **12**, 1929-1936

4. Ott, H. C., Matthiesen, T. S., Goh, S. K., Black, L. D., Kren, S. M., Netoff, T. I., and Taylor, D. A. (2008) Perfusion-decellularized matrix: using nature's platform to engineer a bioartificial heart. *Nat Med* **14**, 213-221

5. Yoo, J. J., Meng, J., Oberpenning, F., and Atala, A. (1998) Bladder augmentation using allogenic bladder submucosa seeded with cells. *Urology* **51**, 221-225

6. Zhang, Y., Kropp, B. P., Lin, H. K., Cowan, R., and Cheng, E. Y. (2004) Bladder regeneration with cell-seeded small intestinal submucosa. *Tissue Eng* **10**, 181-187

7. Gilbert, T. W., Sellaro, T. L., and Badylak, S. F. (2006) Decellularization of tissues and organs. *Biomaterials* **27**, 3675-3683

8. Grounds, M. D. (1991) Towards understanding skeletal muscle regeneration. *Path Res Pract* **187**, 1-22

9. Cornelison, D. D., Filla, M. S., Stanley, H. M., Rapraeger, A. C., and Olwin, B. B. (2001) Syndecan-3 and syndecan-4 specifically mark skeletal muscle satellite cells and are implicated in satellite cell maintenance and muscle regeneration. *Dev Biol* **239**, 79-94

10. Crawley, S., Farrell, E. M., Wang, W., Gu, M., Huang, H. Y., Huynh, V., Hodges, B. L., Cooper, D. N., and Kaufman, S. J. (1997) The alpha7beta1 integrin mediates adhesion and migration of skeletal myoblasts on laminin. *Exp Cell Res* **235**, 274-286

11. Flaumenhaft, R., Moscatelli, D., Saksela, O., and Rifkin, D. B. (1989) Role of extracellular matrix in the action of basic fibroblast growth factor: matrix as a source of growth factor for long-term stimulation of plasminogen activator production and DNA synthesis. *J Cell Physiol* **140**, 75-81

12. Di Benedetto, G., Zura, G., Mazzucchelli, R., Santinelli, A., Scarpelli, M., and Bertani, A. (1998) Nerve regeneration through a combined autologous conduit (vein plus acellular muscle grafts). *Biomaterials* **19**, 173-181

13. Ide, C. (1984) Nerve regeneration through the basal lamina scaffold of the skeletal muscle. *Neurosci Res* **1**, 379-391

14. Borschel, G. H., Dennis, R. G., and Kuzon, W. M., Jr. (2004) Contractile skeletal muscle tissue-engineered on an acellular scaffold. *Plast Reconstr Surg* **113**, 595-602; discussion 603-594

15. Fawcett, J. W., and Keynes, R. J. (1986) Muscle basal lamina: a new graft material for peripheral nerve repair. *J Neurosurg* **65**, 354-363

16. Gamba, P. G., Conconi, M. T., Lo Piccolo, R., Zara, G., Spinazzi, R., and Parnigotto, P. P. (2002) Experimental abdominal wall defect repaired with acellular matrix. *Pediatr Surg Int* **18**, 327-331

17. Liu, X. L., Arai, T., Sondell, M., Lundborg, G., Kanje, M., and Dahlin, L. B. (2001) Use of chemically extracted muscle grafts to repair extended nerve defects in rats. *Scand J Plast Reconstr Surg Hand Surg* **35**, 337-345

18. Merritt, E. K., Hammers, D. W., Tierney, M., Suggs, L. J., Walters, T. J., and Farrar, R. P. (2010) Functional assessment of skeletal muscle regeneration utilizing homologous extracellular matrix as scaffolding. *Tissue Eng Part A* **16**, 1395-1405

19. Mligiliche, N., Tabata, Y., Endoh, K., and Ide, C. (2001) Peripheral nerve regeneration through a long detergent-denatured muscle autografts in rabbits. *Neuroreport* **12**, 1719-1722

20. Qing, Q., and Qin, T. (2009) Optimal method for rat skeletal muscle decellularization. *Chinese J Reparative Reconstr Surg* **23**, 836-839

21. Stern, M. M., Myers, R. L., Hammam, N., Stern, K. A., Eberli, D., Kritchevsky, S. B., Soker, S., and Van Dyke, M. (2009) The influence of extracellular matrix derived from skeletal muscle tissue on the proliferation and differentiation of myogenic progenitor cells ex vivo. *Biomaterials* **30**, 2393-2399

22. Zhang, Y., He, Y., Bharadwaj, S., Hammam, N., Carnagey, K., Myers, R., Atala, A., and Van Dyke, M. (2009) Tissue-specific extracellular matrix coatings for the promotion of cell proliferation and maintenance of cell phenotype. *Biomaterials* **30**, 4021-4028

23. Granzier, H. L., and Irving, T. C. (1995) Passive tension in cardiac muscle: contribution of collagen, titin, microtubules, and intermediate filaments. *Biophys J* **68**, 1027-1044

24. Farndale, R. W., Buttle, D. J., and Barrett, A. J. (1986) Improved quantitation and discrimination of sulphated glycosaminoglycans by use of dimethylmethylene blue. *Biochim Biophys Acta* **883**, 173-177

25. Stegemann, H., and Stalder, K. (1967) Determination of hydroxyproline. *Clin Chim Acta* **18**, 267-273

26. Neuman, R. E., and Logan, M. A. (1950) The determination of collagen and elastin in tissues. *J Biol Chem* **186**, 549-556

27. Wood, D. S., Zollman, J., Reuben, J. P., and Brandt, P. W. (1975) Human skeletal muscle: properties of the "chemically skinned" fiber. *Science* **187**, 1075-1076

28. Friden, J., and Lieber, R. L. (2003) Spastic muscle cells are shorter and stiffer than normal cells. *Muscle Nerve* **27**, 157-164

29. Lieber, R. L., Runesson, E., Einarsson, F., and Friden, J. (2003) Inferior mechanical properties of spastic muscle bundles due to hypertrophic but compromised extracellular matrix material. *Muscle Nerve* **28**, 464-471

30. Mertens, G., Cassiman, J. J., Van den Berghe, H., Vermylen, J., and David, G. (1992) Cell surface heparan sulfate proteoglycans from human vascular endothelial cells. Core protein characterization and antithrombin III binding properties. *J Biol Chem* **267**, 20435-20443

31. Gratzer, P. F., Harrison, R. D., and Woods, T. (2006) Matrix alteration and not residual sodium dodecyl sulfate cytotoxicity affects the cellular repopulation of a decellularized matrix. *Tissue Eng* **12**, 2975-2983

32. Wainwright, J. M., Czajka, C. A., Patel, U. B., Freytes, D. O., Tobita, K., Gilbert, T. W., and Badylak, S. F. (2010) Preparation of cardiac extracellular matrix from an intact porcine heart. *Tissue Eng Part C Methods* **16**, 525-532

33. Yang, B., Zhang, Y., Zhou, L., Sun, Z., Zheng, J., Chen, Y., and Dai, Y. (2010) Development of a porcine bladder acellular matrix with well-preserved extracellular bioactive factors for tissue engineering. *Tissue Eng Part C Methods* **16**, 1201-1211

34. Purslow, P. P., and Trotter, J. A. (1994) The morphology and mechanical properties of endomysium in series-fibred muscles: variations with muscle length. *J Muscle Res Cell Motil* **15**, 299-308

35. Trotter, J. A., and Purslow, P. P. (1992) Functional morphology of the endomysium in series fibered muscles. *J Morphol* **212**, 109-122

36. Engler, A. J., Griffin, M. A., Sen, S., Bonnemann, C. G., Sweeney, H. L., and Discher, D. E. (2004) Myotubes differentiate optimally on substrates with tissue-like stiffness: pathological implications for soft or stiff microenvironments. *J Cell Biol* **166**, 877-887

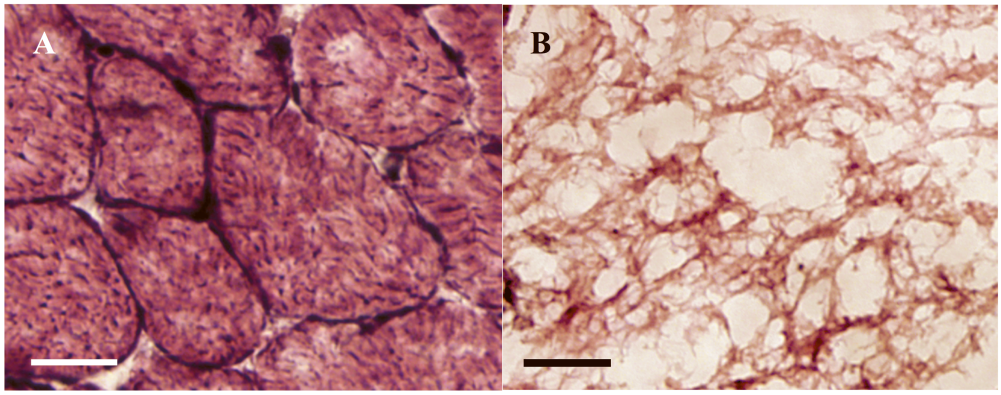

Figure 3.1: Hematoxylin and eosin staining of untreated **(A)** and decellularized **(B)** mouse tibialis anterior muscles. Absence of dark stained peripheral nuclei was confirmed in decellularized muscle. Scale bars represent 20μm.

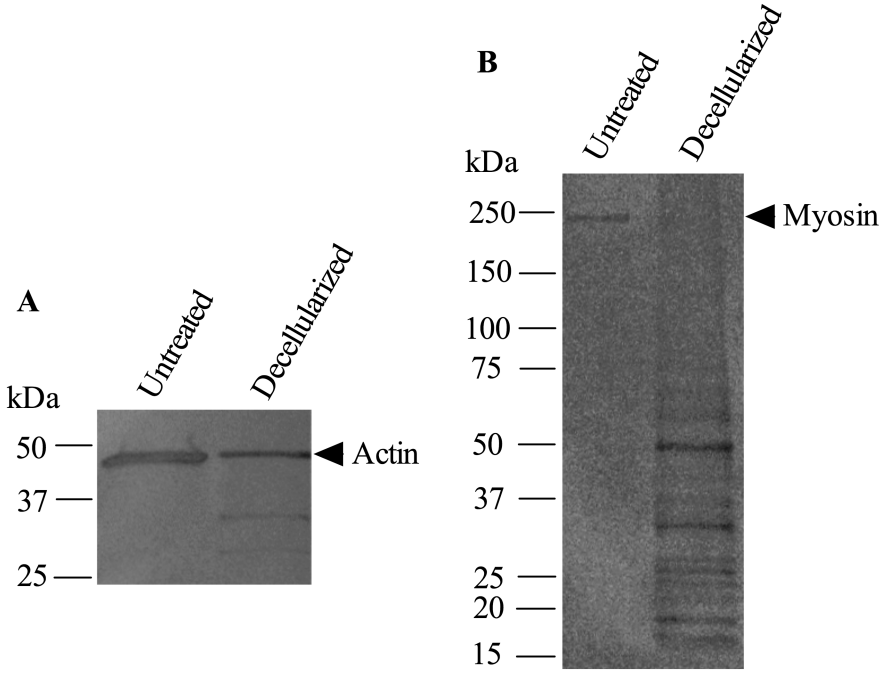

Figure 3.2: Western blots of untreated and decellularized mouse tibialis anterior muscles for actin **(A)** and myosin **(B)**. Both actin and myosin content were greatly reduced in decellularized muscles, however a small 43 kDa band for actin was still present. A 200 kDa band for myosin was not observed in decellularized muscles.

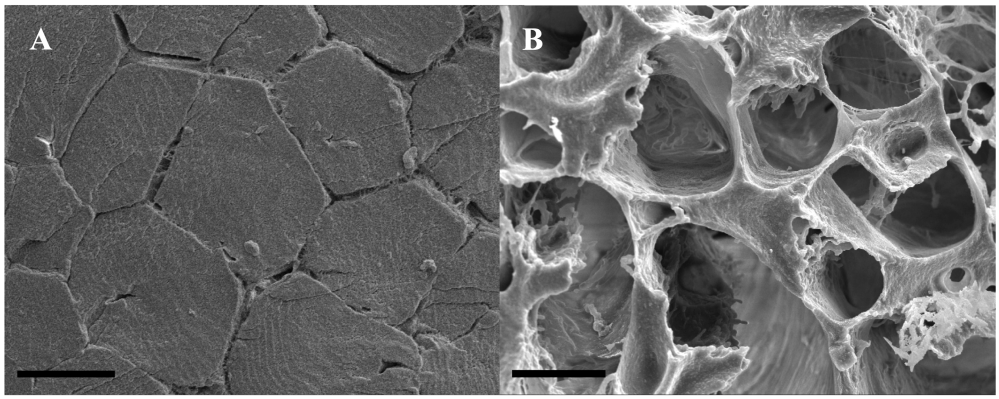

Figure 3.3: Scanning electron micrographs of untreated **(A)** and decellularized **(B)** mouse tibialis anterior muscles cut transversely to fiber direction. Unlike untreated muscles, decellularized muscles had a hollow tubular structure, suggesting the removal of muscle fibers. Scale bar represents 20μm.

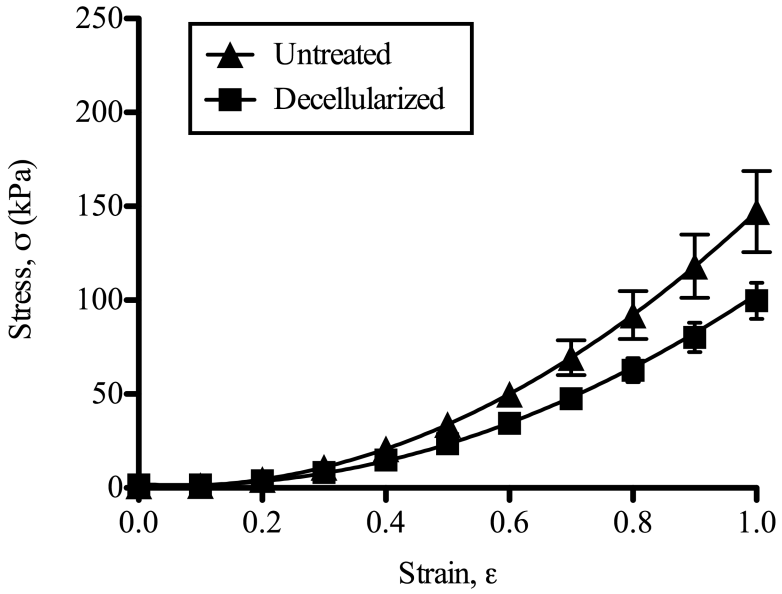

Figure 3.4: Mechanical properties of untreated and decellularized mouse tibialis anterior muscle bundles. Stress (σ) vs. strain (ε) relationship represented as average stress (untreated: n=9; decellularized: n=8) ± SE. Relationships were approximated by quadratic fits with $\sigma = 162\varepsilon^2 - 15.7\varepsilon + 1.18$ ($r^2 = 0.979$) for untreated bundles and $\sigma = 117\varepsilon^2 – 16.0\varepsilon + 2.09$ ($r^2 = 0.993$) for decellularized bundles.

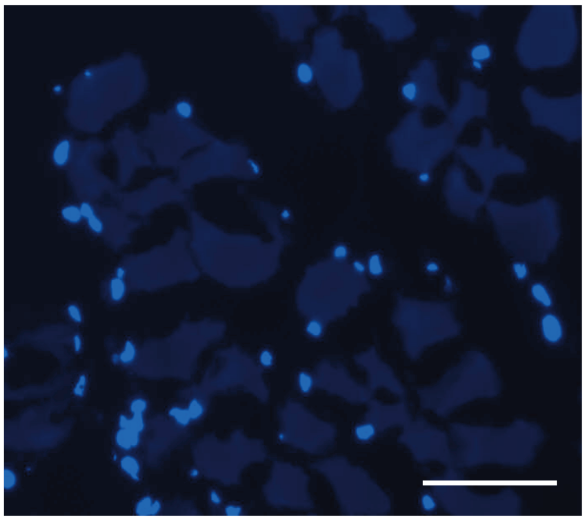

Figure 3.5: Cryosection of C2C12 cells cultured on decellularized mouse tibialis anterior muscle for 4 days and stained with DAPI. The fact that the cells survived 4 days and the presence of the DAPI-stained nuclei indicated the cytocompatibility of decellularized muscles and confirmed the removal of any potentially cytotoxic decellularization reagents. Scale bar represents 50μm.

CHAPTER 4

Three-Dimensional Reconstruction of Perimysial Collagen in Skeletal Muscle Extracellular Matrix

4.1 Abstract

Recent studies have shown that the extracellular matrix (ECM) of skeletal muscle may play an important role in altered tissue mechanics and muscle function with disease and injury, but the tools available to investigate *in vivo* ECM structure are lacking. Scanning block face electron microscopy, a recently developed method that reveals high-resolution nanostructure of tissues, was explored as a tool to examine skeletal muscle ECM ultrastructure for the first time. Addition of ruthenium red improved tissue contrast and utilization of variable pressure imaging modality reduced electron charging artifacts, allowing for continuous imaging over a relatively large volume of ECM. Previously unappreciated perimysial collagen structures were reconstructed via manual and semi-automated segmentation methods. Perimysial collagen structures in the ECM may provide a target for clinical therapies aimed at reducing skeletal muscle fibrosis.

4.2 Introduction

Electron microscopy of skeletal muscle dates back to the 1940s with the first structural investigation of myofibrils (1). To date, most ultrastructural studies of skeletal muscle have focused on muscle fibers, the sarcoplasmic reticulum (2), membranes, and the neuromuscular junction (3). The structure of the skeletal muscle extracellular matrix (ECM) has largely been overlooked due to its perceived lack of functional organization and is traditionally defined as being subdivided into endomysium, perimysium, and epimysium based upon cross-sectional morphology. There are, however, notable exceptions to this oversight. In the early 1980s, Borg & Caulfield and Rowe first describe the endomysial collagen network and large collagen bundles in the perimysium of several muscles (4, 5). The next major advancements in understanding ECM structure came from the work of Trotter and Purslow who observed and quantified endomysial collagen organization (6, 7) and more recently the observation of perimysial junctional plates by Passerieux et al. (8). Conversely, the extracellular matrix of cardiac muscle has been studied more in depth to reveal alterations in ECM structure with pathology and how these structural changes affect tissue mechanics (9).

Skeletal muscle ECM has recently been shown to be important in muscle adaptation (10), yet structural changes that occur during these adaptations are not well understood and typically described as a thickening of the endomysium and/or perimysium. Microscopy methods that have previously been used to observe ECM alterations are not sufficient to describe ECM ultrastructure because they lack in resolution capability (immunohistochemistry, confocal microscopy), provide only a 2-dimensional view (transmission electron microscopy), and/or preparation methods are

disruptive to in vivo tissue organization (scanning electron microscopy). However, with the development of 3-dimensional imaging technology and improved staining techniques it has become possible to investigate tissue ultrastructure. Serial block face scanning electron microscopy (SBFSEM) combines the benefits of TEM-scale resolution and tissue structure preservation with the 3D visualization of SEM (11). Imaging skeletal muscle ECM using SBFSEM presents specific challenges, therefore the purpose of this study was to develop a method to image and reconstruct skeletal muscle ECM. To our knowledge, this is the first report of 3D electron microscopy investigation of skeletal muscle ECM structure.

4.3 Methods

Tissue preparation and staining

All animal work was approved by the UCSD IACUC. Fixation and embedding reagents were obtained from Electron Microscopy Sciences (Hartfield, PA) unless otherwise noted. Aged (>12 mo) 129/SV mice were anesthetized with intraperitoneal injection of either pentobarbital (100 mg/kg) or rodent cocktail (100 mg/kg ketamine, 10 mg/kg xylazine, 3 mg/kg acepromazine) and transcardially perfused with mammalian Ringers solution warmed to 35°C containing heparin (20 units/ml) and 0.2% dextrose for 2 minutes followed by 2% paraformaldehyde, 2.5% glutaraldehyde, 0.05% ruthenium red, and 0.2% tannic acid in 0.15M sodium cacodylate buffer containing 2mM calcium chloride at 35°C for 5 minutes. After complete fixation extensor digitorum longus (EDL) muscles were dissected and incubated in the same

fixative solution overnight at 4°C. Tissue was prepared following a modified version of the West et al. method (12). Briefly, tissues were washed with sodium cacodylate buffer followed by incubation with 2% osmium tetroxide containing 1.5% potassium ferrocyanide and 0.05% ruthenium red (13) in 0.15M sodium cacodylate buffer for 30 minutes. Tissues were washed in distilled water and incubated in 1% thiocarbohydrazide for 20 minutes. Tissues were washed with distilled water, incubated in 2% osmium tetroxide for 30 minutes, washed with distilled water, and placed in 2% uranyl acetate overnight at 4°C. The next day tissues were stained en bloc with Warton's lead aspartate for 15 minutes at 60°C followed by washing with distilled water and dehydration in graded ethanol. Tissues were embedded in Durcupan ACM resin. Embedded tissues were trimmed to ~1mm3 and mounted on aluminum pins.

Serial block face scanning electron microscopy (SBFSEM)

Specimens were loaded in a Zeiss Sigma scanning electron microscope outfitted with a serial block face imaging chamber (Gatan 3View). Digital Micrograph software (Gatan) was used to control knife and specimen movement within the chamber and for data collection. Images were obtained at 3kV accelerating voltage with a 60mm aperture under variable pressure (chamber pressure was varied from 28 to 35 Pa to offset charging). Beam stigmation and aperture alignment were performed as necessary. Tissue blocks were sectioned at 70nm thickness, although thinner sections were possible. Images were recorded at 2,300X magnification and a raster size of 8K x 8K with 1µs dwell time, resulting in 4.51 nm per pixel. Approximately

2,000 images were obtained during each session, with focus and stigmation corrected periodically. Cutting speed was set to 0.5mm/second with oscillation.

Image analysis

Images were converted to 8bit for analysis. Cross-correlation was calculated and images aligned and stacked. Images were binned by a factor of 6 prior to segmentation. Both semi-automated and manual segmentation methods were used to identify objects of interest including muscle fibers, fibroblasts, capillaries, grouped collagen fibrils (collagen cables), and myonuclei. Initial attempts at segmentation were performed manually with IMOD software (14). Contours were linearly interpolated over 10 images unless object branching necessitated drawing contours on each section. For comparison, Analyze 11.0 software (AnalyzeDirect, Inc.) was also used to segment the same datasets. Objects were defined by thresholding and seeded on neighboring images to grow the object throughout the volume. Voxel sizes were dependent upon imaging parameters. The time required for volume segmentation was measured for both methods.

4.4 Results

Data acquisition from a single volume took approximately 36 hours given the above imaging parameters. A typical image obtained from an ECM volume is shown in Figure 4.1. Manual segmentation required >40 hours, and while semi-automated segmentation took about the same amount of total time, it required approximately 20%

of the hands-on time that is required for manual segmentation. This is due to only a fraction of time spent seeding an object in Analyze, with the software generating a model during the rest of the time. The total time for Analyze segmentation includes manual corrections that were required after semi-automated segmentation. A comparison of IMOD and Analyze reconstructions showed that IMOD modeling was better for segmenting large objects, such as fibroblasts, that have similar contrast to nearby objects such as muscle fibers and collagen cables (Fig. 4.2). However, the seed-growing algorithm utilized by Analyze more accurately defined the fine structure of individual collagen fibrils, provided that they were not localized close to other structures.

Final segmentation yielded a surprisingly long network of collagen fibrils bundled together into "cables" that undulated through the tissue and in some cases split into multiple cables. Because the structure of these cables does not correspond to the historical definition of endomysium, we defined them to be perimysial collagen. Perimysial collagen cables were in close proximity to fibroblasts and myonuclei, and were generally oriented along the muscle fiber axis. In addition to perimysial cables, fibroblasts were also segmented and interactions between fibroblasts and perimysial cables were identified (Fig. 4.3). Long fibroblast processes were closely associated with perimysial cables across long distances as well as the muscle fiber surface. Fibroblasts also formed long projections, but these projections did not appear to be fibripositors (15). Projections were flat, wide and sheet-like (Fig. 4.3A) or finger-like (Fig. 4.3B).

4.5 Discussion

Three-dimensional SBFSEM imaging of skeletal muscle has revealed high resolution nanoscale structural information that was previously only achieved through serial sectioning, although the limited available data on skeletal muscle were obtained as proof of concept and focused mainly on muscle fibers (11). Because the skeletal muscle ECM contains a large volume of non-electron dense space, it presents special challenges to the use of SBFSEM that have not been previously addressed. Earlier tissue preparation methods (11, 12) were modified to enhance staining of the ECM by incorporating ruthenium red during fixation and primary osmium staining to enhance contrast of structures containing glycosaminoglycans. By incorporating SEM variable pressure modality, electron charging artifacts were reduced in areas of non-conductive space within the ECM and images could be recorded over a relatively large volume depth.

Manual and semi-automated segmentation methods were compared for ECM volumes. Although semi-automated segmentation could be performed in less time, it was less able to identify and segment finer details of perimysial collagen cables and fibroblasts. Objects with similar intensities were often segmented as the same object when in close proximity, for example perimysial cables and fibroblasts, therefore manual corrections were usually required. Myonuclei were especially difficult to automatically segment due to inability to threshold myonuclei separately from muscle fibers. Although there is no minimum object size for extracting objects in Analyze, the

ability to segment an object throughout the volume depends upon the thresholding parameters that are set independently for each seed point. For this reason multiple seed points were occasionally required to segment a single object. Semi-automated reconstructions successfully modeled the general shape and organization of perimysial collagen cables, capillaries, and fibroblasts, but manual segmentation was required to view structures/connections at a smaller scale (Fig. 4.3).

This report is the first to visualize 3D skeletal muscle ECM ultrastructure. Perimysial collagen cables were identified that have been referred to previously (4, 16), but never viewed at this level of detail. The location and wavy structure of the perimysial cables suggest that they can act as a parallel elastic element in skeletal muscle that can bear load. Unique interactions of perimysial collagen cables with fibroblasts were also observed, suggesting that fibroblasts may be involved in the formation and/or regulation of perimysial collagen cables.

Discovery of the ECM ultrastructure may lead to identification of potential targets for therapy in muscle injury and disease. After inadequate or failed regeneration, skeletal muscle becomes fibrotic resulting in increased muscle stiffness and decreased muscle function. Previous measurements of muscle stiffness correlate relatively poorly with measures of endomysial content such as percent collagen and area fraction of ECM (10, 17). We propose that this is due to the lack of consideration of structures identified here as perimysial cables. Therapies that target these structures may reverse the effects of fibrosis and thereby improve muscle function.

In conclusion, a three-dimensional electron microscopy method for imaging and reconstructing skeletal muscle ECM ultrastructure has been described. Perimysial

collagen cables and their physical interaction with fibroblasts and muscle fibers were identified using manual and semi-automatic volume segmentation. In future studies this method may be used to determine how these structures change in response to muscle pathology. By defining the ultrastructure of fibrotic skeletal muscle ECM, therapeutic targets may be identified to reduce fibrosis and associated muscle stiffness in patients with limited muscle function.

4.6 Acknowledgements

I would like to acknowledge the co-authors of this paper. Chapter 4 is currently being prepared for submission for publication of the material, Gillies AR, Bushong E, Deerinck TJ, Ellisman MH, Lieber RL. No authors have competing interests.

Research supported by NIH grants R24 HD05083 and R01 AR057393. Mason Mackey and Andrea Thor from the National Center for Microscopy and Imaging Research are thanked for assistance with 3View tissue preparation.

4.7 References

1. Hall, C. E., Jakus, M. A., and Schmitt, F. O. (1946) An investigation of cross striations and myosin filaments in muscle. *Biol Bull* **90**, 32-50

2. Eisenberg, B. R., Kuda, A. M., and Peter, J. B. (1974) Stereological analysis of mammalian skeletal muscle. I. Soleus muscle of the adult guinea pig. *J Cell Biol* **60**, 732-754

3. Rash, J. E., and Ellisman, M. H. (1974) Studies of excitable membranes. I. Macromolecular specializations of the neuromuscular junction and the nonjunctional sarcolemma. *J Cell Biol* **63**, 567-586

4. Borg, T. K., and Caulfield, J. B. (1980) Morphology of connective tissue in skeletal muscle. *Tissue Cell* **12**, 197-207

5. Rowe, R. W. (1981) Morphology of perimysial and endomysial connective tissue in skeletal muscle. *Tissue Cell* **13**, 681-690

6. Trotter, J. A., and Purslow, P. P. (1992) Functional morphology of the endomysium in series fibered muscles. *J Morphol* **212**, 109-122

7. Purslow, P. P., and Trotter, J. A. (1994) The morphology and mechanical properties of endomysium in series-fibred muscles: variations with muscle length. *J Muscle Res Cell Motil* **15**, 299-308

8. Passerieux, E., Rossignol, R., Chopard, A., Carnino, A., Marini, J. F., Letellier, T., and Delage, J. P. (2006) Structural organization of the perimysium in bovine skeletal muscle: Junctional plates and associated intracellular subdomains. *J Struct Biol* **154**, 206-216

9. Weber, K. T., Pick, R., Jalil, J. E., Janicki, J. S., and Carroll, E. P. (1989) Patterns of myocardial fibrosis. *J Mol Cell Cardiol* **21 Suppl 5**, 121-131

10. Smith, L. R., Lee, K. S., Ward, S. R., Chambers, H. G., and Lieber, R. L. (2011) Hamstring contractures in children with spastic cerebral palsy result from a stiffer extracellular matrix and increased in vivo sarcomere length. *J Physiol* **589**, 2625-2639

11. Denk, W., and Horstmann, H. (2004) Serial block-face scanning electron microscopy to reconstruct three-dimensional tissue nanostructure. *PLoS Biol* **2**, e329

12. West, J. B., Fu, Z., Deerinck, T. J., Mackey, M. R., Obayashi, J. T., and Ellisman, M. H. (2010) Structure-function studies of blood and air capillaries in chicken lung using 3D electron microscopy. *Respir Physiol Neurobiol* **170**, 202-209

13. Luft, J. H. (1971) Ruthenium red and violet. I. Chemistry, purification, methods of use for electron microscopy and mechanism of action. *Anat Rec* **171**, 347-368

14. Kremer, J. R., Mastronarde, D. N., and McIntosh, J. R. (1996) Computer visualization of three-dimensional image data using IMOD. *J Struct Biol* **116**, 71-76

15. Canty, E. G., Lu, Y., Meadows, R. S., Shaw, M. K., Holmes, D. F., and Kadler, K. E. (2004) Coalignment of plasma membrane channels and protrusions (fibripositors) specifies the parallelism of tendon. *J Cell Biol* **165**, 553-563

16. Gillies, A. R., and Lieber, R. L. (2011) Structure and function of the skeletal muscle extracellular matrix. *Muscle Nerve* **44**, 318-331

17. Meyer, G. A., and Lieber, R. L. (2012) Skeletal muscle fibrosis develops in response to desmin deletion. *Am J Physiol Cell Physiol* **302**, C1609-1620

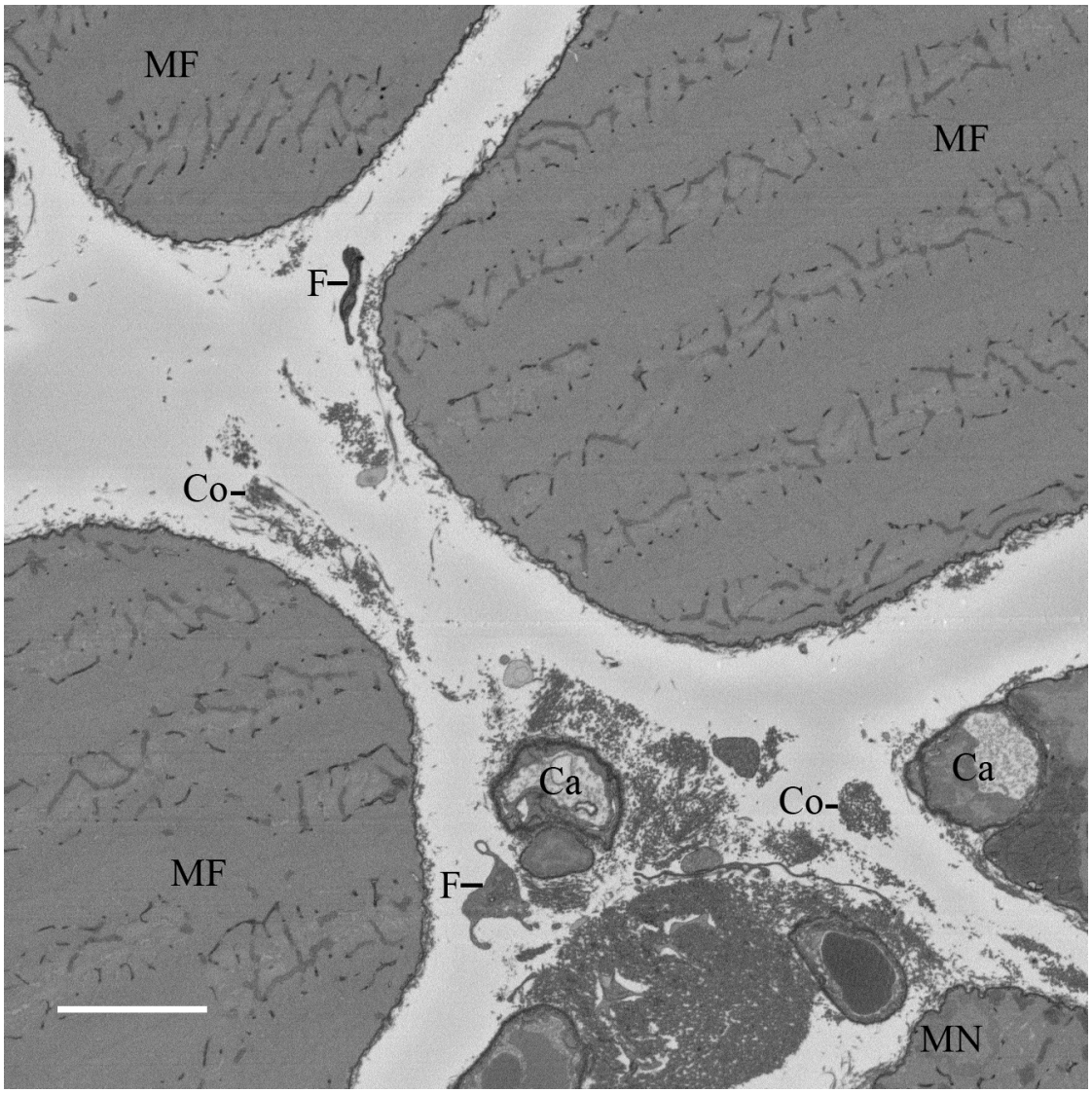

Figure 4.1: Representative x-y slice obtained from serial block face scanning electron microscopy of skeletal muscle ECM (z=400; z range 0-1,999). Scale bar = 5 μm. MF, myofiber; Ca, capillary; MN, myonucleus; F, fibroblast; Co, perimysial collagen cable.

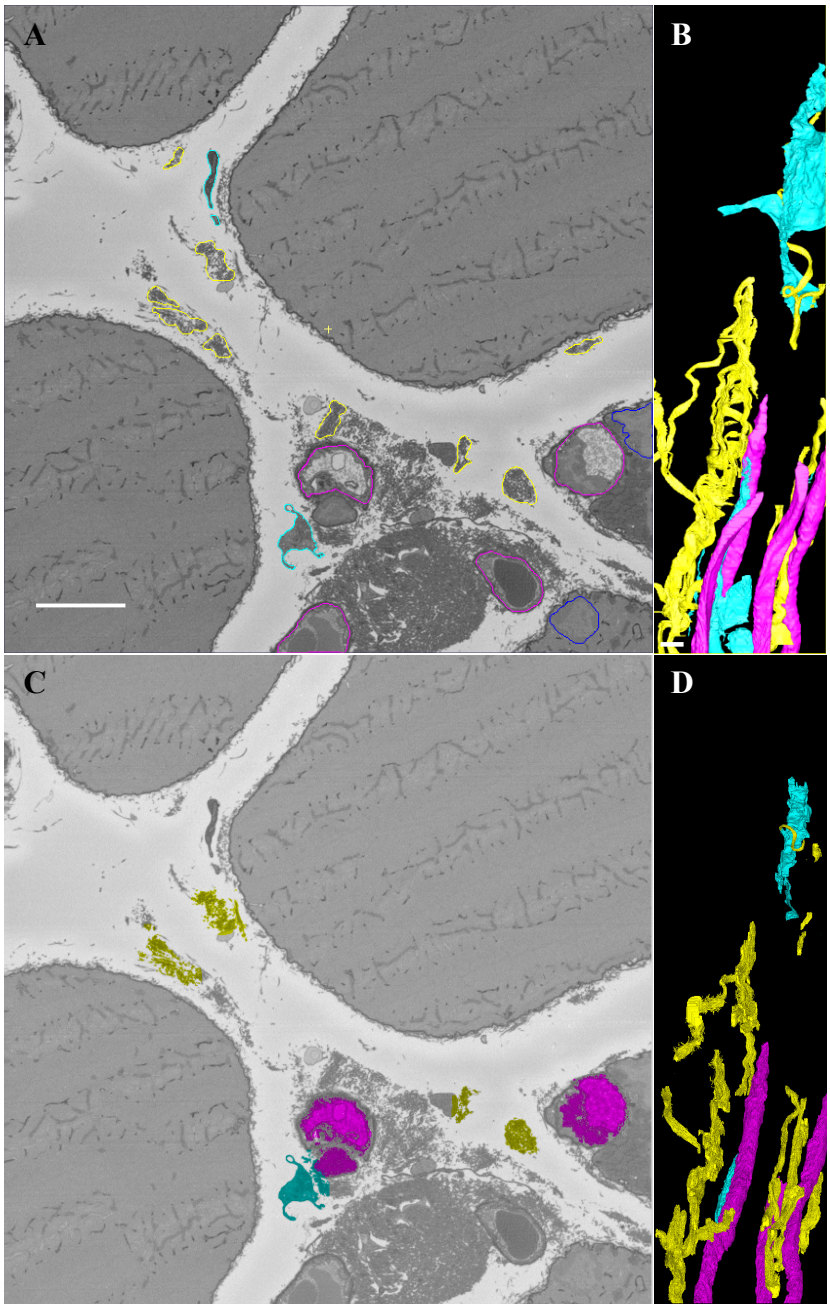

Figure 4.2: Comparison of dataset segmented and reconstructed manually with IMOD (A and B) and semi-automatically with Analyze (C and D). The same x-y slice from Figure 1 is shown with object contours defined in IMOD (A) or Analyze (C). Projections of the manual (B) and semi-automated (D) models are shown for comparison. Capillary = pink, fibroblast = light blue, collagen cable = yellow. Scale bars = 5 μm.

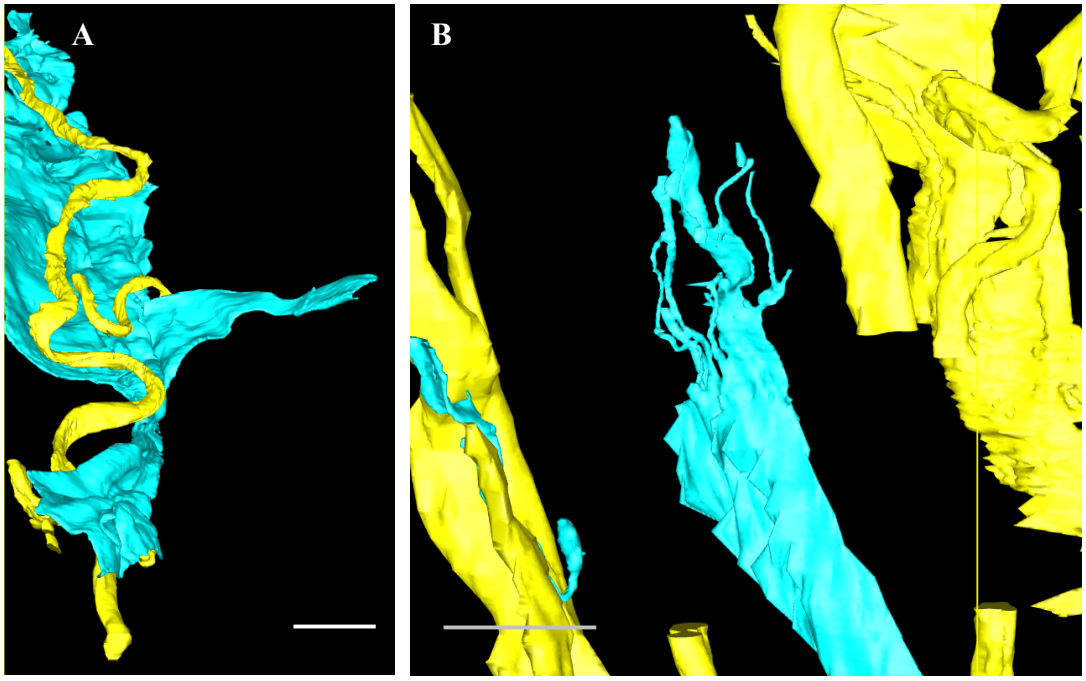

Figure 4.3: Perimysial collagen cables were found in close proximity to fibroblasts and appear to connect in some areas. A) Fibroblast (light blue) and perimysial collagen cables (yellow) viewed at a 60° rotation around the x-axis to highlight the long arm-like projections of the fibroblast and the interaction of the perimysial collagen with the fibroblast. B) Thin finger-like projections from the end of a fibroblast. Scale bars = 5 μm; from manual reconstruction.

CHAPTER 5

Perimysial Collagen Volume Fraction is Increased in Fibrotic Skeletal Muscle Extracellular Matrix

5.1 Abstract

Fibrosis and concomitant increased stiffness often occur after skeletal muscle injury and disease, thereby limiting muscle function. The source of passive stiffness in skeletal muscle is unknown, however collagen in the extracellular matrix is thought to be a primary source due to its structural properties. Skeletal muscle perimysium contains large bundles of collagen fibrils, or "cables", that were viewed by serial block face scanning electron microscopy reconstructions and appeared to be capable of load-bearing, therefore we hypothesized that fibrotic skeletal muscle contains a higher volume fraction of perimysial collagen cables. In the desmin knockout model of progressive fibrosis, perimysial collagen cables accounted for a significantly higher volume fraction than that measured for wild type muscle. Current treatments to alleviate skeletal muscle fibrosis have been largely unsuccessful, thus perimysial collagen cables may be a future therapeutic target for reducing fibrosis related muscle stiffness.

5.2 Introduction

Fibrosis commonly develops in response to skeletal muscle disease and injury and is generally described as an increase in the extracellular matrix (1, 2). Many factors are involved in the development of fibrosis including growth factor signaling, macrophage phenotype, fibroblast activation/proliferation, and dysregulated proteolysis (3). The most obvious hallmark of fibrosis is increased area of the extracellular matrix (ECM) in muscle cross-sections. The ECM is traditionally defined as the epimysium, surrounding the muscle body, the perimysium, which surrounds muscle fascicles, and the endomysium, which ensheaths individual muscle fibers. Collagen is the most abundant structural protein found in ECM and is upregulated at the transcriptional level (4-6) and increased at the protein level (4, 7) with fibrosis. The organization of collagen in fibrotic ECM is not well understood, yet it could have a large impact on muscle mechanical properties and function even though it accounts for only a small volume fraction.

Secondary to fibrosis, increased muscle stiffness and/or contracture may progressively occur, thereby limiting muscle function and mobility (8, 9). Children with cerebral palsy can develop fibrosis secondary to an upper motoneuron lesion and present with limited range of motion and muscle spasticity. Mechanical testing of muscle biopsies from these patients showed that bundles of muscle fibers are approximately twice as stiff as muscle from control subjects (7). Similarly, in a model of progressive skeletal muscle fibrosis (desmin knockout, $des^{-/-}$), bundles of fibers are stiffer than control muscle (4). This increase in stiffness is not observed at the single fiber level, indicating that the increase in stiffness is most likely due to the presence of passive elements, such as collagen, included in muscle bundle mechanical testing

preparations. However, data from our laboratory indicate that collagen content alone is not predictive of muscle bundle stiffness. It is possible that another property of collagen, such as its organization, may affect tissue stiffness. In cardiac ECM, perimysial collagen fibers have been described that increase in size with left ventricular hypertrophy (10, 11). Similar structures have been identified in skeletal muscle (12-14), however it is unknown how these structures reorganize in response to skeletal muscle fibrosis. Therefore, the purpose of this study was to describe and quantify perimysial collagen cables in skeletal muscle fibrosis. We hypothesized that fibrotic *des*$^{-/-}$ muscle would contain a larger volume fraction of perimysial collagen cables.

5.3 Results

Three-dimensional reconstruction of perimysial collagen cables reveals altered morphology in *des*$^{-/-}$ muscle

Micrographs obtained from serial block face scanning electron microscopy were stacked into a volume and segmented in three dimensions to identify perimysial collagen cables, fibroblasts, muscle fibers, and myonuclei within *wt* and *des*$^{-/-}$ extensor digitorum longus (EDL) muscle. Reconstruction showed groups of collagen fibrils associated over relatively long distances that generally aligned with the muscle fiber axis, which we defined as perimysial collagen cables (Fig. 5.1). Perimysial cables had a wavy, but not coiled, morphology and occasionally branched in both *wt* and *des*$^{-/-}$ muscle. Fibroblasts were often found between muscle fibers and formed long

processes extending beyond the nucleus. Perimysial cables were closely associated with these processes, and processes occasionally appeared to guide cable direction. It was not clear if collagen fibrils within perimysial cables formed a physical connection with fibroblast processes directly or through an intermediate matrix structural protein. Dense areas of collagen were observed in "grooves" of the sarcolemma overlying myonuclei, but these collagen structures could not be identified as perimysial cables based on morphology (Fig. 5.2). The most obvious difference between the *wt* and *des*$^{-/-}$ reconstructions was the presence of more cables that appeared to be oriented closer to the muscle fiber axis than *wt* perimysial cables.

Desmin knockout EDL muscle has a higher volume fraction of perimysial collagen cables compared to *wt*

Volume fractions of muscle components were measured in *wt* and *des*$^{-/-}$ EDL relative to total muscle volume. A total of 421,041 points were classified on transmission electron micrographs obtained from 16 animals. The extracellular space accounted for 26.8% ± 3.6% volume of *des*$^{-/-}$ muscle and 24.1% ± 3.0% of *wt* muscle (not significant). Within the extracellular space no change was detected in the volume of single collagen fibrils, satellite cells, or fibroblasts, but the volume fraction of collagen fibrils in cables was almost doubled in *des*$^{-/-}$ muscle (Fig. 5.3).

5.4 Discussion

Extracellular matrix organization is altered in fibrotic muscle

Perimysial collagen cables were followed over distances as long as 150 μm along the muscle fiber axis. Cables were present in close proximity with fibroblast processes as well as muscle fibers. Physical connections between fibroblasts and perimysial cables were not directly shown, however non-electron dense linker proteins may be present that link fibroblasts to cables. As cables straighten with muscle strain (Supplementary Fig. 5.1), connected fibroblasts may be able to "sense" muscle strain. Collagen dense structures observed in sarcolemmal "grooves" adjacent to myonuclei may serve as a mechanosensing strategy for muscle fibers (Fig. 5.2). Collagen fibrils perpendicular to the sarcolemma were observed at these grooves, suggesting that collagen fibrils may be linked to cytoskeletal or nuclear components at these locations. Costameres are known to localize ECM components to the cytoskeleton, but they are not known to be co-localized with myonuclei (15). Cables appeared to be more aligned with the muscle fiber axis in *des*$^{-/-}$ muscle but still showed the same wavy morphology as *wt* muscle. Muscles were fixed in plantarflexion, so EDL muscles were slightly lengthened and cables may have stretched/realigned accordingly.

Fibrotic perimysial collagen volume fraction is increased

Perimysial collagen volume fraction was significantly increased in *des*$^{-/-}$ EDL muscle (Fig. 5.3). It is assumed that the perimysial collagen cables observed in this study were primarily composed of type I collagen based on morphology and confocal imaging (Supplementary Fig. 5.1), however type III collagen may also be present (16). Whether the increased volume fraction of perimysial cables is present as more cables

of the same size or the same number of cables that are larger will be the subject of future study.

It is striking that such a small volume change in perimysial cables (+1.7%) is the only measured component that exhibits the same trend as muscle stiffness. It is possible that the volume fraction of extracellular space is overrepresented due to artificially increased intrafascicular spaces during the resin embedding process. This would lead to a relative increase in the calculated perimysial volume fraction. Still, on the order of only a few percent of total muscle volume, this would not seem to have a large effect on the volume fraction estimations presented here.

No differences were found in the volume fraction of satellite cells or fibroblasts from des-/- muscle. Genetic deletion of desmin leads to a continuous injury and inflammation, which eventually results in fibrosis (4). Controls in this study were age matched and the satellite cell pool decreases with age (17), so a small volume fraction of satellite cells was expected in both genotypes. Since no difference was observed in the fibroblast compartment, fibroblasts in *des*$^{-/-}$ muscle may alter gene transcription, instead of proliferating, to increase collagen production or tissue inhibitors of matrix metalloproteinases that prevent normal collagen turnover.

As muscle fibers stretched, perimysial collagen cables realigned with the muscle axis (Supplementary Fig. 5.1) suggesting that the wavy orientation of perimysial collagen cables may provide a strain relief function. Given the very high tensile strength of collagen fibrils (18), it is feasible that the increase in perimysial collagen cable volume fraction could be a factor in increased *des*$^{-/-}$ muscle stiffness (4). The degree of collagen crosslinking was not measured in this study, but could

increase stiffness (19). Also, the volume fraction of collagen cables was only measured in the EDL, a fast muscle in mice. Muscles composed primarily of slow fibers may have different stiffness properties as well as collagen organization.

Perimysial collagen cables may be a potential target for anti-fibrotic therapies

Because perimysial collagen volume fraction increases with muscle bundle stiffness, anti-fibrotic therapies that target these structures may improve muscle function in patients with skeletal muscle fibrosis. Current therapies for improving function of fibrotic muscle include tendon lengthening (20), physical therapy (21), and pharmacotherapy. These approaches to date have only partially alleviated symptoms associated with fibrosis (22, 23). Recently, anti-fibrotic research has shifted to focus on the cellular and molecular levels. New evidence shows that antibodies may be used to block procollagen type I polymerization (24) and collagen crosslinking enzymes (25) and may prevent fibrosis progression in various tissues. These strategies, however, would theoretically target all type I collagen polymerization and enzyme crosslinking activity. By specifically targeting the structures responsible for reduced function (higher stiffness), adverse side effects, such as reduced tissue integrity, may be circumvented.

5.5 Materials and Methods

Animals

All procedures were performed in accordance with the National Institutes of Health's Guide for the Use and Care of Laboratory Animals and were approved by the University of California San Diego Institutional Animal Care and Use Committee. All experiments were performed on muscles from aged (>12 months old) wild type (*wt*) 129/SV and desmin knockout ($des^{-/-}$) 129/SV mice. Animals for transmission electron microscopy and serial block face scanning electron microscopy analysis (n = 8 per genotype) were anesthetized by intraperitoneal injection of either pentobarbital (100 mg/kg) or rodent cocktail (100 mg/kg ketamine, 10 mg/kg xylazine, 3 mg/kg acepromazine) and transcardially perfused with mammalian Ringers solution warmed to 35°C containing heparin (20 units/ml) and 0.2% dextrose for 2 minutes followed by 2% paraformaldehyde, 2.5% glutaraldehyde, 0.05% ruthenium red, and 0.2% tannic acid in 0.15M sodium cacodylate buffer containing 2mM calcium chloride at 35°C for 5 minutes. After complete fixation, both fifth toe extensor digitorum longus (EDL) muscles were dissected from each animal with one EDL prepared for transmission electron microscopy and the other for 3View analysis (randomized). Animals for whole muscle mechanical testing (n = 8 per genotype) and confocal microscopy (n = 4 *wt*) were killed by CO_2 asphyxiation and cervical dislocation followed by removal of hindlimbs for analysis.

Serial block face scanning electron microscopy

Perfusion fixed muscles were incubated in fixative solution overnight at 4°C. Tissues were washed with 0.15M sodium cacodylate buffer followed by incubation with 2% osmium tetroxide containing 1.5% potassium ferrocyanide and 0.05%

ruthenium red in 0.15M sodium cacodylate buffer for 30 minutes on ice. After washing in distilled water, tissues were incubated in 1% thiocarbohydrazide for 20 minutes then washed with distilled water followed by a final incubation in 2% osmium tetroxide for 30 minutes. Tissues were washed with distilled water and placed in 2% uranyl acetate overnight at 4°C. Tissues were then stained *en bloc* with Warton's lead aspartate for 15 minutes at 60°C followed by washing with distilled water and dehydration in 50%, 70%, 90%, 100%, and 100% ethanol for 5 minutes each. Tissues were embedded in Durcupan ACM resin. Embedded tissues were trimmed to ~1mm^3 and mounted on aluminum pins.

Mounted specimens were viewed in a Zeiss Sigma scanning electron microscope outfitted with a specialized specimen chamber for serial block face imaging (Gatan 3View). Specimens were imaged at 3 kV under variable pressure (~32 Pa), high current mode, at 2300X magnification with aperture size 60 mm. Images were acquired with a Gatan backscattered electron detector (1 mm aperture) and visualized with Gatan Digital Micrograph software at 8k x 8k raster, 1 μs dwell time, at 70 nm cutting thickness. Acquired images were converted to TIFF format and serial images were imported as a volume in Analyze 11.0 software (AnalyzeDirect, Inc.). Object segmentation was performed using the object extractor tool. Using this tool, a seed point was placed on each object of interested, the object boundaries were defined by thresholding, and the defined seed-growing algorithm traced the object throughout the tissue volume. Manual corrections of object boundaries were performed as necessary.

Transmission electron microscopy

After removal, EDL muscles were cut to 5 pieces of equal length and incubated in fixative solution overnight at 4°C. Tissues were washed with 0.15M sodium cacodylate buffer followed by incubation with 2% osmium tetroxide containing 1.5% potassium ferrocyanide and 0.05% ruthenium red in 0.15M sodium cacodylate buffer for 30 minutes on ice. Tissues were washed in distilled water and placed in 2% uranyl acetate at 4°C overnight, followed by washing in distilled water and dehydration in 50%, 70%, 90%, 100%, and 100% ethanol for 5 minutes each. Dehydrated tissues were placed in anhydrous acetone and then embedded in Durcupan ACM resin. Cross-sections of tissue blocks were sectioned at 70nm thickness on a Leica Ultracut UCT ultramicrotome with a Diatome diamond knife, and collected on 300 hexagonal mesh thin bar copper grids. Sections were post-stained for 10 minutes in 2% uranyl acetate, washed with distilled water, and stained for 1 minute in Sato's lead. Sections were observed at 80kV using a FEI Tecnai Spirit TEM with objective aperture size 40 μm and condenser aperture size 100 μm. Images were acquired with a 2k x 2k Gatan CCD camera and SerialEM Software (26).

Volume fraction estimation by stereology

Transmission electron micrographs for stereological analysis were acquired following a multi-stage sampling scheme. One section from each tissue block (n = 5 per muscle) was imaged. Eight low magnification (1650x) and five high magnification (11,000x) micrographs were randomly acquired from each section, with high magnification images acquired only from areas containing extracellular space. If the

randomly selected 11,000x field of view contained no extracellular space, another field of view was randomly selected. Sections were discarded if they contained tendon tissue (n=2 out of 80 total). Images were analyzed with IMOD software using the stereology plug-in (27). A 20 x 20 square grid (grid spacing 0.79 μm, 400 points/grid) was overlaid on each low magnification micrograph and each point was classified as myofibril, mitochondria, myonucleus, satellite cell, fibroblast, extracellular space, nerve, capillary, or other. To quantify objects within the extracellular space, 27 x 27 square grids (grid spacing 85.6 nm, 729 points/grid) were overlaid on high magnification micrographs and points within the extracellular space were classified as interstitial space (no visible object), single collagen fibril, collagen fibril in bundle, or basal lamina (Supplementary Fig. 2). Points lying on objects not within the extracellular space were left unclassified and not counted. Object point counts were summed for each animal and volume fractions of myofibrils, mitochondria, myonuclei, satellite cells, fibroblasts, extracellular space, nerves, and capillaries were defined as the total object point count divided by the total number of points counted at low magnification. Volume fractions for single collagen fibril, collagen fibrils in cable, and basement membrane were calculated using the following equation:

$$\frac{V_{col}}{V_M} = \frac{V_{col}}{V_s} \times \frac{V_s}{V_M}$$

where V_{col}/V_s is the fraction of collagen (single fibril, fibril in cable, or basement membrane) in the extracellular space calculated at high magnification and V_s/V_M is the fraction of extracellular space in the muscle calculated at low magnification.

Immunohistochemistry and confocal microscopy

After dissection, fifth toe EDL muscles were pinned to cork at slack length and stored at -20°C in glycerinated storage solution containing (in mM): K-propionate (170), K_3EGTA (5), $MgCl_2$ (5.3), imidazole (10), Na_2ATP (21.2), NaN_3 (1), glutathione (2.5), 50 μM leupeptin, and 50% (vol/vol) glycerol. Mouse anti-type I collagen antibodies (Chondrex) were labeled with Alexa Fluor 488 using an antibody labeling kit (Life Technologies). Antibody conjugates were purified prior to use to remove any unlabeled antibody or dye. Muscles for confocal analysis were pinned to sylgard coated dishes in a relaxing solution containing (in mM): imidazole (59.4), KCH_4O_3S (86), $Ca(KCH_4O_3S)_2$ (0.13), $Mg(KCH_4O_3S)_2$ (10.8), K_3EGTA (5.5), KH_2PO_4 (1), Na_2ATP (5.1), and 50.0 μM leupeptin at pCa 8.0 and pH 7.1. Bundles of muscle fibers (5-10 fibers) were isolated and placed in a custom stretching chamber with a cover glass bottom designed for confocal imaging of skeletal muscle bundles (28). Bundles were attached using 10 – 0 monofilament nylon suture on one end to a stationary titanium pin and on the other end to a titanium wire attached to a micrometer. Bundles were blocked in 1% bovine serum albumin in relaxing solution for 30 minutes, followed by blocking in 15 μl/ml goat serum and 10% mouse serum in 0.1% BSA in relaxing solution for 15 minutes. Bundles were incubated with Alexa Fluor conjugated anti-type I collagen (1:250) overnight at 4°C. After removing primary antibodies, DRAQ5 (1:1,000) was added to label nuclei.

Confocal imaging was performed at 21°C with a Leica True Confocal Scanner SP5 microscope using a 63X planapochromat oil immersion lens (1.3 numerical aperture). Muscle bundle length was adjusted to slack length, measured as the suture

knot-to-knot distance. Image stacks of muscle bundles were obtained at slack length and at 10% strain increments. Bundles that slipped on the pin with strain or were damaged were not included in image analyses. X-Y image stacks (512x512 raster, 400 Hz) were acquired at 0.99 μm optical section thickness in Leica Application Suite Advanced Fluorescence (LAS AF) software. Three-dimensional projections of image stacks were created in LAS AF software using the 3D Projection tool in the x-y plane. Because fluorescence intensity decreased with imaging time (photobleaching) and distance from the cover glass, black and white levels were adjusted in Adobe Photoshop CS6 when necessary to extend the image histogram to the full range of 0 to 255, without adjusting midtone.

Statistical analysis

Volume fraction data were analyzed with GraphPad Prism 5 statistical software. Significance was determined using Student's t tests with significance level (α) set to 0.05. Data are presented as means ± SEM.

5.6 Acknowledgements

I would like to acknowledge the co-authors of this paper. Chapter 5 is currently being prepared for submission for publication of the material, Gillies AR, Bushong E, Deerinck TJ, Ellisman MH, Lieber RL. No authors have competing interests.

This work was supported by grants from the National Institutes of Health (R24 HD05083 and R01 AR057393). We acknowledge Dr. Samuel Ward and Ana

Rodríguez-Soto for helpful discussion and Mason Mackey, Andrea Thor, Michael Villongco, Blair Conner, and Shannon Bremner for technical assistance.

5.7 References

1. Lieber, R. L., Runesson, E., Einarsson, F., and Friden, J. (2003) Inferior mechanical properties of spastic muscle bundles due to hypertrophic but compromised extracellular matrix material. *Muscle Nerve* **28**, 464-471

2. Cullen, M. J., and Mastaglia, F. L. (1980) Morphological changes in dystrophic muscle. *Br Med Bull* **36**, 145-122

3. Serrano, A. L., and Munoz-Canoves, P. (2010) Regulation and dysregulation of fibrosis in skeletal muscle. *Exp Cell Res* **316**, 3050-3058

4. Meyer, G. A., and Lieber, R. L. (2012) Skeletal muscle fibrosis develops in response to desmin deletion. *Am J Physiol Cell Physiol* **302**, C1609-1620

5. Haslett, J. N., Sanoudou, D., Kho, A. T., Bennett, R. R., Greenberg, S. A., Kohane, I. S., Beggs, A. H., and Kunkel, L. M. (2002) Gene expression comparison of biopsies from Duchenne muscular dystrophy (DMD) and normal skeletal muscle. *Proc Natl Acad Sci U S A* **99**, 15000-15005

6. Smith, L. R., Ponten, E., Hedstrom, Y., Ward, S. R., Chambers, H. G., Subramaniam, S., and Lieber, R. L. (2009) Novel transcriptional profile in wrist muscles from cerebral palsy patients. *BMC Med Genomics* **2**, 44

7. Smith, L. R., Lee, K. S., Ward, S. R., Chambers, H. G., and Lieber, R. L. (2011) Hamstring contractures in children with spastic cerebral palsy result from a stiffer extracellular matrix and increased in vivo sarcomere length. *J Physiol* **589**, 2625-2639

8. Kerr Graham, H., and Selber, P. (2003) Musculoskeletal aspects of cerebral palsy. *J Bone Joint Surg Br* **85**, 157-166

9. Cornu, C., Goubel, F., and Fardeau, M. (1998) Stiffness of knee extensors in Duchenne muscular dystrophy. *Muscle Nerve* **21**, 1772-1774

10. Weber, K. T., Janicki, J. S., Shroff, S. G., Pick, R., Chen, R. M., and Bashey, R. I. (1988) Collagen remodeling of the pressure-overloaded, hypertrophied nonhuman primate myocardium. *Circ Res* **62**, 757-765

11. Jalil, J. E., Doering, C. W., Janicki, J. S., Pick, R., Shroff, S. G., and Weber, K. T. (1989) Fibrillar collagen and myocardial stiffness in the intact hypertrophied rat left ventricle. *Circ Res* **64**, 1041-1050

12. Borg, T. K., and Caulfield, J. B. (1980) Morphology of connective tissue in skeletal muscle. *Tissue Cell* **12**, 197-207

13. Gillies, A. R., and Lieber, R. L. (2011) Structure and function of the skeletal muscle extracellular matrix. *Muscle Nerve* **44**, 318-331

14. Passerieux, E., Rossignol, R., Chopard, A., Carnino, A., Marini, J. F., Letellier, T., and Delage, J. P. (2006) Structural organization of the perimysium in bovine skeletal muscle: Junctional plates and associated intracellular subdomains. *J Struct Biol* **154**, 206-216

15. Ehmer, S., Herrmann, R., Bittner, R., and Voit, T. (1997) Spatial distribution of beta-spectrin in normal and dystrophic human skeletal muscle. *Acta Neuropathol* **94**, 240-246

16. Robinson, T. F., Geraci, M. A., Sonnenblick, E. H., and Factor, S. M. (1988) Coiled perimysial fibers of papillary muscle in rat heart: morphology, distribution, and changes in configuration. *Circ Res* **63**, 577-592

17. Shefer, G., Van de Mark, D. P., Richardson, J. B., and Yablonka-Reuveni, Z. (2006) Satellite-cell pool size does matter: defining the myogenic potency of aging skeletal muscle. *Dev Biol* **294**, 50-66

18. Burton, A. C. (1954) Relation of structure to function of the tissues of the wall of blood vessels. *Physiol Rev* **34**, 619-642

19. Iimoto, D. S., Covell, J. W., and Harper, E. (1988) Increase in cross-linking of type I and type III collagens associated with volume-overload hypertrophy. *Circ Res* **63**, 399-408

20. Beals, R. K. (2001) Treatment of knee contracture in cerebral palsy by hamstring lengthening, posterior capsulotomy, and quadriceps mechanism shortening. *Dev Med Child Neurol* **43**, 802-805

21. Wiart, L., Darrah, J., and Kembhavi, G. (2008) Stretching with children with cerebral palsy: what do we know and where are we going? *Pediatr Phys Ther* **20**, 173-178

22. Tilton, A. H. (2006) Therapeutic interventions for tone abnormalities in cerebral palsy. *NeuroRx* **3**, 217-224

23. Zhou, L., and Lu, H. (2010) Targeting fibrosis in Duchenne muscular dystrophy. *J Neuropathol Exp Neurol* **69**, 771-776

24. Chung, H. J., Steplewski, A., Chung, K. Y., Uitto, J., and Fertala, A. (2008) Collagen fibril formation. A new target to limit fibrosis. *J Biol Chem* **283**, 25879-25886

25. Barry-Hamilton, V., Spangler, R., Marshall, D., McCauley, S., Rodriguez, H. M., Oyasu, M., Mikels, A., Vaysberg, M., Ghermazien, H., Wai, C., Garcia, C. A., Velayo, A. C., Jorgensen, B., Biermann, D., Tsai, D., Green, J., Zaffryar-Eilot, S., Holzer, A., Ogg, S., Thai, D., Neufeld, G., Van Vlasselaer, P., and Smith, V. (2010) Allosteric inhibition of lysyl oxidase-like-2 impedes the development of a pathologic microenvironment. *Nat Med* **16**, 1009-1017

26. Mastronarde, D. N. (2005) Automated electron microscope tomography using robust prediction of specimen movements. *J Struct Biol* **152**, 36-51

27. Kremer, J. R., Mastronarde, D. N., and McIntosh, J. R. (1996) Computer visualization of three-dimensional image data using IMOD. *J Struct Biol* **116**, 71-76

28. Shah, S. B., and Lieber, R. L. (2003) Simultaneous imaging and functional assessment of cytoskeletal protein connections in passively loaded single muscle cells. *J Histochem Cytochem* **51**, 19-29

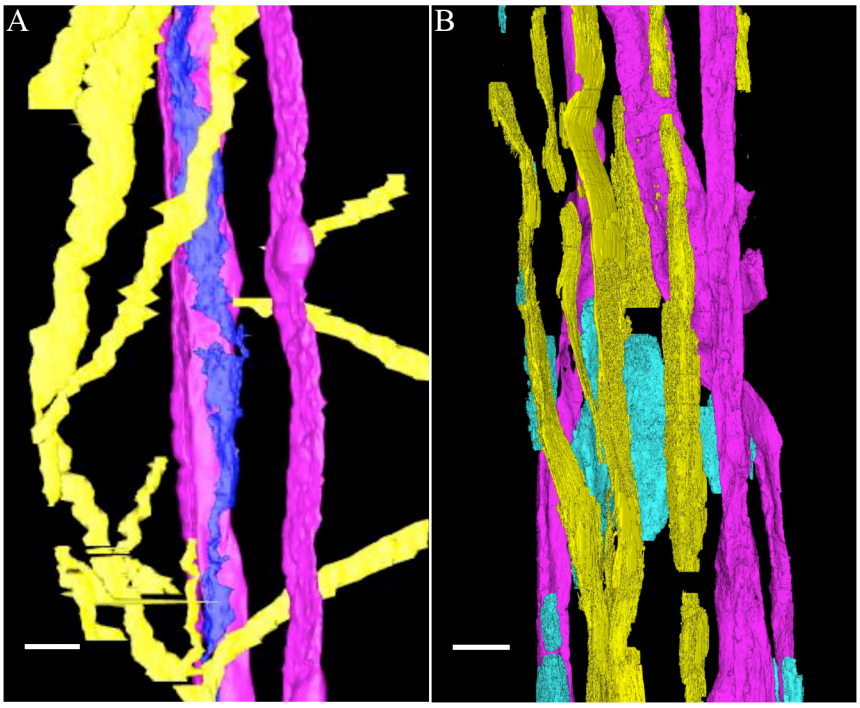

Figure 5.1: Three-dimensional reconstruction of serial block face scanning electron micrographs from *wt* (A) and *des*$^{-/-}$ (B) EDL. Muscle fibers were aligned vertically but were not shown for clarity. Interactions between perimysial collagen cables (yellow), capillaries (pink), and fibroblasts (blue) are shown. Scale bars = 5 μm.

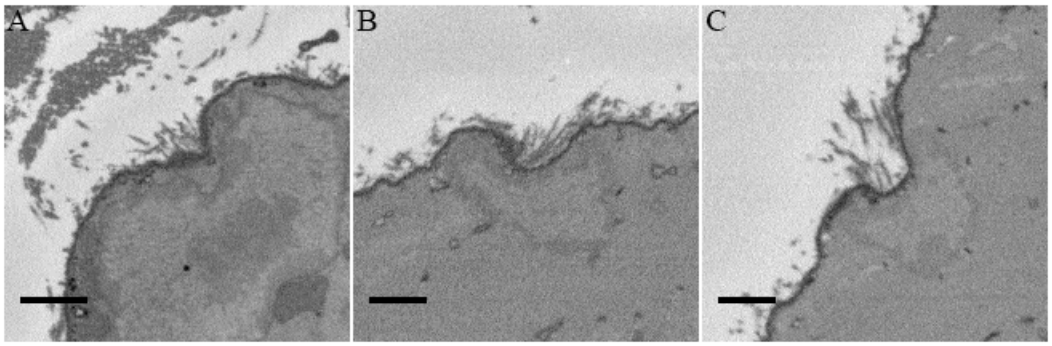

Figure 5.2: 3View cross-sectional scanning electron micrographs of sarcolemmal grooves localized with myonuclei and extracellular matrix components in *des*$^{-/-}$ (A) and *wt* (B & C) muscle fibers. Collagen fibrils are organized transversely to the muscle fiber within sarcolemmal grooves. Scale bars = 1 μm.

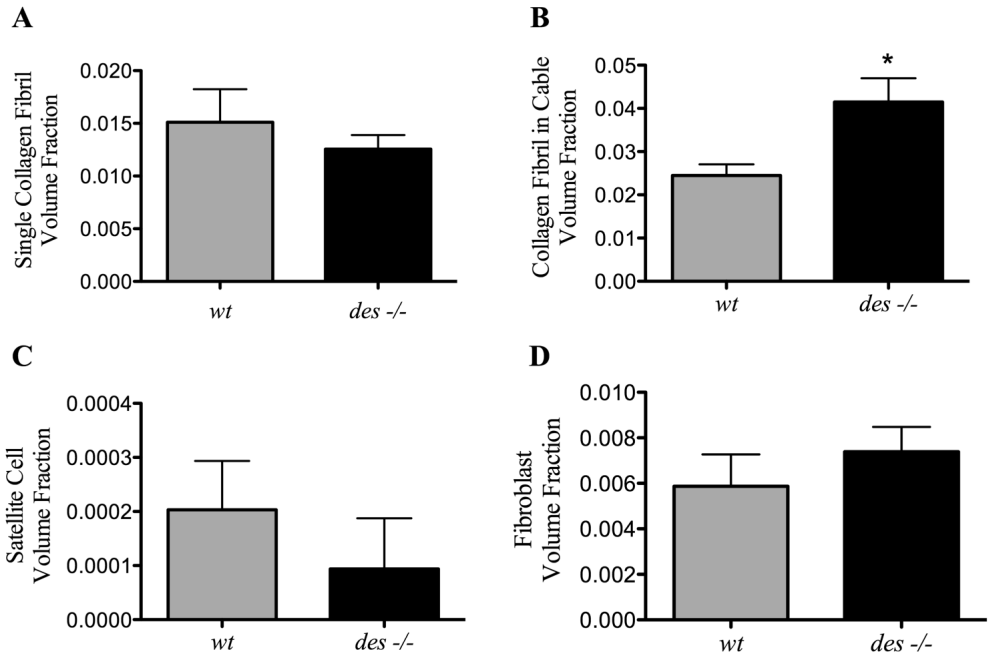

Figure 5.3: Volume fraction estimation of muscle components from wt and *des*$^{-/-}$ EDL muscle. Single collagen fibril (A), satellite cell (C), and fibroblast (D) volume fraction were not changed, however collagen fibrils in cables (B) were almost doubled in *des*$^{-/-}$ muscle. * indicates $p < 0.05$.

CHAPTER 6

Summary and Significance

6.1 Summary of Findings

The objective of this dissertation was to improve understanding of the skeletal muscle extracellular matrix structure and function in normal and fibrotic muscle. This dissertation presents evidence of collagenous structures in skeletal muscle perimysium that were previously unappreciated (Chapter 2). Based on confocal microscopy, they appear to be composed of primarily type I collagen and have been shown to reorganize with muscle strain in real time. Because of their wavy morphology and sensitivity to strain they were deemed likely candidates for load bearing in muscle, and further investigation was performed to determine their role in skeletal muscle fibrosis.

Previous research indicated that fibrotic muscles were stiffer than normal, and this increase in stiffness was presumed to result from an increase in the extracellular matrix stiffness (1, 2). Initial experiments were designed to develop a method that would allow for direct investigation of muscle ECM mechanical properties (Chapter 3). This was achieved by decellularizing muscle tissue, leaving behind the intact ECM. However, this method inherently altered the native tissue structure despite the lack of proteolytic enzymes and detergents for removing muscle fibers, and other microscopy methods were explored to prevent disturbing the *in vivo* organization of ECM collagen.

With the development of new electron microscopy tools for the observation of large tissue volumes, it became possible to study the three-dimensional ultrastructure of extracellular collagen networks. Because muscle ECM contains relatively large "spaces" devoid of electron dense material (interstitial spaces), it presents specific challenges for this type of imaging. These challenges were addressed and existing serial block face scanning electron microscopy methods were optimized for use with muscle ECM (Chapter 4). The importance of this development is that it allowed for nanoscale reconstruction of collagen structures over long distances, which previously would be considered extremely tedious and nearly impossible. The improved staining techniques and automated data acquisition and segmentation allowed for analysis of large datasets over a short period of time. Perimysial cables in normal muscle that had been observed over limited distances with scanning electron microscopy were reconstructed, and their interactions with muscle fibers and fibroblasts were observed. Armed with the appropriate tools, the structure and function of perimysial cables in fibrotic muscle was examined.

The major finding of this dissertation is that fibrotic muscle contains a higher volume fraction of perimysial collagen cables (Chapter 5). The increase in stiffness and doubling of perimysial collagen volume fraction in fibrotic muscle suggests that the increased cables could be responsible for increased stiffness, however correlation could not be determined. This is the first quantitative observation at the electron microscopy level that the ECM of fibrotic muscle has an inherently different structure compared to normal ECM. Other interesting findings include unique interactions between transverse collagen fibrils and sarolemmal grooves with underlying

myonuclei, and interactions of collagen cables with fibroblasts and muscle fibers. Long processes extending from fibroblast cell bodies appeared to guide perimysial cables, and fibroblasts may form physical connections (focal adhesions) with collagen cables.

6.2 Significance of Findings

The morphological findings of this study are a significant contribution to the literature on skeletal muscle ECM. The data presented here suggest that ECM is not simply divided into epi-, peri-, and endomysium based on location in a muscle cross-section, but that these levels of ECM have different compositions and structures, and are not confined to intrafascicular areas based on ECM "thickness." Without the correct understanding of normal ECM structure and organization, it is impossible to determine its specific functions in skeletal muscle with respect to force transmission and passive tension. The observation of laterally oriented collagen fibrils localized to sarcolemmal grooves and underlying myonuclei could direct future research on force transmission and mechanosensing in muscle.

Most muscle research has focused on the actively contracting components, which make up the majority of muscle volume. However, this dissertation has shown that a change of only a *few percent* in the volume fraction of perimysial collagen is associated with the clinically significant increase in stiffness that is measured in fibrotic muscle. For researchers studying antifibrotic therapies, this is good news! A single component of muscle ECM (perimysial cables) *may* be responsible for the

majority of the increased stiffness and ensuing decreased range of motion and contracture seen clinically. This provides a target for clinical therapies aimed at reducing skeletal muscle fibrosis.

6.3 Future Directions

The knowledge gained from this dissertation opens several avenues for future study. The reported structure and volume fraction of perimysial collagen for aged wild type and desmin knockout mice may differ in different mouse muscles, in muscles from different species, and/or muscles with a different fibrosis initiator. The systematic tissue sampling for stereology data analysis could be applied to other muscles to quantify perimysial cables, but this process is laborious and time consuming. Another approach for measuring amounts of perimysial collagen in pathologic muscle could be to develop an assay for perimysial collagen. If all muscle components were digested from muscle tissue except collagen (similar to the hydroxyproline assay (3)) and collagen cables maintain their association into bundles of fibrils, cables may be fractionated from dissociated fibrillar collagens and measured. Such an assay would allow for mechanical testing and perimysial collagen quantification to be performed on the same sample, thus correlation between collagen cable quantity and muscle stiffness could be determined.

Because collagen structure and quantity are not the only factors that can affect fibrotic muscle stiffness, other components must be measured. Collagen crosslinking is another factor that can affect tissue mechanical properties, and increased collagen

crosslinking in various tissues corresponds with increase stiffness (4-6). The transcription of collagen crosslinking enzyme genes was slightly increased in biopsies from patients with cerebral palsy compared to typically developing age-matched controls, but this increase was not significant (7). Nevertheless, collagen crosslinking should be measured in fibrotic muscle to determine if this is another factor in the observed increased stiffness.

The three-dimensional microscopy methods developed in this dissertation could be applied to a number of muscle injury and disease models, or to normal muscle to assess the role of perimysial cables in force transmission. Serial block face scanning electron microscopy is automated once the specimen is prepared and microscope settings are adjusted, so it is theoretically possible to collect data from a single sample over several days to a week. The ultramicrotome apparatus limits imaging depth, but very short muscles (e.g. mouse flexor digitorum brevis) could be analyzed over their entire length. Serial images may then be reconstructed to identify perimysial cables and determine if they extend from tendon to tendon, or from tendon to the muscle belly and terminate on muscle fibers, etc. This type of information is necessary to understand how ECM transmits force laterally from muscle fibers to tendons.

If perimysial collagen cables are primarily responsible for the increased stiffness associated with muscle fibrosis, then clinical therapies could be developed to target these structures. Therapeutic approaches could aim to prevent formation of perimysial cables, or dissociate existing cables. Chung *et al.* have developed an antibody that binds the C-terminal telopeptide of the α2-chain of type I collagen (8).

Binding of the antibody to type I collagen creates steric hindrance that prevents cleavage of C-terminal propeptides and therefore type I collagen fibril formation. Although this method shows promise for reducing collagen deposition in fibrotic muscle, antibody dosing must be carefully defined so that structural collagen in surrounding tissues is not affected.

If crosslinking of perimysial cables is required to maintain their structure, then therapies targeting collagen crosslinking enzymes may promote dissociation of perimysial collagen. Another example of antibody use for fibrosis treatment comes from Barry-Hamilton *et al.* who describe creation of an inhibitory antibody against the matrix enzyme lysyl oxidase–like-2 (LOXL2) (9). LOXL2 functions in normal tissue to crosslink collagens and elastin, however it is upregulated in fibrotic lung and liver tissue. Antibody treatment to block LOXL2 activity in lung and liver fibrosis models resulted in fewer activated fibroblast and decreased fibrosis signaling. A clinical trial is currently underway to determine if LOXL2-blocking antibodies can prevent progression of liver fibrosis (10). Perimysial collagen cable-like structures may be ubiquitous across fibrotic tissues, therefore therapies developed to treat skeletal muscle fibrosis may be applicable to other tissues and vice versa.

6.4 References

1. Smith, L. R., Lee, K. S., Ward, S. R., Chambers, H. G., and Lieber, R. L. (2011) Hamstring contractures in children with spastic cerebral palsy result from a stiffer extracellular matrix and increased in vivo sarcomere length. *J Physiol* **589**, 2625-2639

2. Meyer, G. A., and Lieber, R. L. (2012) Skeletal muscle fibrosis develops in response to desmin deletion. *Am J Physiol Cell Physiol* **302**, C1609-1620

3. Neuman, R. E., and Logan, M. A. (1950) The determination of collagen and elastin in tissues. *J Biol Chem* **186**, 549-556

4. Georges, P. C., Hui, J. J., Gombos, Z., McCormick, M. E., Wang, A. Y., Uemura, M., Mick, R., Janmey, P. A., Furth, E. E., and Wells, R. G. (2007) Increased stiffness of the rat liver precedes matrix deposition: implications for fibrosis. *Am J Physiol Gastrointest Liver Physiol* **293**, G1147-1154

5. Badenhorst, D., Maseko, M., Tsotetsi, O. J., Naidoo, A., Brooksbank, R., Norton, G. R., and Woodiwiss, A. J. (2003) Cross-linking influences the impact of quantitative changes in myocardial collagen on cardiac stiffness and remodelling in hypertension in rats. *Cardiovasc Res* **57**, 632-641

6. Norton, G. R., Tsotetsi, J., Trifunovic, B., Hartford, C., Candy, G. P., and Woodiwiss, A. J. (1997) Myocardial stiffness is attributed to alterations in cross-linked collagen rather than total collagen or phenotypes in spontaneously hypertensive rats. *Circulation* **96**, 1991-1998

7. Smith, L. R., Chambers, H. G., Subramaniam, S., and Lieber, R. L. (2012) Transcriptional abnormalities of hamstring muscle contractures in children with cerebral palsy. *PLoS One* **7**, e40686

8. Chung, H. J., Steplewski, A., Chung, K. Y., Uitto, J., and Fertala, A. (2008) Collagen fibril formation. A new target to limit fibrosis. *J Biol Chem* **283**, 25879-25886

9. Barry-Hamilton, V., Spangler, R., Marshall, D., McCauley, S., Rodriguez, H. M., Oyasu, M., Mikels, A., Vaysberg, M., Ghermazien, H., Wai, C., Garcia, C. A., Velayo, A. C., Jorgensen, B., Biermann, D., Tsai, D., Green, J., Zaffryar-Eilot, S., Holzer, A., Ogg, S., Thai, D., Neufeld, G., Van Vlasselaer, P., and Smith, V. (2010) Allosteric inhibition of lysyl oxidase-like-2 impedes the development of a pathologic microenvironment. *Nat Med* **16**, 1009-1017

10. Gilead Sciences. A Phase 2b, Dose-Ranging, Randomized, Double-Blind, Placebo-Controlled Trial Evaluating the Safety, and Efficacy of GS-6624, a Monoclonal Antibody Against Lysyl Oxidase-Like Molecule 2 (LOXL2) in

Subjects With Advanced Liver Fibrosis But Not Cirrhosis Secondary to Non-Alcoholic Steatohepatitis (NASH). In: ClinicalTrials.gov [Internet]. Bethesda (MD): National Library of Medicine (US). 2000- [cited 2013 Apr 14]. Available from: http://clinicaltrials.gov/ct2/show/study/NCT01672866 NLM Identifier: NCT01672866.

APPENDIX A

Supplementary material from Chapter 5

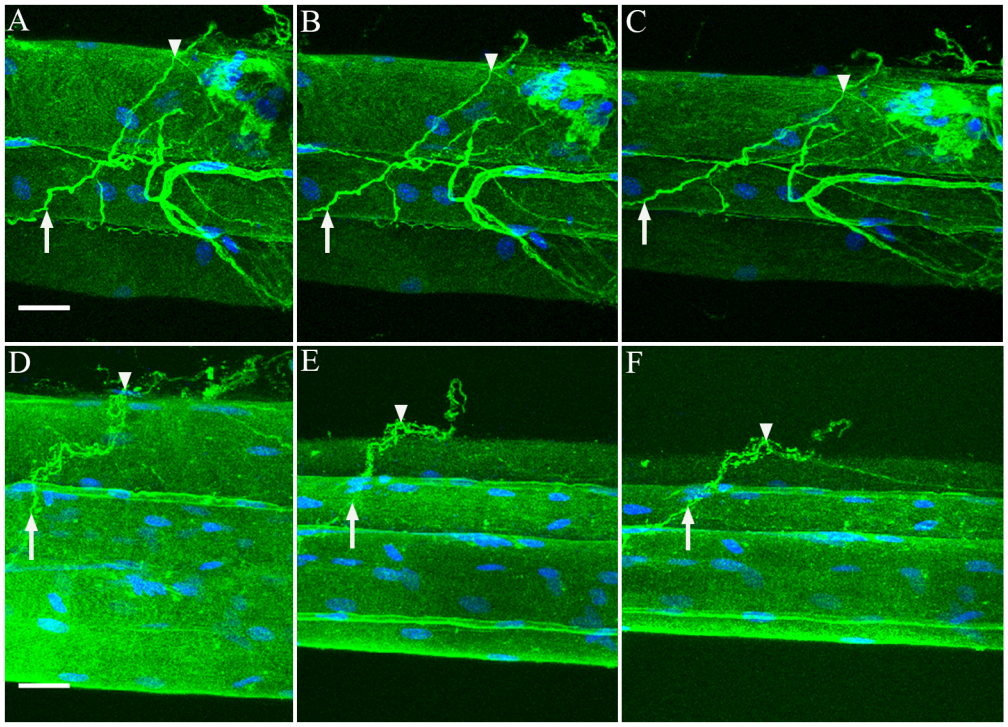

Supplementary Figure 5.1: Confocal microscopy of *wt* fifth toe EDL muscle bundles showing reorganization of perimysial collagen cables with strain. Two separate preparations (A-C and D-F) were immunostained for type I collagen (green) and nuclei (blue). At slack length (0% strain; A and C) intensely stained type I collagen positive structures that traverse multiple fibers are defined as perimysial collagen cables. Two points on a cable are identified (arrow and arrowhead) and these points are again identified at 20% strain (B and E) and 40% strain (C and F) showing reorganization of the cable with strain. Scale bars = 25 μm.

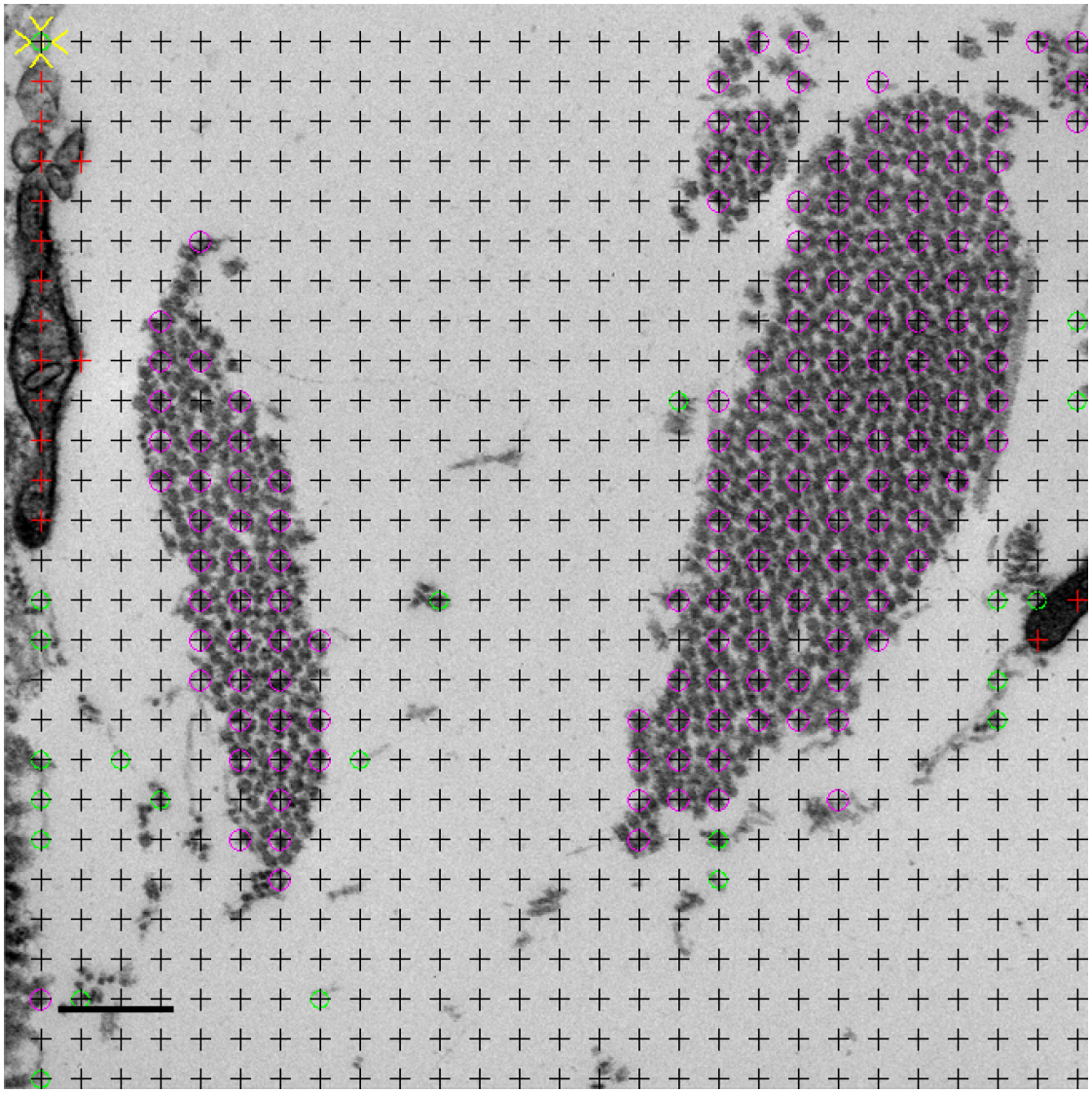

Supplementary Figure 5.2: High magnification (11,000x) transmission electron micrograph with stereology grid generated in IMOD. Each point (at crosshair) was classified as a single collagen fibril (green), collagen fibril in cable (pink), or interstitial space (black). Points lying on objects that were not part of the extracellular space were not classified (red) or included in point count totals. Scale bar = 250 nm.

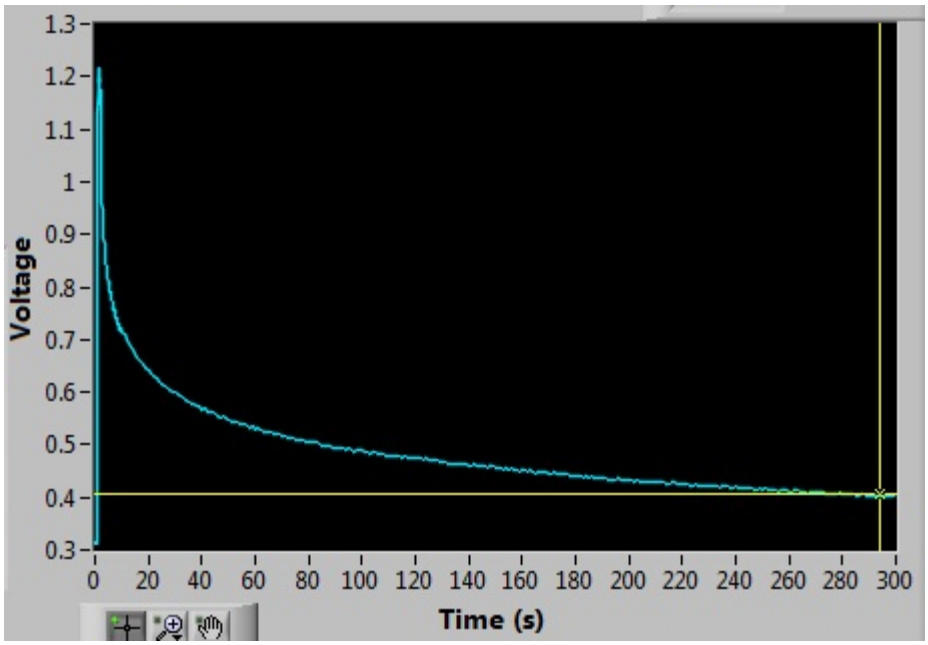

Supplementary Figure 5.3: Example of force record from whole muscle passive mechanical testing. With each step-wise increase in muscle strain, force (shown here in terms of transducer voltage) increases initially to peak force and then voltage declines non-linearly (stress-relaxation) over a period of 5 minutes while muscle strain is held constant.